AD-A050 114 SYSTEMS SCIENCE AND SOFTWARE LA JOLLA CALIF F/G 18/3
NEAR-SURFACE NUCLEAR DUST CLOUD STUDIES.(U)
JAN 77 J W KIRSCH DNA001-73-C-0128
UNCLASSIFIED SSS-R-76-2828 DNA-4332F NL

1 OF 2
AD A050 114

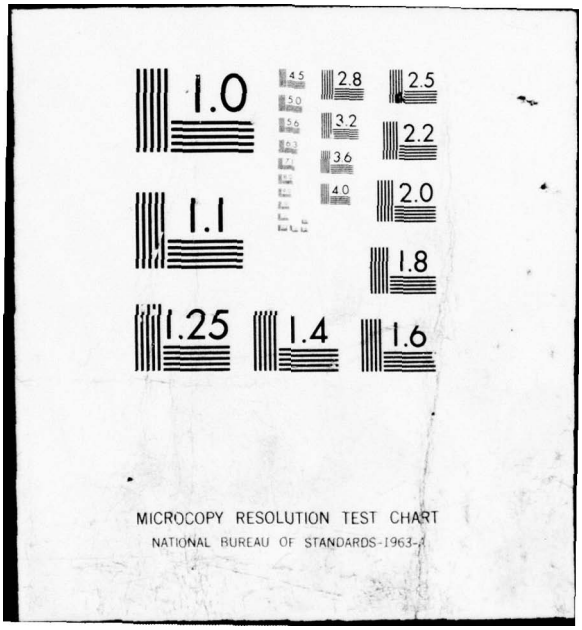
1.0
1.1
1.25
1.4
1.6
1.8
2.0
2.2
2.5
2.8
3.2
3.6
4.0
4.5
5.0
5.6
MICROCOPY RESOLUTION TEST CHART
NATIONAL BUREAU OF STANDARDS-1963-A

DNA 4332F

NEAR-SURFACE NUCLEAR DUST CLOUD STUDIES

Systems, Science and Software
P.O. Box 1620
La Jolla, California 92038

January 1977

Final Report for Period March 1973—February 1974

CONTRACT No. DNA 001-73-C-0128

APPROVED FOR PUBLIC RELEASE;
DISTRIBUTION UNLIMITED.

THIS WORK SPONSORED BY THE DEFENSE NUCLEAR AGENCY
UNDER RDT&E RMSS CODE B344073464 Y99QAXSA00140 H2590D.

Prepared for
Director
DEFENSE NUCLEAR AGENCY
Washington, D. C. 20305

(18) DNA, SBIE (19) 4332F, AD-E300 085

UNCLASSIFIED

SECURITY CLASSIFICATION OF THIS PAGE (When Data Entered)

REPORT DOCUMENTATION PAGE	READ INSTRUCTIONS BEFORE COMPLETING FORM
1. REPORT NUMBER: DNA 4332F ✓	2. GOVT ACCESSION NO. / 3. RECIPIENT'S CATALOG NUMBER
4. TITLE (and Subtitle): (6) NEAR-SURFACE NUCLEAR DUST CLOUD STUDIES.	(9) 5. TYPE OF REPORT & PERIOD COVERED: Final Report. Mar 73–Feb 74,
	6. PERFORMING ORG. REPORT NUMBER: (14) SSS-R-76-2828 ✓
7. AUTHOR(s): (10) J. W. Kirsch	8. CONTRACT OR GRANT NUMBER(s): (15) DNA 001-73-C-0128 now
9. PERFORMING ORGANIZATION NAME AND ADDRESS: Systems, Science and Software ✓ P. O. Box 1620 La Jolla, California 92038	10. PROGRAM ELEMENT, PROJECT, TASK AREA & WORK UNIT NUMBERS: (16) Subtask Y99QAXSA001-40 (17) AD01
11. CONTROLLING OFFICE NAME AND ADDRESS: Director Defense Nuclear Agency ✓ Washington, D. C. 20305	(11) 12. REPORT DATE: Jan 77
	13. NUMBER OF PAGES: 152 (12) 148p.
14. MONITORING AGENCY NAME & ADDRESS (if different from Controlling Office)	15. SECURITY CLASS. (of this report): UNCLASSIFIED
	15a. DECLASSIFICATION/DOWNGRADING SCHEDULE

16. DISTRIBUTION STATEMENT (of this Report)

Approved for public release; distribution unlimited.

17. DISTRIBUTION STATEMENT (of the abstract entered in Block 20, if different from Report)

18. SUPPLEMENTARY NOTES

This work sponsored by the Defense Nuclear Agency under RDT&E RMSS Code B344073464 Y99QAXSA00140 H2590D.

19. KEY WORDS (Continue on reverse side if necessary and identify by block number)

Dust Lofting, Suspension, Saltation, Fluidization, Dust Storms, Rough Wall Boundary Layer, Wind Erosion, Nuclear Dust Clouds, Fluidized Beds, Reverse Percolation, Blowoff, Particulate Lofting, Blast Wave Dust Clouds, MIXED COMPANY Dust Cloud, MIDDLE GUST Dust Cloud, Precursor Dust Clouds

20. ABSTRACT (Continue on reverse side if necessary and identify by block number)

The report completes the documentation of SCOUR2 development and calculations. It covers, primarily, the period from March 1973 to February 1974, but also includes some unreported work from later periods. The results of approximately fifteen calculations of nuclear dust clouds are summarized in this report. They include surface burst calculations from 32.5 KT to 20 MT, and the results of the first SCOUR calculation with a precursor flow field (36.6 KT at 350 ft HOB). These results, although

DD FORM 1 JAN 73 1473 EDITION OF 1 NOV 65 IS OBSOLETE

UNCLASSIFIED

SECURITY CLASSIFICATION OF THIS PAGE (When Data Entered)

388 507

20. ABSTRACT (Continued)
superseded by later SCOUR calculations, provide an excellent introduction to the predictive capacity of the SCOUR code.

A comprehensive comparison is made between the SCOUR code predictions and experimental observations of the near-surface dust clouds produced by the MIDDLE GUST II (100 tons TNT) and MIXED COMPANY (500 tons TNT) high explosive detonations. Included are the results of the most recent (1975) SCOUR calculations that were made with an improved version of the SCOUR code. These results indicated that the nominal SCOUR prescription of dust lofting and diffusion parameters appear to be appropriate for the positive and early negative phase of these HE blast wave events. At later times, the particle impact/deposition model in SCOUR plays a major role in the level of predicted concentrations. By adjusting model parameters, it was possible to explain the discrepancies between SCOUR results and the 5 mm glass beads particulate lofting experiment (MIDDLE GUST II). This suggests that impact and deposition phenomenology should be further studied.

The last area of investigation was the application of a new S^3 code, FLUB, to the calculation of the phenomenon known as "reverse percolation". This is the condition that occurs when the air in porous soils is trapped and pressurized during the early positive phase of the blast wave flow field. The trapped air is capable of rapidly percolating up through the soil matrix when the overpressure is reduced. The present results demonstrate that with a one-dimensional treatment of the problem, porous (strengthless) soils can be fluidized down to a depth of a meter, and significant quantities of sand/dust will be raised above the original surface. It is speculated that this can affect the mass lofting of the blast wave flow field, but due to more pressing research and development problems on precursor dust storms, the study was terminated.

PREFACE

The author wishes to take this opportunity to thank Mr. J. E. Welch and Mr. P. L. Anderson for their assistance in the development and operation of the SCOUR code during this work period. In addition, the fluidized bed computer code, FLUB, used in these studies to analyze the reverse percolation process, was the result of a Systems, Science and Software IR&D Project under the direction of Mr. John W. Pritchett and Dr. Sabodh K. Garg. I appreciate the opportunity to include a description of relevant parts of their effort in this report and thank Mr. Pritchett and Dr. Garg for their cooperation and consultation during this phase of the research project.

TABLE OF CONTENTS

I. INTRODUCTION AND SUMMARY

Systems, Science and Software (S^3) has developed a computer code (SCOUR2) that calculates the time varying structure and intensity of the near-surface dust storm produced in the aftermath of nuclear detonations. This information is required by systems designers concerned with "hardening" missile sites to withstand the high dust dynamic pressures in the positive phase of the blast wave flow field, and for those concerned with near-surface dust concentrations in the late time (negative phase) dust environment.

SCOUR2 was developed over a five year period from December 1970 to December 1975. Most of the S^3 effort has been reported in References 1-4. This report completes the documentation of SCOUR2 development and calculations. It covers, primarily, the third annual report period from March 1973 to February 1974, but also includes some unreported work from later periods.

The SCOUR code is briefly described in the second chapter of this report. An appendix is provided that lists code parameters, nomenclature, and input-output formats. The latter are taken from the most recent version of the code.

Our primary interest in this time period was the prediction of the nuclear dust storm cloud dimensions, concentrations, and dynamic pressure. Approximately fifteen calculations were performed to provide state of the art input data for particular detonations that were of interest to the defense community.[5-7] The results of these calculations are summarized in the third chapter of this report. They include surface burst calculations from 32.5 KT to 20 MT, and the results of the first SCOUR calculation with a precursor flow field (36.6 KT at 350 ft HOB).

It should be noted, however, that the results presented in Chapter III have been superseded by the more recent calculations reported in References 3-4. The latter were necessary because a number of minor coding errors in the original SCOUR computer program were detected towards the end of the third report period.[3] Nevertheless, these earlier results (reported in Chapter III) are very close to those calculated with the SCOUR2 code[3,4] and they were crucial to the continued development of the SCOUR code. In addition to providing enhanced insight of surface burst dust cloud phenomena, the precursor calculation demonstrated the feasibility of using the SCOUR code in more complicated flow field calculations.

Chapter IV is a presentation of SCOUR results for the MIDDLE GUST (100 tons of TNT) and MIXED COMPANY (500 tons of TNT) high explosive detonations. Near-surface dust cloud observations and concentration measurements (at the 25 psi overpressure station) are compared to SCOUR predictions. The earlier SCOUR results, some of which have been reported in Reference 2, were very encouraging but the coding errors (referred to above) necessitated a recalculation of the HE dust storms. These later results (SCOUR2-1975) are published in Chapter IV to provide a convenient comparative study with the SCOUR calculations of 1973-74. It is shown that the SCOUR2 predictions differ in detail from the earlier results. For large diameter pebbles and sand grains, the aerodynamic shear lofting is greater than with more claylike soils. It was also shown that the particle impact model seriously affects the late time dust concentrations just above the surface.

The fifth and final chapter is a presentation of the S^3 study of "reverse percolation". This is the condition that occurs when the air in porous soils is trapped and pressurized during the early positive phase of the blast

wave flow field. Initially, the air flow is into the ground, but when the overpressure decays, the trapped air rapidly percolates up through the soil matrix. Under nuclear blast wave conditions this percolation could be so intense as to blow off surface dust and/or "prepare" the surface for aerodynamic shear lofting of soil particles. This effect has been observed in experiments conducted in an inverted shock tube,[8] and was analyzed by S^3 with the aid of a simple model[9] for flow-through porous media in Reference 2. In Chapter V, some examples of reverse percolation have been computed with the aid of a new S^3 code (FLUB) that was developed to study the dynamics of fluidized beds.[10,11] The FLUB calculations demonstrate that the potential exists for massive blowoff due to reverse percolation; but under the assumption of uniform fluidization, the velocities are too small for particles to be actually ejected into the flow field. Rather, the effect would be to make particles more susceptible to aerodynamic shear pickup and to modify the impact lofting processes currently included in the SCOUR model.

II. SCOUR CODE

The S^3 SCOUR code has been described in the other annual reports. In this chapter, the 1973 version of SCOUR is briefly described with special emphasis on those subroutines and models that are discussed in subsequent chapters. An appendix is provided that summarizes 1975 SCOUR2 nomenclature, input, output, and special diagnostic routines.

2.1 BASIC DESCRIPTION

SCOUR was originally written to calculate the dust sweepup contributions to the nuclear dust cloud. The surface around the blast center is divided into annular rings. Given an axisymmetric hydrodynamic flow field input (from SHELL or HULL calculations), SCOUR calculates the amount of dust mass lofted from each ring, the time at which it is ejected from the surface, and the trajectories of representative dust particles as they move in the near-surface boundary layer or the (free stream, hydrodynamic) blast wave flow field.

The air equation of state, spherical particle drag coefficient routines (including Mach number dependence), and the routines for retrieving the hydrodynamic flow field properties for the trajectory calculations have been obtained from the AFWL's DUSTY code. During this report period, a new subroutine was written that allows tracer particles to be preloaded at specified positions and velocities.

A typical SCOUR calculation proceeds as follows. The preload particles are input, along with soil particle size distribution, and any special parameter changes from the nominal SCOUR prescription. The radial increment for the SCOUR zones are scaled by the cube root of the yield of the burst that was the source for the input hydrodynamic flow field. At 1 MT, these zones are 50 meters wide. The air

shock is located in the hydro flow field at the maximum air density position. As the air shock traverses a surface zone, the mass of dust for each particle size to be lofted via aerodynamic shear is calculated from the aerodynamic mass lofting equation using the free stream air flow conditions. This determines the mass, M_p, to be represented by shear lofted particles from that surface zone. The mass lofting rate is then time-integrated for each subsequent time step in the calculation. Whenever a zone's mass integral for any of the particle sizes exceeds M_p, or some specified fraction of M_p, a new SCOUR particle is created. During this time period it was decided to use 0.2 M_p as the mass lofting criteria for all particles launched after the first batch of shock lofted particles were introduced to the flow field. (This has the advantage of improving the resolution of the SCOUR code by more than doubling the number of particles to be tracked in a SCOUR calculation.) During the positive phase it is possible that a finite time delay exists between the air shock's arrival and significant vertical motion of the activated surface particles. This occurs because the shear first moves particles in a nearly horizontal direction. Should the delay time for the particle be less than the time step in the hydro flow field input, the representative particle is ejected into the boundary layer. If the reverse is true, particles are stored until the accumulated time exceeds the delay time. All particles are lofted from random positions in the zone.

Particles in the boundary layer are subjected to turbulent diffusion and advection by the local air flow. Those particles that are transported out of the boundary layer are moved only by the free stream wind field. As the winds die down, particles may impact the surface. SCOUR's impact model enables particles with sufficient momentum to eject new particles. In such a manner, the negative phase dust storm will degenerate to a saltation type of dust transport, as

described in Reference 12. Should a particle impact the surface with sufficient momentum, a new particle with equal representative mass is ejected. The diameter of the new particle is randomly selected from the in situ soil distribution. The mass of impacting dust is subtracted from the aerodynamic mass lofting integral so that at late times there is very little mass added to the dust cloud. Finally, when impacting particles do not have sufficient momentum, new particles are not ejected and the dust is deposited. This is referred to as a particle "kill" and the dust mass is subtracted from the total lofted dust mass for the zone where deposition occurs.

SCOUR2 has been initially written to use four particle sizes to represent the in situ soil. The mass distribution among these particles is prescribed as code input. (This is not mandatory, however, and randomly selected particle diameters between certain ranges could easily be included, although the price of each calculation would increase with each additional particle size class.)

In a typical calculation, approximately 5,000 particles are tracked in SCOUR at a given time. Once introduced to the flow field, particle trajectories are calculated during hydro flow field time steps. Each particle's mass, position, and velocity are stored as it is moved by the flow field. A 180 second surface burst SCOUR2 calculation will require approximately one hour of computer time on the Univac 1108. With a complete set of output, a typical price per calculation is approximately $300.

The on-line output of SCOUR is geared for rapid diagnosis of the dust environment. It includes:

- Particles' mass, position, and velocity stored for each hydro cycle – available for printout. This includes the tracking of pre-selected

particles (e.g., positive phase dust, pre-loaded dust, etc.).

- Local dust concentrations and dust dynamic pressure for combined and individual particle sizes in a grid superposed on the dust flow.
- Total mass airborne.
- Mass above given surface zone.
- Mass in disc between two altitudes.
- Boundary layer details.
- Local erosion/deposition depth.
- Maximum altitudes of particles.

A second off-line output format is also available. The code user specifies the overpressure locations, vertical zones of interest, and dust cloud parameters of interest. The new output routine averages the time histories of the specified variables over a spread of three radial zones for each radial/vertical location. The spatial averaging eliminates troublesome "zeros" in the digital output. Computer plots of these time histories can be provided per user requirements. Currently, SCOUR2 off-line output covers the following variables:

- Dust concentration.
- Dust flux, horizontal.
- Dust flux impulse.
- Dust flux, vertical.
- Dust flux impulse, vertical.
- Mass averaged dust velocity, horizontal.
- Mass averaged dust velocity, vertical.
- Dust dynamic pressure.
- Dust dynamic pressure impulse.

The input-output format for SCOUR2 is fully described in the appendix to this report.

2.2 NON-INTERACTIVE FORMULATION

The basic SCOUR model was formulated during the first year of the S^3 dust sweepup program. A number of basic assumptions were made at the outset that define the scope of the modeling problem. These were based on measurements of dust clouds and earlier calculations of the dust cloud[13-15] which indicated that only in the near-surface region may particulate concentrations become dense enough to measurably affect the local flow field.* Typical dust loading ratios[16] indicate that dust concentrations in the stem and mushroom portion of the cloud are between 10^{-6} g/cc and 10^{-10} g/cc. It is entirely reasonable, therefore, to approach the dust lofting problem with the following non-interactive formulation:

- Particles are moved by the flow field but do not affect it.
- Characteristic particles, representing a large number of real particles, are introduced to the flow field in lieu of following each and every particle or treating the raised dust statistically.
- Trajectories of characteristic particles are independent of other particles.
- The boundary layer at the surface may be computed under the assumption that the input hydrodynamic flow field provides the free stream information.

The non-interactive model is an important simplification as it precludes the expenditure of time, funds, and effort on reformulating the air flow hydro codes. Hence for a

*This was confirmed in the original (and subsequent) SCOUR calculations.

given weapon yield and HOB, the most appropriate calculation in the tape library of SHELL or HULL hydro calculations can be used to compute the dust cloud.

2.3 SCOUR2 BOUNDARY LAYER MODEL

The boundary layer model in SCOUR2 is almost identical to that described in References 1 and 2. It was derived on the basis of a set of simplifying assumptions, consistent with the non-interactive formulation, that make the problem tractable within the scope of the overall study. One of these is the assumption that the roughness effect of the dust particles moving just above the surface is similar to that produced by very rough walls, i.e., the "perfectly rough" regime of turbulent boundary layers. The shear in the near-surface "perfectly rough" boundary layer is dependent only on free stream velocity and a suitably selected "effective roughness". On the basis of high velocity wind tunnel tests,[17] it was determined that the average height of the near-surface particles provides an adequate measure of effective roughness.

The SCOUR formulation has

$$\frac{u_*}{U_e} = \frac{0.707}{\left(2.87 + 0.7 \ln \frac{x}{k_s}\right)} , \quad \frac{x}{k_s} \geq 1 \qquad (2.1)$$

where

u_* = shear velocity in the boundary layer

$= \sqrt{\tau_0 / \rho}$, τ_0 = shear at wall

ρ = air density

U_e = free stream velocity

x = distance behind air shock for the positive phase, and $\int U_e dt$ in the negative phase (t_0 is time)

k_s = roughness height

The maximum ratio of u_*/U_e is 0.248, but in our calculations $0.15 > \frac{u_*}{U_e} > 0.03$ is a typical range of values.

From the "perfectly rough" shear law, it was also possible to derive integral expressions for the blast wave boundary layer that are evaluated under the assumptions that the local air flow is quasi-steady (i.e., keyed to shock motion), incompressible, and the horizontal velocity in the boundary layer is governed by

$$\frac{u}{U_e} = \left(\frac{y}{\delta}\right)^{1/n}, \quad y \leq \delta \tag{2.2}$$

where

u = radial component of air velocity

Y = altitude above original ground surface

δ = boundary layer thickness

n = boundary layer profile exponent, $8 > n \geq 2$;
(n = 2 in SCOUR, on the basis of wind tunnel experiments[17]).

The turbulent boundary layer development behind the blast wave from a 100 ton HE detonation (MIDDLE GUST) was measured at the 30 and 70 psi overpressure locations.[18] These results for the blast wave boundary layer and the predictions of turbulent boundary layer growth behind the air shock are provided by more sophisticated boundary layer models and compared to the SCOUR boundary layer predictions in Figure 2.1. The SCOUR results at early times are independent of particle roughness effects because the topographical roughness dominates the SCOUR boundary layer development. It is interesting to note that the SCOUR results are in good agreement with the other theories, except at later times where the

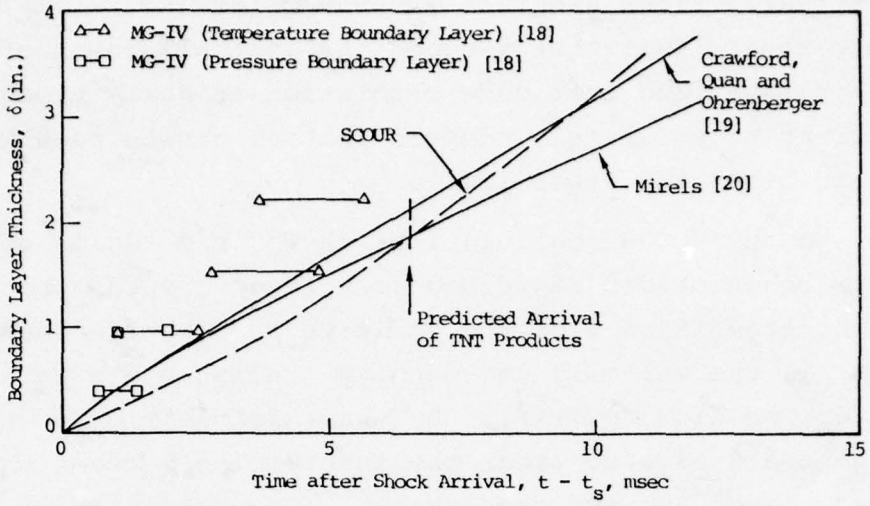

Figure 2.1a. Comparison of SCOUR boundary layer thickness to other predictions and the experimental data at the nominal 70 psi overpressure location (280 ft station) for MIDDLE GUST. [18]

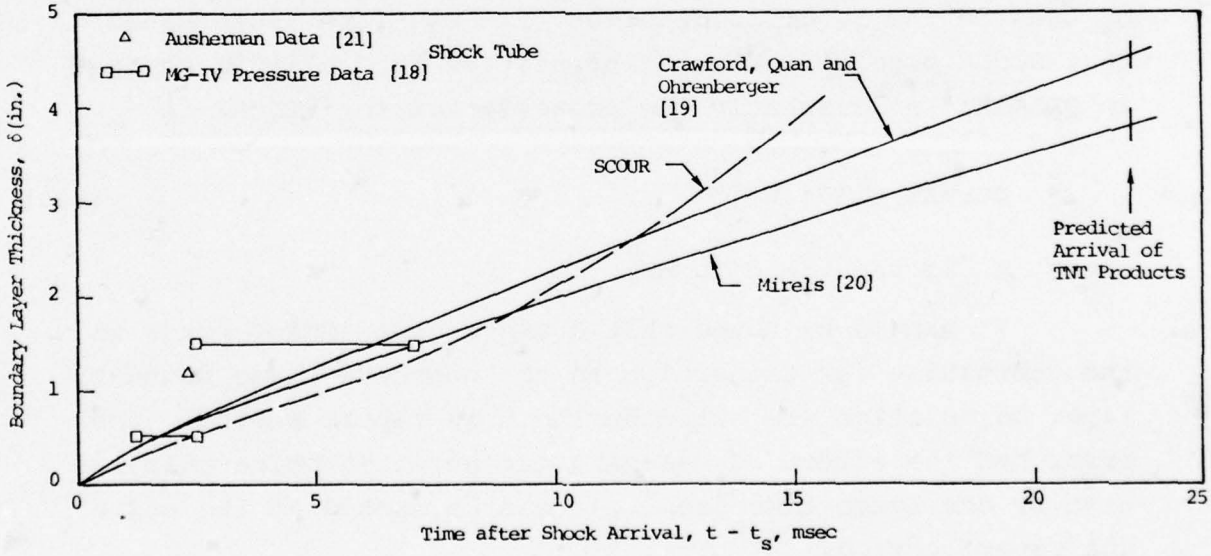

Figure 2.1b. Comparison of SCOUR boundary layer thickness to other predictions and the experimental data at the nominal 30 psi overpressure location (260 ft station) for MIDDLE GUST. [18]

rough wall assumption leads to significantly greater boundary layer growth. The major reasons for the slight underprediction at early times are that the shear law (Eq. (2.1)) has a maximum shear limit that reduces the initial growth of the boundary layer and that code resolution at early times is insufficient to accurately compute initial growth even when the shear is below the upper limit.

In any SCOUR2 calculation, there is a regime of non-uniform behavior and rapid boundary layer growth associated with the transition from the positive to negative phase. Generally, the velocity and density gradients are relatively small during flow reversal. An exact formulation of the problem would have to treat the interaction between the boundary layer and the free stream. To avoid this difficult (but not crucial) portion of the boundary layer calculation, a maximum boundary layer height, DELMAX, is prescribed for each SCOUR calculation. DELMAX was originally based on the maximum size of the zones in the hydrodynamic flow field to be used in the SCOUR calculation. It was later determined that SCOUR predictions were insensitive to realistic changes in DELMAX.[2] Currently the prescription for DELMAX is

$$\text{DELMAX} = 175(W)^{1/3} \tag{2.3}$$

where W is the yield in MT.

It should be noted that a minor programming error in the subroutine for transition to the negative phase boundary layer calculation was noted during this report period. The error had the effect of delaying the negative phase calculation by one hydro time step. It was corrected at the end of the report period.

2.4 AERODYNAMIC LOFTING

The aerodynamic mass lofting prescription in SCOUR2 is based on a simple premise.

> The force required to loft particles out of the fluidized surface layer is supplied by some fraction, b_{ND}, of the net shear in the near-surface boundary layer. For a given particle size,

$$\dot{M}_p V_0 = b_{ND} \left\{ \rho_a u_*^2 - \tau_{th} \right\} dA_i \qquad (2.4)$$

where

b_{ND} = shear transfer coefficient

τ_{th} = threshold shear (taken as 1 dyne/cm^2)

dA_i = surface area of zone

$\dot{M}_p$ = lofting rate (at dA)

V_0 = initial ejection speed of particulates

Conceptually, b_{ND}, V_0 and τ_{th} are all dependent on: particle size, soil type, local wind conditions, soil surface cohesion, vegetation cover, etc. In SCOUR2, the nominal prescription is that there is an overall 10 percent conversion of near-surface aerodynamic shear to the vertical force transmitted to lofted particles.* The lofting efficiency for each particle size class is directly proportional to its mass fraction, i.e.,

$$b_{ND} = \mu_D b_N \qquad (2.5)$$

---

*According to Bagnold,[22] b_N could be as high as 0.3 for dry, hard soils that are characterized by both large and small surface particles.

where

μ_D = mass fraction of soil represented by particle with diameter, D

b_N = overall shear conversion coefficient (nominally 0.1)

The remainder of the shear is assumed to be dissipated in the near-surface tangential motion of the particulates (the so-called "creep" layer). Hence, the SCOUR code tracks only those particles which are ejected out of the near-surface "creep" layer.

Based on recent observations[21,23] of particle entrainment at high velocities, the particle ejection speed, V_0, is randomly selected between 0.5 u_* and u_*, with initial direction chosen so that the slowest particles are ejected at an angle of 10° to the horizontal while the fastest are ejected at 90°. The horizontal component of the particle velocity was programmed to be in the direction of the positive phase flow, even in the negative phase. This error was detected at the end of this report period and the present version of SCOUR2 contains the prescription that ejects particles with horizontal velocities in the same direction as the instantaneous local air flow above a surface zone.

2.5 IMPACT LOFTING AND DEPOSITION

When the wind speeds decay, the bigger particles will fall back to the ground (particularly those above 1 mm in diameter). The SCOUR impact model treats this situation by re-ejecting a particle, whose diameter is randomly selected from the in situ particle size distribution, and which represents the same mass as the impacting particle. It is ejected vertically with 0.1 of the horizontal momentum and all of the vertical momentum of the impacting particle. The mass ejected is

subtracted from the mass lofting integral, for the i^{th} surface zone,

$$(m_p)_{\Delta A_i} = \int_t \dot{M}_p dt, \text{ (mass lofting integral)} \qquad (2.6)$$

which computes the amount of mass being lofted due to shear for a given particle size ($\dot{M}_p$ from Eq. (2.5)). Hence, as particles fall out, the mass lofting integrals at a given surface zone may no longer increase, resulting in the establishment of the equilibrium saltation mode of particulate motion at the surface (wherein no net erosion or deposition is occurring).

Experiments in both natural and laboratory conditions have revealed that there are threshold levels of shear in the boundary layer, below which saltation ceases.[22] In the shear threshold regime, impacting particles begin to deposit (rather than cause the ejection of other particles). As one might expect, this process is dependent on soil type and particle size. Figure 2.2 shows the variation of the threshold shear velocity, u_{*th}, with particle size for uniform sandy soils.

The particle deposition model in SCOUR is based on the principle that particle motion at the surface is directly linked to the existence of the threshold shear. That is, particle impacts will no longer be self-sustaining if the ejection velocity for a SCOUR particle is less than the threshold ejection velocity (u_{*th} in Figure 2.2). Thus, for an impact where the particle ejection velocity is less than u_{*th}, SCOUR "kills" the impact particle and the deposition is recorded in the surface zone erosion integral. When subsequent new particles are created by the action of aerodynamic shear, they replace the killed particles in the SCOUR data storage subroutine.

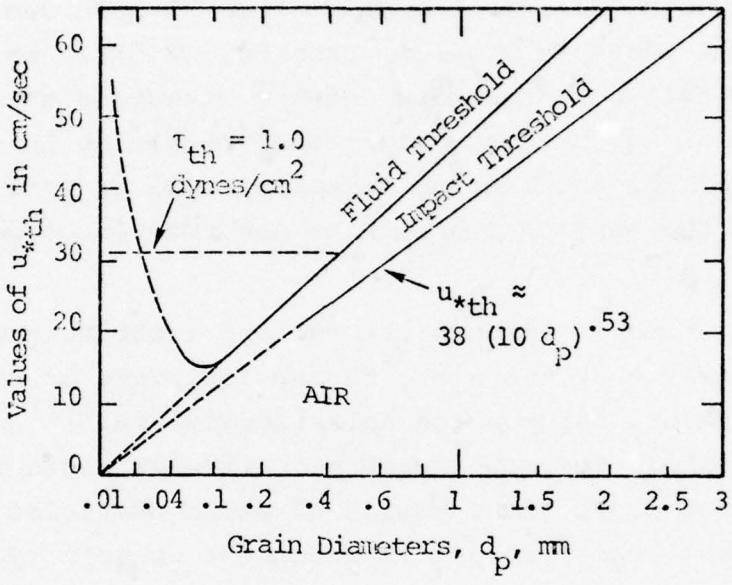

Figure 2.2. Plot of the fluid threshold and impact threshold shear velocities that are necessary to induce saltation (from Reference 22). For aerodynamic lofting, the fluid threshold is appropriate (τ_{th} = 1.0 dynes/cm used in SCOUR). Impact lofting is governed by the impact threshold.

2.6 PARTICLE ENTRAINMENT

The movement of the enormous quantities of dust raised by the blast wave winds is treated in SCOUR by monitoring the motion of numerous ($\sim$ 5,000) individual particles, each representing a much larger number of particles in a certain diameter class. The trajectories of the representative particles are computed by integrating the equations of motion in time steps corresponding to the time sequence of data "dumps" in the hydro flow field being used in a particular SCOUR calculation. The equations are

$$m_p \frac{d^2Y_p}{dt^2} = -m_p g + C_D\left(\frac{1}{2}\rho_a\right)\left(V_p - V_a\right)\left(\dot{Y}_p - v_a\right)\frac{\pi d_p^2}{4} \qquad (2.7)$$

$$m_p \frac{d^2X_p}{dt^2} = C_D\left(\frac{1}{2}\rho_a\right)\left(V_p - V_a\right)\left(\dot{X}_p - u_a\right)\frac{\pi d_p^2}{4} \qquad (2.8)$$

where

V_p = speed of particle $= \sqrt{\dot{X}_p^2 + \dot{Y}_p^2}$

V_a = local wind speed $= \sqrt{u_a^2 + v_a^2}$

$\dot{Y}_p$, $\dot{X}_p$ = components of particle velocity in y, x directions

v_a, u_a = component of wind velocity in y, x directions

The drag coefficient, C_D, is a function of Reynolds number (Re) and Mach number (both based on the relative speed between air and particle). A subroutine for C_D and the air equation of state was extracted from AFWL's DUSTY code.

2.6.1 Diffusion Model

It is evident from Eqs. (2.7) and (2.8) that, except for the initial conditions given to each particle, all dust motion

is governed by the action of aerodynamic drag and gravity forces exerted on the individual dust particles. The hydro flow fields used as input to the SCOUR calculations do not include boundary layer effects or turbulent diffusion in the free stream. Hence, particles injected into an unmodified flow field can only be entrained and suspended if the vertical components of the air velocity are great enough.

SCOUR takes into account the diffusion of particles in the boundary layer by prescribing diffusional (or transport) velocities that are superposed on the horizontal and vertical velocity boundary layer profiles. Hence, particles will be suspended and/or transported out of the boundary layer depending on the particles' susceptibility to the prescribed transport velocity.

The SCOUR model for transport velocity is based on the analogy to diffusion in atmospheric boundary layers. Assuming that dust concentrations will change over the same spatial scale as the dominant mixing eddies, it can be shown that the transport velocity in the boundary layer, V_f, is approximated by

$$V_f \simeq (0.45)\ \sigma_e u \tag{2.9}$$

where

σ_e = standard deviation of the horizontal wind angle fluctuation

u = local horizontal wind velocity

This suggests that a simple prescription for V_f would be of the form

$$V_f = k'u\ , \tag{2.10}$$

where

$$k' = 0.45\ \sigma_e \ . \tag{2.11}$$

This is the diffusion prescription in the SCOUR2 model.

The observed values of σ_e yields values of k' in the range[2]

$$0.004 < k' < 0.12 \ , \tag{2.12}$$

where the lower end of the range is associated with very stable stratified boundary layers (i.e., cold air near the ground, warmer air above). At neutral stability where the thermal gradient matches the temperature loss associated with the adiabatic rise of a gas particle through the atmosphere, $k' \approx 0.06$. The high end of the spectrum is associated with unstable atmospheres.

The nominal value for k' is 0.08. This value gives good agreement for the dust cloud concentration measurements obtained from the MIDDLE GUST and MIXED COMPANY HE detonations. It could be anticipated that for the case of a preheated surface layer, the dust transport would be intensified due to boundary layer instabilities. For this reason, k' is 0.20 for precursor cloud calculations. The advection of the dust behind the shock wave in these cases is dominated by the free stream precursor flow field, and the exact value of k' does not play a significant role in dust cloud development.

To account for the effects of near-surface diffusion phenomena in the SCOUR2 model, numerical turbulence was superposed on the boundary layer velocity prescription to simulate a randomized mixing process due to local disturbances.[2] Specifically,

$$V_f = k'u + 0.1\ u_*, \ y \leq \delta \tag{2.13}$$

where the sign in front of $0.1\ u_*$ is randomly chosen.

2.6.2 Entrainment at the Shock

The SCOUR boundary layer model does not compute the boundary layer parameters above a surface zone until the air shock has completely traversed the zone. As a result, particles which are being swept along by the shock and are in the same radial zone as the shock will not be subjected to either of the entrainment models discussed above. To compensate for the enhanced entrainment and diffusion that has been observed in shock tube experiments,[21] the velocity field in the shock radial zone is prescribed as follows:

$$u = U_e \left(1 - \frac{y_p}{X_s}\right) \tag{2.14}$$

$$V = 0.08\ U_e + U_e \left(\frac{\delta}{X_s - x_{is}}\right) \tag{2.15}$$

where

y_p = particle altitude

X_s = radial location of shock

x_{is}, δ = radial location and boundary layer height at nearest zone completely traversed by shock

III. NUCLEAR DUST CLOUDS

Two sets of dust cloud calculations were made during this report period. The first group (I) consisted of calculations for 32.5 KT and 5 MT surface bursts and a 36.6 KT detonation at 350 ft HOB. These were primarily intended to provide "state of the art" dust cloud information and order of magnitude comparative predictions for input to other defense contractors,[5-7] prior to the setting of nominal values for SCOUR parameters. These results are summarized in Sections 3.1 and 3.2.

The second set of nuclear dust cloud calculations (II) were made for surface burst yields of 0.1 MT, 1.0 MT, and 20 MT. SCOUR parameters were set at nominal values so that the effect of scale on the SCOUR dust cloud predictions could be studied. The particle size distribution of the soil was the same as that used in most of the previous SCOUR calculations;[1,2] i.e., representative particles of 0.8 cm, 0.3 cm, and 0.07 cm in diameter were assigned 20 percent each of the total soil mass. The remaining 40 percent was assigned to representative particles with a diameter of 0.005 cm. These results are summarized in Section 3.3.

The SCOUR code results presented in this chapter, as has been previously explained, have been superseded by later calculations published in References 3 and 4. Nevertheless, they provide a qualitative indication of the SCOUR code's predictive capacity.

3.1 SURFACE BURST DUST CLOUD PARAMETERS – I

A number of SCOUR calculations were made in the first half of the report period, at yields between 32.5 KT and 5.0 MT. For the purposes of this report, the results for the 32.5 KT and 5.0 MT surface bursts are briefly reviewed to

illustrate the sensitivity of the code to changes in the diffusion model in the old[1,2] and newer version of SCOUR (fully described in Reference 2). The 32.5 KT calculation was made with a scaled version of AFWL/SHELL flow field No. 1002.055 (100 KT surface burst, 0-300 secs). The 5.0 MT calculation utilized AFWL problem No. 143.000 (1.4 MT surface burst, 0-600 secs). Both used the nominal in situ particle distribution (20 percent mass to 0.8 cm, 0.3 cm, 0.07 cm diameter, 40 percent mass to 0.005 cm diameter).

Typical concentrations in the dust sweepup cloud for a 5 MT surface burst are presented in Figure 3.1. During the positive phase, these range from 2×10^{-3} g/cc to 0.2×10^{-3} g/cc, over an overpressure range of 500 psi to 2 psi. Negative phase concentrations are predicted to be approximately 0.25×10^{-3} g/cc with the old SCOUR diffusion model,[1,2] and 0.05×10^{-3} g/cc in the (more diffusive) new SCOUR calculations. (This is the present diffusion model in SCOUR.) Predicted values of the near-surface cloud height as a function of radial distance from ground zero (at t = 180 secs) are plotted in Figure 3.2 for a (typical) surface burst.

The mass loading of the cloud for two new SCOUR calculations for a 32.5 KT surface burst are presented in Figure 3.3. These curves represent mass (MT) per MT yield that is lofted above the indicated altitudes. In one case, the diffusion constant, k' (in Eq. (2.10)), was maintained at 0.225. These results are compared to that of a second calculation wherein the diffusion velocities were reduced to one-tenth the previous values ($k' = 0.0225$).

The order of magnitude change in k', the diffusion parameter, has the greatest effect on sweepup contribution to the high altitude dust cloud. These results are similar to that obtained in the 1 MT calculations presented in Figure 6.7

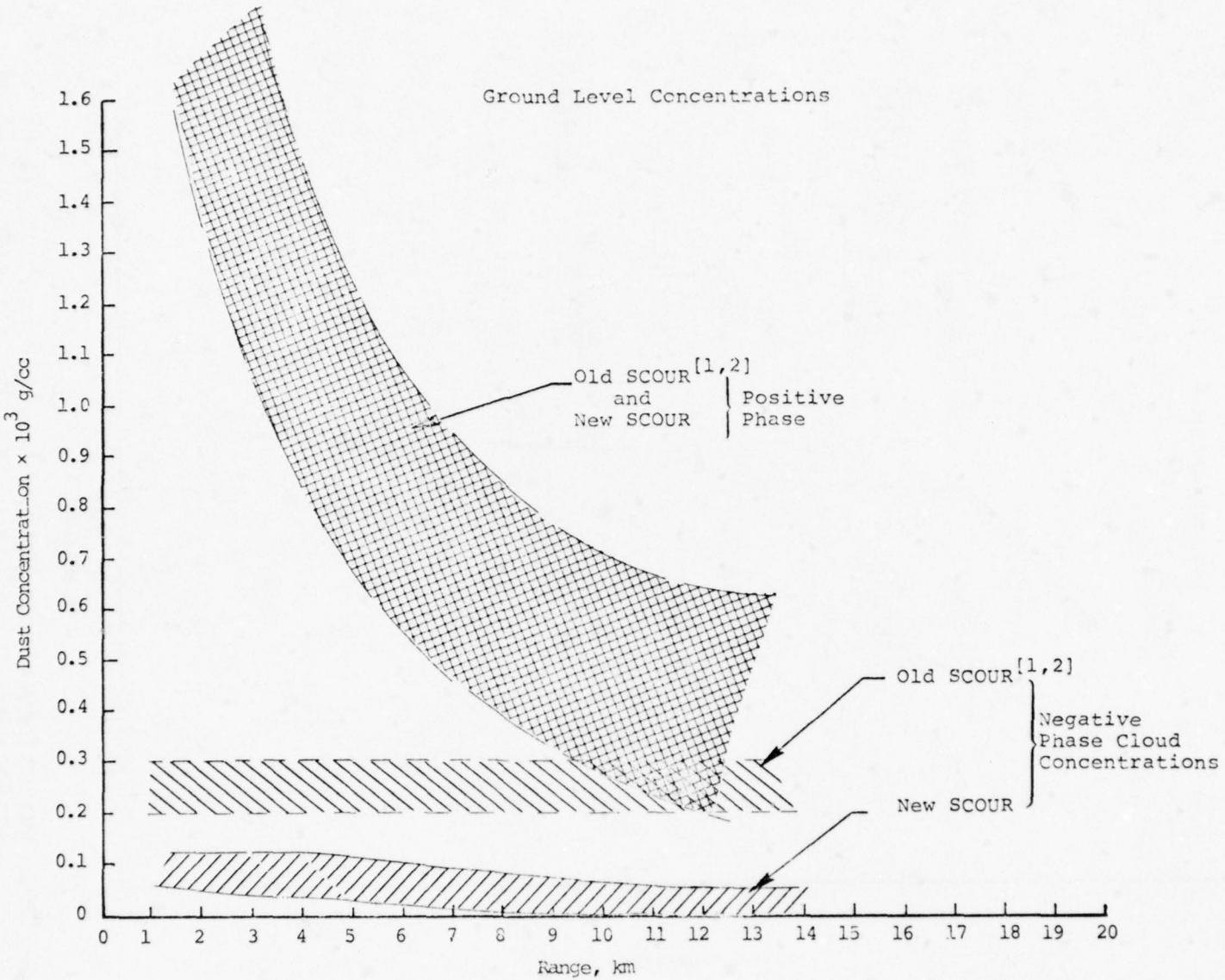

Figure 3.1. Dust concentrations in positive and negative phase for a 5 MT surface burst. Plot shows range of values predicted by SCOUR code. Note that these results, while qualitatively consistent with subsequent SCOUR2 calculations, are superseded by results published in References 3 and 4.

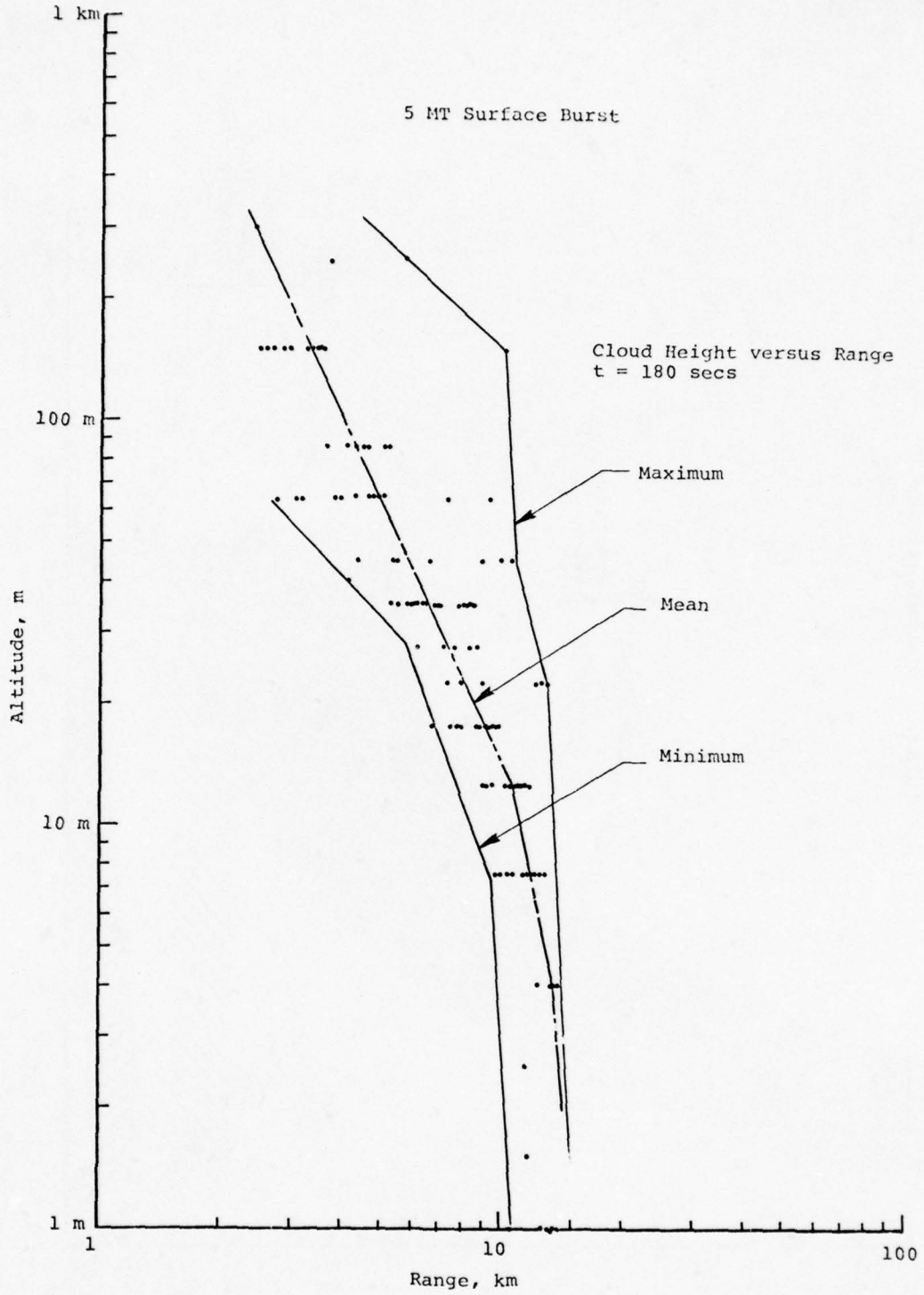

Figure 3.2. Variations of cloud height with range for a 5 MT surface burst. Points represent altitude of cells above individual surface zones populated with dust above 10^{-6} g/cc. Note that these results, while qualitatively consistent with subsequent SCOUR2 calculations, are superseded by results published in References 3 and 4.

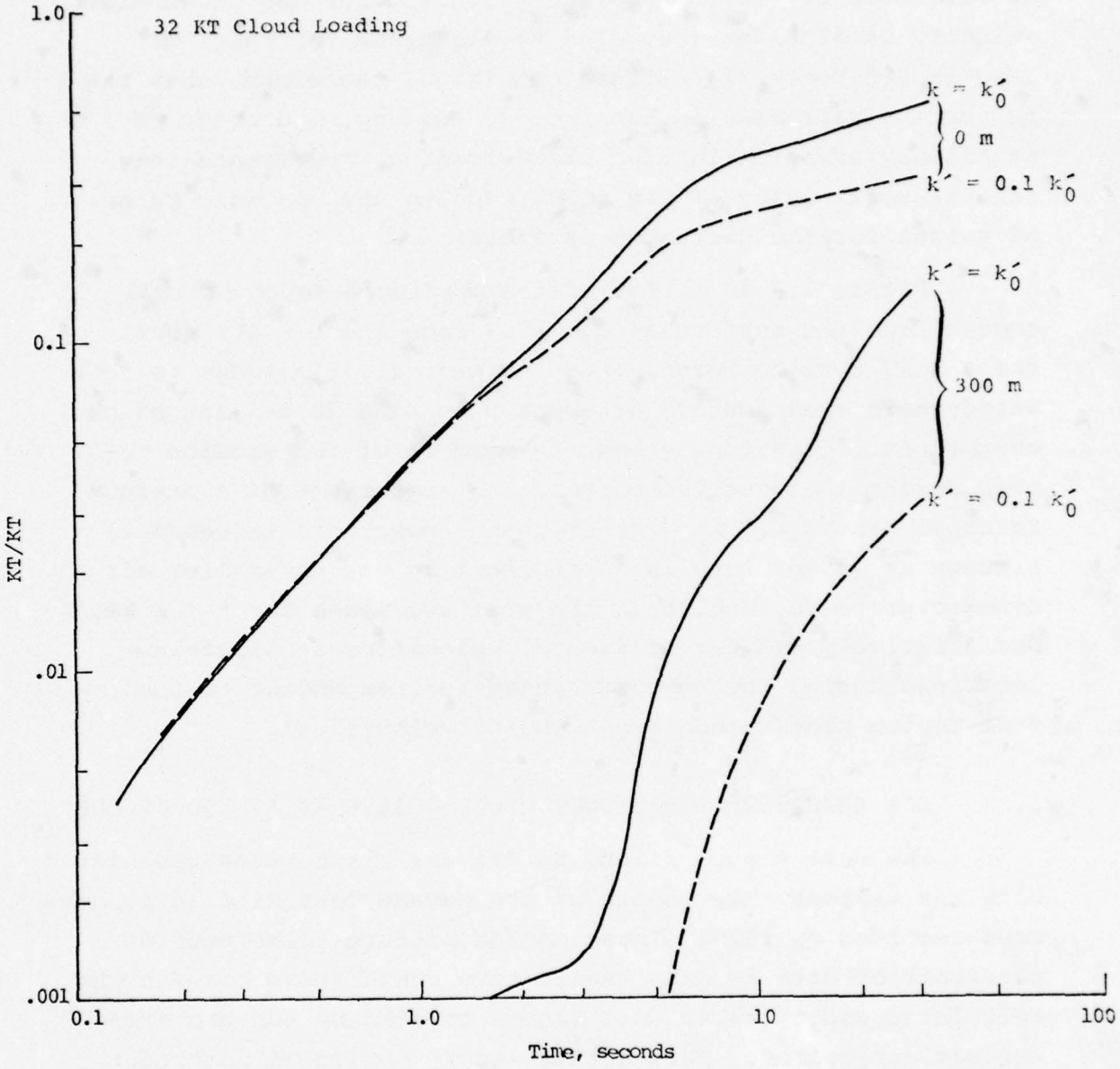

Figure 3.3. Dust loading due to sweepup. Curves show mass lofted above ground level (0 m) and 300 m for a 32.5 KT (surface burst) using two different values of k' ($k'_0 = 0.255$). Note that these results, while qualitatively consistent with subsequent SCOUR2 calculations, are superseded by results published in References 3 and 4.

of Reference 2. In the present calculations, the cloud rise velocity is 57 m/sec (compared to 115 m/sec for the 1 MT case in Reference 2). It was concluded, therefore, that the 50 percent variation in total cloud loading, and order of magnitude variation in high cloud loading, represents the general sensitivity of the SCOUR code to the possible range of values for the diffusion parameter.

Figure 3.4 is a plot of the predicted depth of soil eroded from the surface at t = 18.3 secs and t = 168 secs for a 5 MT surface burst. Peak erosion (1.35 cm) due to aerodynamic shear occurs at about 2 km, the 70 psi air shock overpressure location. About 40 percent of the erosion occurs during the positive phase. The appearance of a maximum in erosion at R $\simeq$ 2 km (rather than a monotonic increase in erosion as ground zero is approached) is due to smaller air dynamic pressure impulse in the positive phase for R < 2 km, and relatively smaller horizontal velocities at close-in locations during the negative phase (corresponding to the stem region containing large updraft velocities).

3.2 LOW HEIGHT OF BURST DUST CLOUD — 36.6 KT AT 350 FT HOB

The dust clouds raised by the air blast waves associated with the various tower shots at the Nevada Test Site (NTS) have been recorded on film. These motion picture films provide a reservoir of data to make qualitative comparisons between the calculated and observed dust clouds created by non-cratering nuclear explosions. During this report period an important review of the NTS dust cloud data was initiated.[24-26] The focus of this study was to develop a phenomenological understanding and model for the development of precursors to the air blast waves. As described in Reference 25, the precursors are distortions in the blastwave structure caused by the radiant preheating of an air layer just above the ground surface.

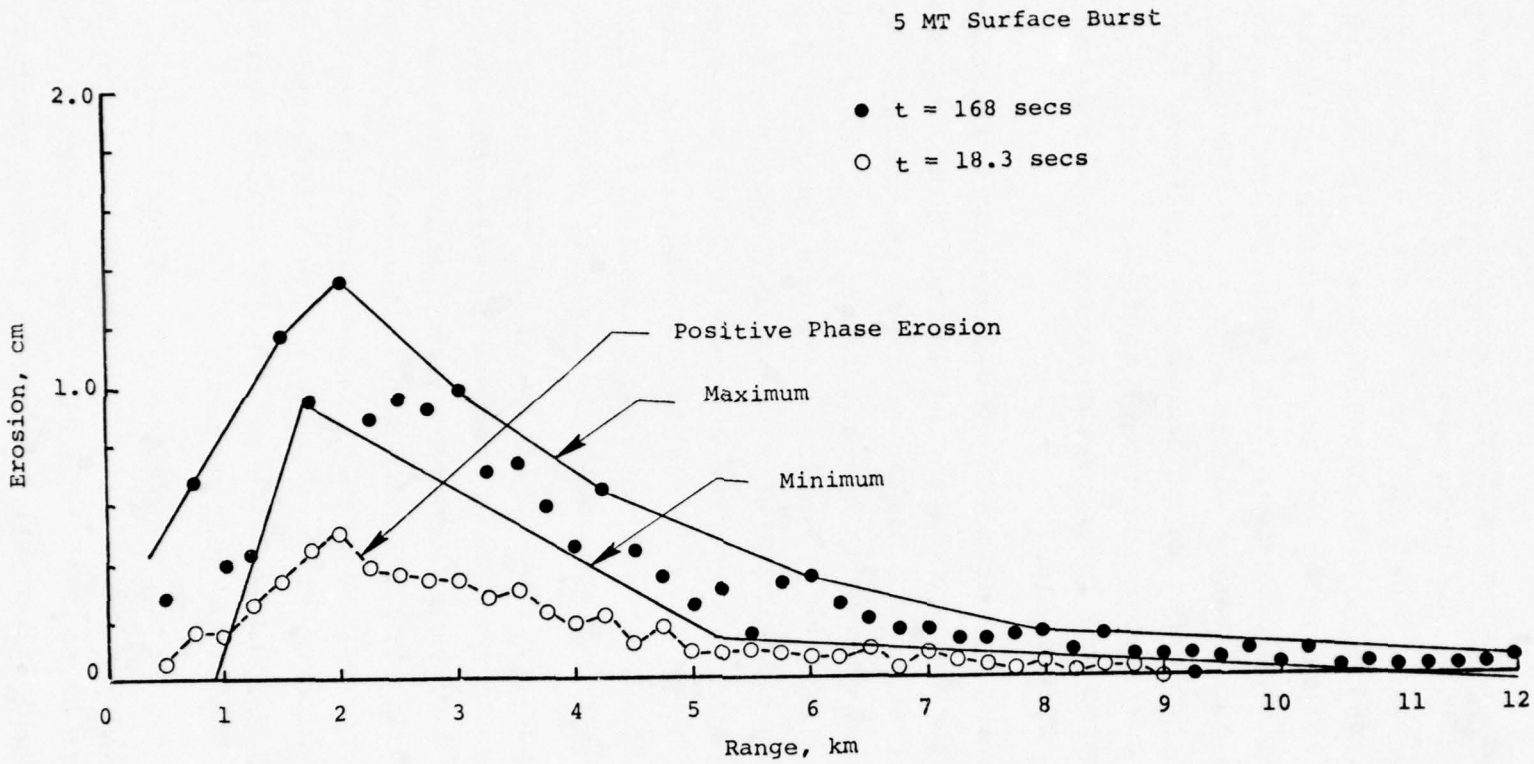

Figure 3.4. Erosion depth calculated for a 5 MT surface burst. Points represent erosion at individual zones located at given range (not all zones plotted). In situ soil density assumed to be 1.8 g/cc. Note that these results, while qualitatively consistent with subsequent SCOUR2 calculations, are superseded by results published in References 3 and 4.

Systems, Science and Software obtained (and converted for use with SCOUR) the hydro output of an AFWL SHELL calculation of a precursor flowfield for a 36.6 KT yield at 350 ft HOB (AFWL No. 362.017, 0.09 sec-5.0 secs). In this AFWL problem, the air near the ground was preheated prior to the inception of the calculation. The preheat layer was roughly 5 meters high and extended out to a range of 420 meters. The presence of a preheated layer causes the shockwave structure to "toe out" just above the ground surface, leading to higher dynamic pressures and lower overpressures when compared to ideal surface flow fields.

Preheating was achieved by designating a fraction of the incident thermal energy on the ground (from the fireball) to be transferred to the air layer above the ground. The flux of incident energy at a slant range, $r_{s\ell}$, was assumed to be equal to $(eh/4\pi r_{s\ell}^2)$ where e is the fireball flux and h is the burst height. AFWL also assumed that the fraction of incident energy transferred to the air layer was equal to the ratio of h to r. To simulate the popcorning threshold of dust, the air layer was not heated until 5.5 calories per square centimeter (or some multiple thereof) were accumulated.

The precursor flow fields resulting from these imposed heating laws, such as those presented in Reference 27, were qualitatively similar to observed flow fields but were different in detail. For the purposes of the SCOUR calculation, however, we were most interested in demonstrating that SCOUR could be used with multiple shockwave flow fields and that the resulting dust cloud structure was in qualitative agreement with observed precursor dust clouds.

Figure 3.5 is a plot of the air velocity vector in the hydro flow field for two times. At 0.38 seconds, the precursor region is shown to consist of a distorted velocity field, with high updraft velocities just behind the leading shock. These

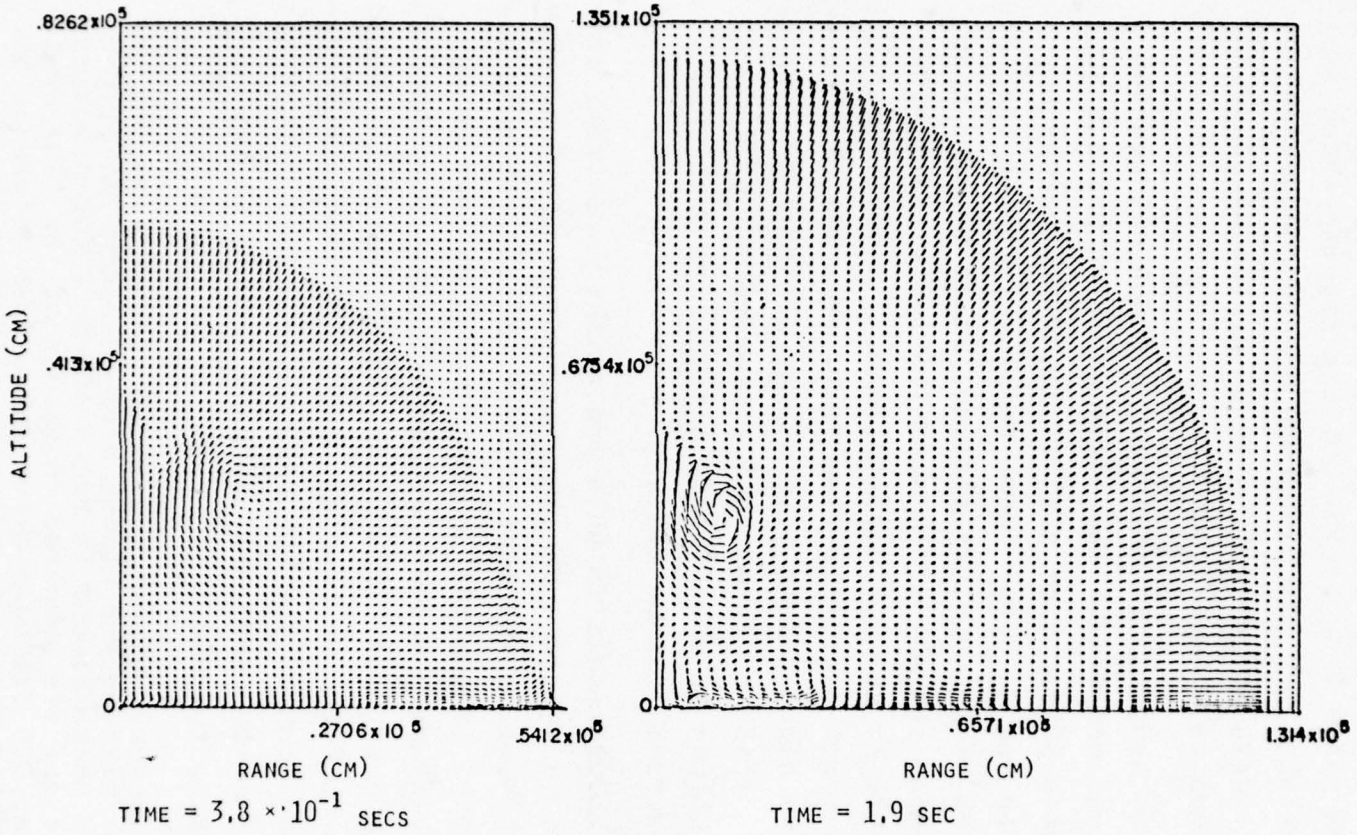

Figure 3.5. Air velocity vector plots from the SHELL calculation which contained a simulation of a thermal precursor. (Note large near-surface updrafts behind the shock at t = 0.38 sec.)

thermal perturbations leave a wake of local eddy disturbances in the negative phase flow field, but the leading shock eventually overtakes the precursor and a more conventional shock structure develops as demonstrated by the air flow at 1.9 seconds shown in Figure 3.5b.

With this hydro field as input, a SCOUR calculation of the dust cloud was made. The early positive phase results are compared to a NTS shot of similar yield and height of burst (HARRY) in Figure 3.6. These results indicate that the predicted height of the precursor cloud, which moves out as hemi-torous behind the shock, is quantitatively and qualitatively comparable to the NTS observations. An additional calculation using a non-precursor flow field (No. 362.018) at the same yield, gave cloud height predictions one-half those shown in Figure 3.6. This indicates that the precursor effect is important to include in dust cloud calculations when theory predicts a precursor will be evident.

An anomalous result in this preliminary precursor calculation, due to a coding error then present in SCOUR boundary layer diffusion models, was most evident in the late time dust cloud predictions. The error in the subroutine lead to extremely large diffusion velocities as particles approached the outer edge of the boundary layer. In effect, particles would slowly diffuse through the boundary layer and then, inadvertently, be ejected out of the boundary layer. This effect was not immediately recognized, and the results were reported in Reference 28 as follows:

> "The agreement between predicted cloud dimensions and the NTS films extend to the early development of the negative phase cloud. Results of the SCOUR precursor calculations are compared to traces of the TURK event (43 KT at 300 ft) dust cloud taken from Reference 28. In Figure 10 the representative particles (d_p = 0.005 cm) entrained in the flow field are plotted on the same axes as traces of the cloud. It is clearly evident that the bulk of the predicted distribution of material lies within the dust cloud traces.

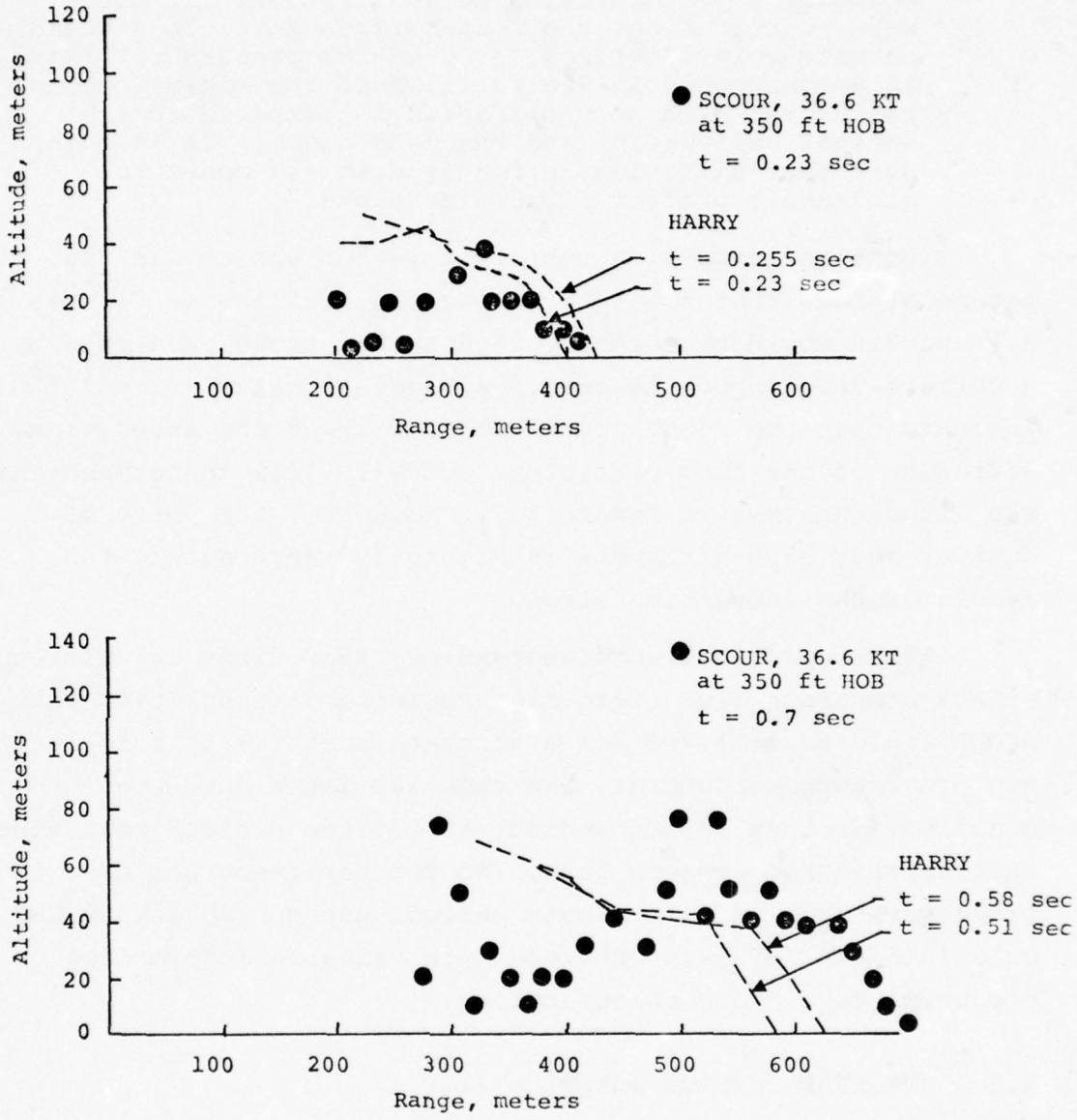

Figure 3.6. Comparison of predicted precursor cloud heights (at t = 0.23 and 0.7 sec) to that obtained from motion pictures of the HARRY event.[24] Note that these results, while qualitatively consistent with subsequent SCOUR2 calculations, are superseded by results published in References 3 and 4.

> This result lends further confidence to the general boundary layer-diffusion model in SCOUR. If there were no diffusion, the near-surface dust cloud would be extremely localized, even with a precursor. This is demonstrated in Figure 11 where the minimal cloud calculated with zero diffusion is compared to the nominal calculation and the TURK cloud. It is evident that diffusion is required in the model to accurately predict cloud dimensions."

Once the diffusion subroutine error was recognized, it became obvious that the late time cloud profiles in Figures 3.7 and 3.8 would be markedly higher than those predicted by a correct version of the code. Subsequent calculations[3,4] indicate that the SCOUR predictions, without the free stream diffusion of the dust particles, actually fall in between the two cloud outlines in Figure 3.7. Moreover, the puffs of dust at very high altitudes in Figure 3.7 were solely the result of the subroutine error.

These problems notwithstanding, this first calculation with a precursor flow field did provide a demonstration that SCOUR could be utilized (on a first-pass basis) to calculate the precursor dust storm. The code was later corrected and modified (in this report period) to include preload particles that represented popcorn dust. No further precursor calculations were made in this report period, but subsequent SCOUR2 calculations[3,4] have provided much valuable information on precursor dust cloud phenomenology.

3.3 NUCLEAR SURFACE BURSTS – (II)

The following calculations were made subsequent to those presented in Sections 3.1 and 3.2. The anomalous diffusion at the outer edge of the boundary layer was corrected, but as previously mentioned, some minor coding errors still were present in SCOUR. Nevertheless, these calculations provided very close estimates of the corrected SCOUR results that are described in References 3 and 4. The diffusion

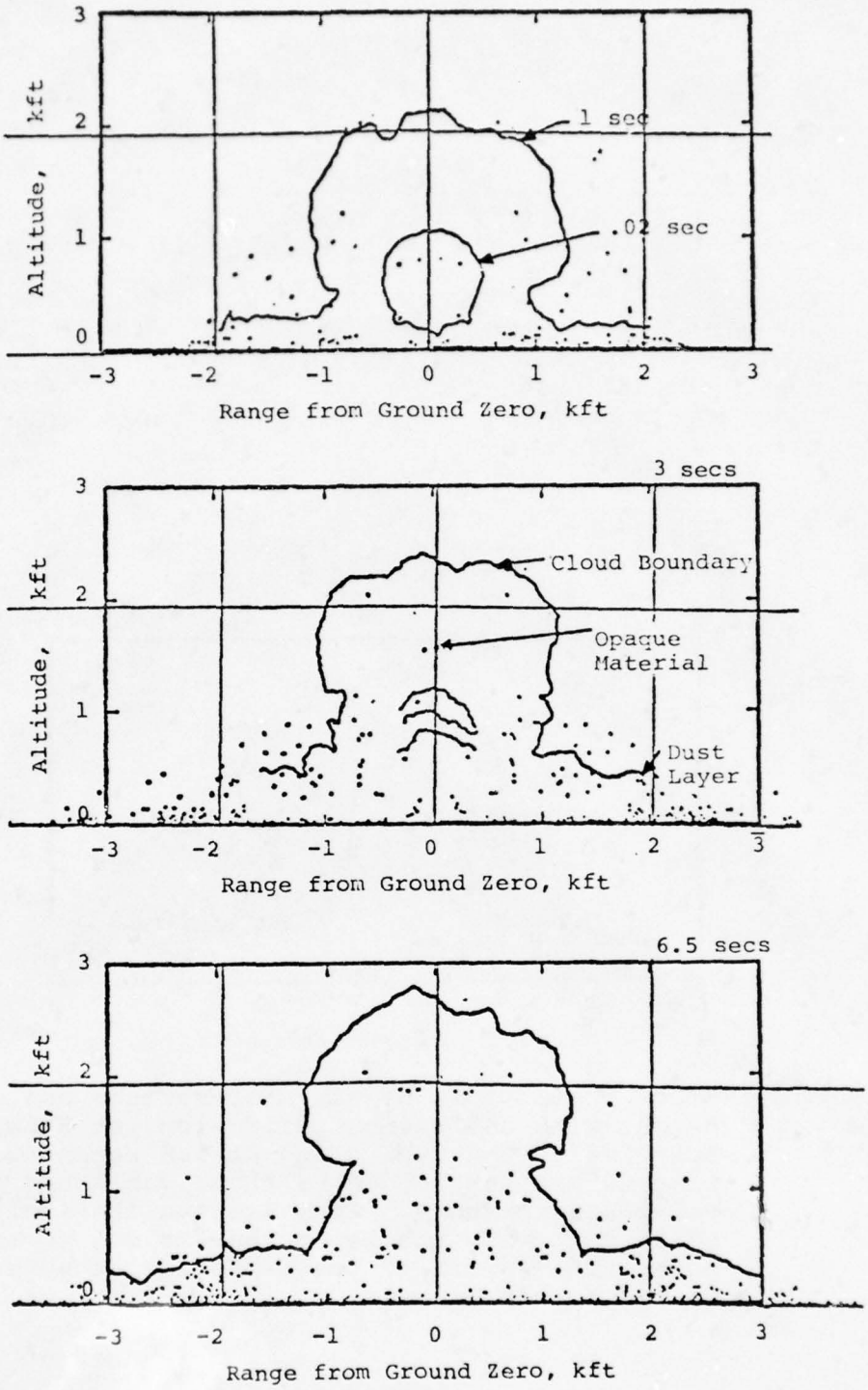

Figure 3.7. Comparison of SCOUR code predictions of positions of representative dust particles to traces of cloud produced during the TURK[29] event. These results are superseded by those published in References 3 and 4. They are qualitatively inconsistent with the later results due to a coding error that magnified the diffusion at outer edge of the boundary layer.

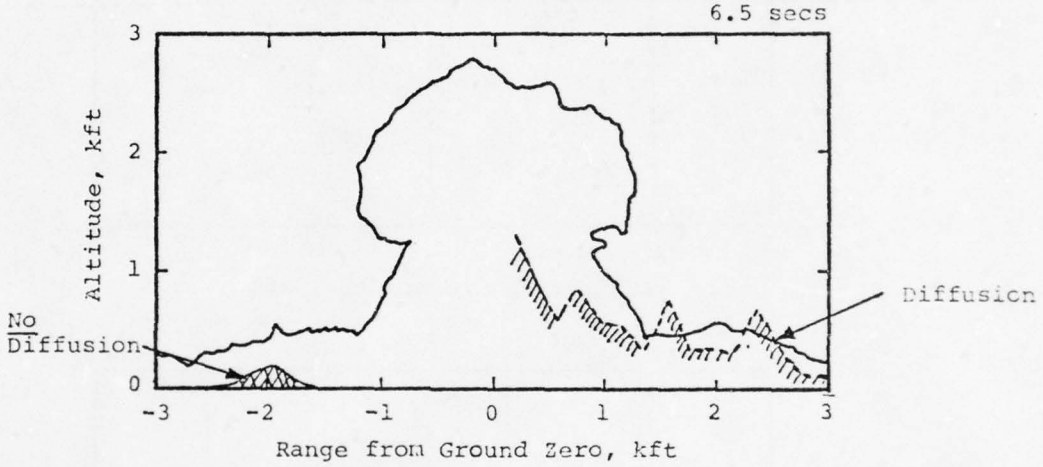

Figure 3.8. SCOUR predictions of the near-surface dust cloud height with and without diffusion, at 5 seconds compared to the TURK cloud at 6.5 seconds. These results are superseded by those published in References 3 and 4. They are qualitatively inconsistent with the later results due to a coding error that magnified the diffusion at outer edge of the boundary layer.

parameter, k', was 0.08 for both the positive and negative phases of these calculations, and the nominal soil particle size distribution was assumed.

3.3.1 Mass Lofting Capacity

The amount of dust lofted by the air blast wave flow field in three different SCOUR2 calculations is plotted in Figure 3.9. Dust mass has been non-dimensionalized by the yield, and time is scaled by the cube root of the yield (in MT). Figure 3.9 also indicates the total dust mass deposited and the dust lofted into the high cloud ($Y > 3$ km).

Roughly speaking, both the total airborne dust and dust deposition fall on the same approximate curve. This indicates that the basic aerodynamic shear dust lofting model can be characterized with a "universal" curve. There is a discrepancy in the 100 KT results between 10 and 100 secs, due primarily to lower speed negative phase winds. However, it is evident that one will not lose much accuracy if a compromise curve is used for this time period.

The rate of dust deposition is comparable to the dust lofting rate at times greater than 100 secs. Maximum airborne mass can, therefore, be estimated from these curves to be 0.4 MT per MT yield.

The blast wave contribution to the high cloud cannot be represented by a single curve, as evidenced by the results of the three calculations. This indicates the significance of energy per unit volume dumped into the fireball and the subsequent influence of the increasing fireball rise velocity at the higher yields. One could anticipate, therefore, that cloud structure and cloud dynamics are closely linked. Nevertheless, it would appear that as much as 0.1 MT of dust per MT yield in the high cloud can be traced back to the air blast wave contribution. This represents approximately

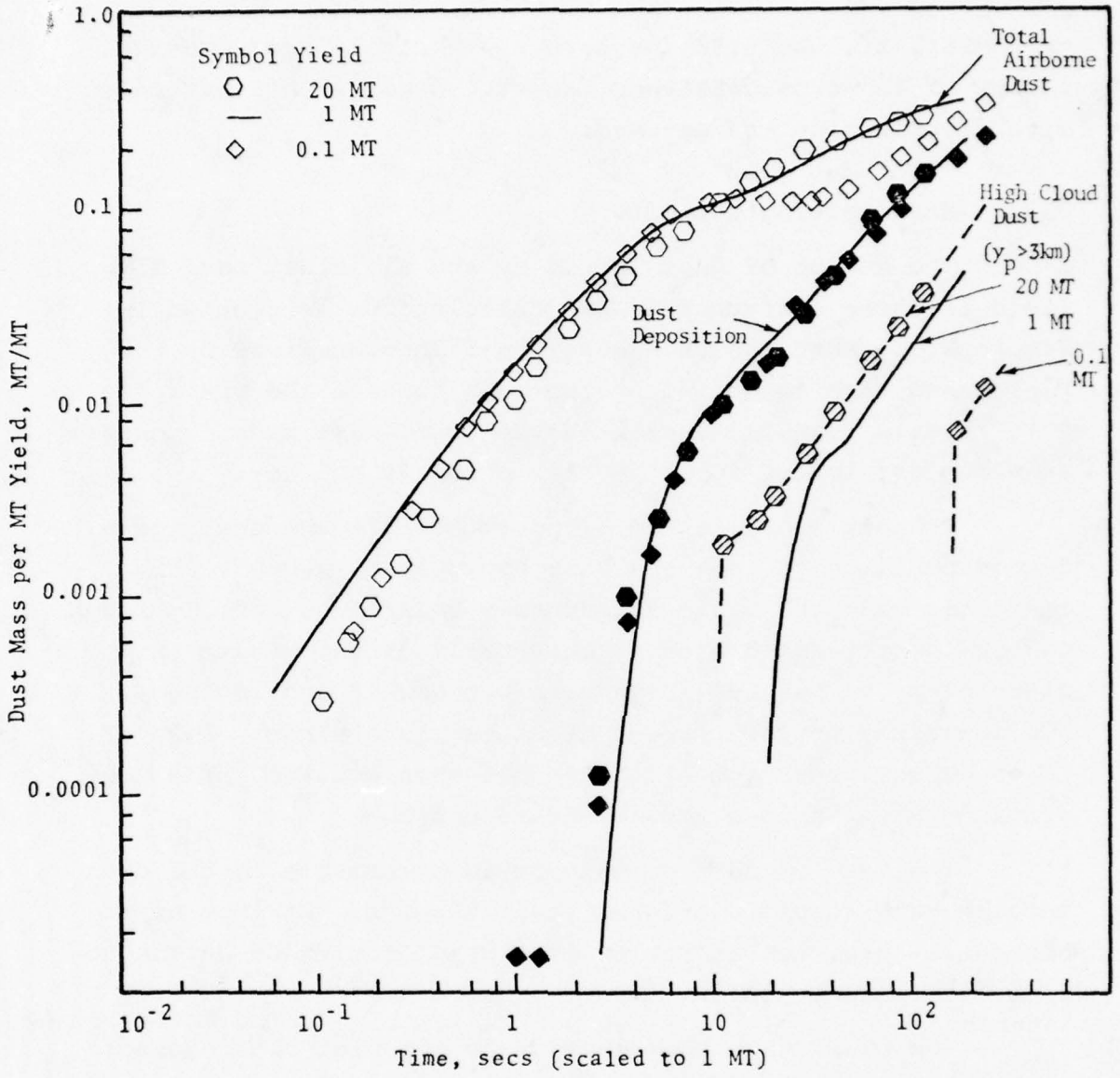

Figure 3.9. Total airborne dust, deposition dust, and high cloud dust in MT dust/MT yield as a function of time (scaled to 1 MT) for three SCOUR surface burst calculations with three different hydro flow fields. Note that these results, while qualitatively consistent with subsequent SCOUR2 calculations, are superseded by results published in References 3 and 4.

one-third the total dust believed to be present in the high altitude cloud produced by surface bursts.

3.3.2 Near-surface Dust Cloud

The extent of the near-surface dust cloud is strongly dependent on the yield of a surface burst. Figure 3.10 shows plots of dust cloud altitude as a function of range from ground zero for 100 KT, 1 MT, and 20 MT. In addition, the lesser yield cloud altitude versus range curves are scaled by the cube root of the yield ratio, $(20/W)^{1/3}$, for direct comparison to the 20 MT results. Note that the times for which the dust clouds are traced are equivalent to approximately 120 secs at 1 MT. Cloud altitude versus range at 180 secs is plotted in Figure 3.11 for the 100 KT, 1 MT, and 20 MT cases, to provide a same-time comparison of the near-surface cloud geometry.

These results give an indication that, at least for the early part of the negative phase, near-surface cloud development can be represented by the time history of a single curve that bounds the three results, where both height and time are scaled by the cube root of the yield ratio.

The potential damage to be caused by the nuclear dust storm is strongly dependent on the augmented dynamic pressure attributable to the blowing dust. Figure 3.12 shows the peak dust dynamic pressure (q_{dust}) calculated at overpressure locations up to 100 psi. Three nuclear bursts are compared to the MIXED COMPANY HE calculation (discussed in Chapter IV). Note that the nuclear burst calculations are only mildly influenced by yield, and within a factor of $\pm$ 25 percent, q_{dust} for surface bursts is a function only of overpressure location.

In all of the nuclear cases, the peak dust dynamic pressure was achieved by dust that was trailing right behind the air shock at an altitude of 1 meter to 3 meters above the

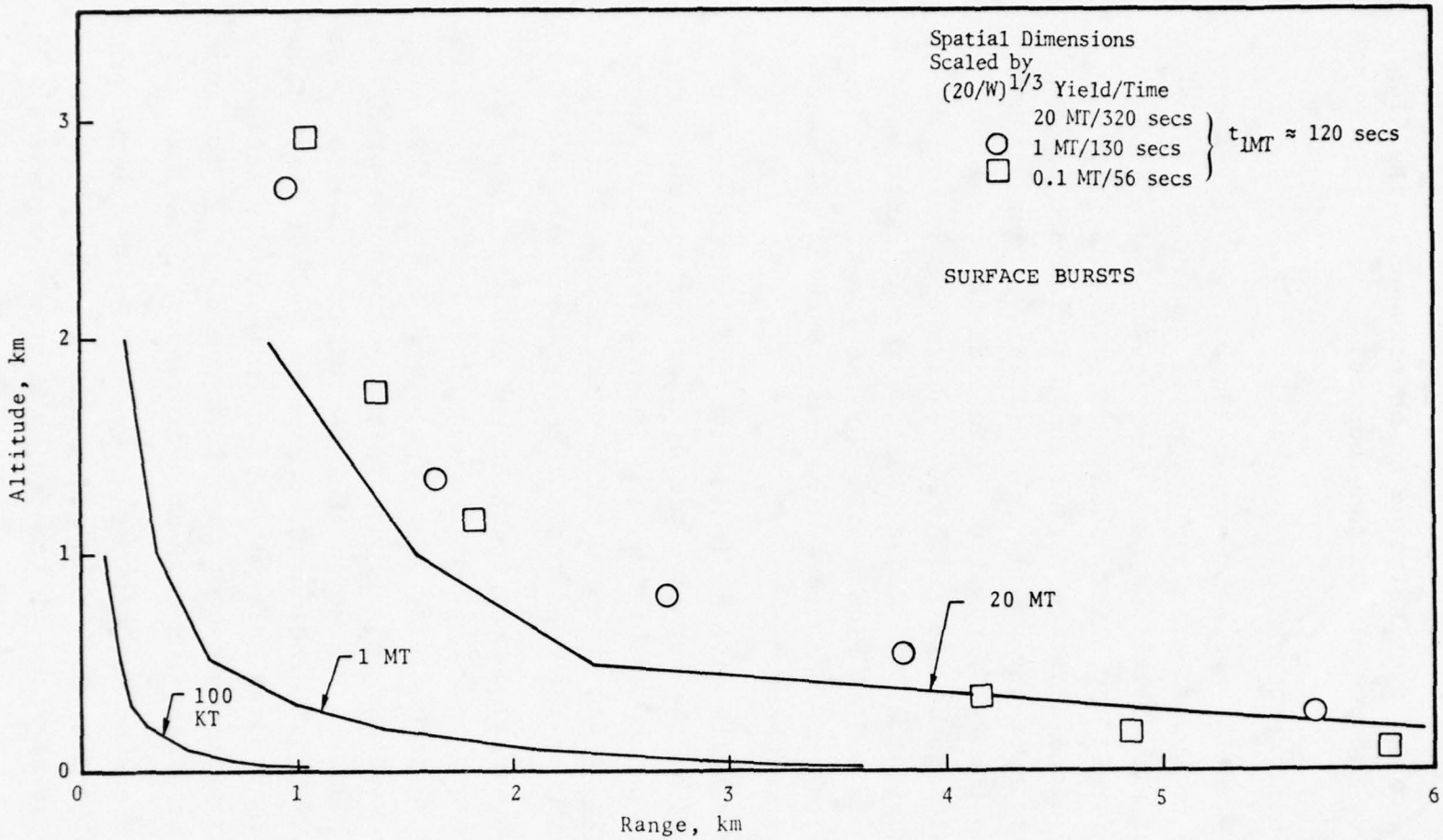

Figure 3.10. The near-surface SCOUR dust cloud altitude versus range for 100 KT, 1 MT, and 20 MT surface bursts at a scaled time of ≈ 120 seconds. Symbols are the spatial dimensions of the lower yield clouds scaled by $(20/W)^{1/3}$. Note that these results, while qualitatively consistent with subsequent SCOUR2 calculations, are superseded by results published in References 3 and 4.

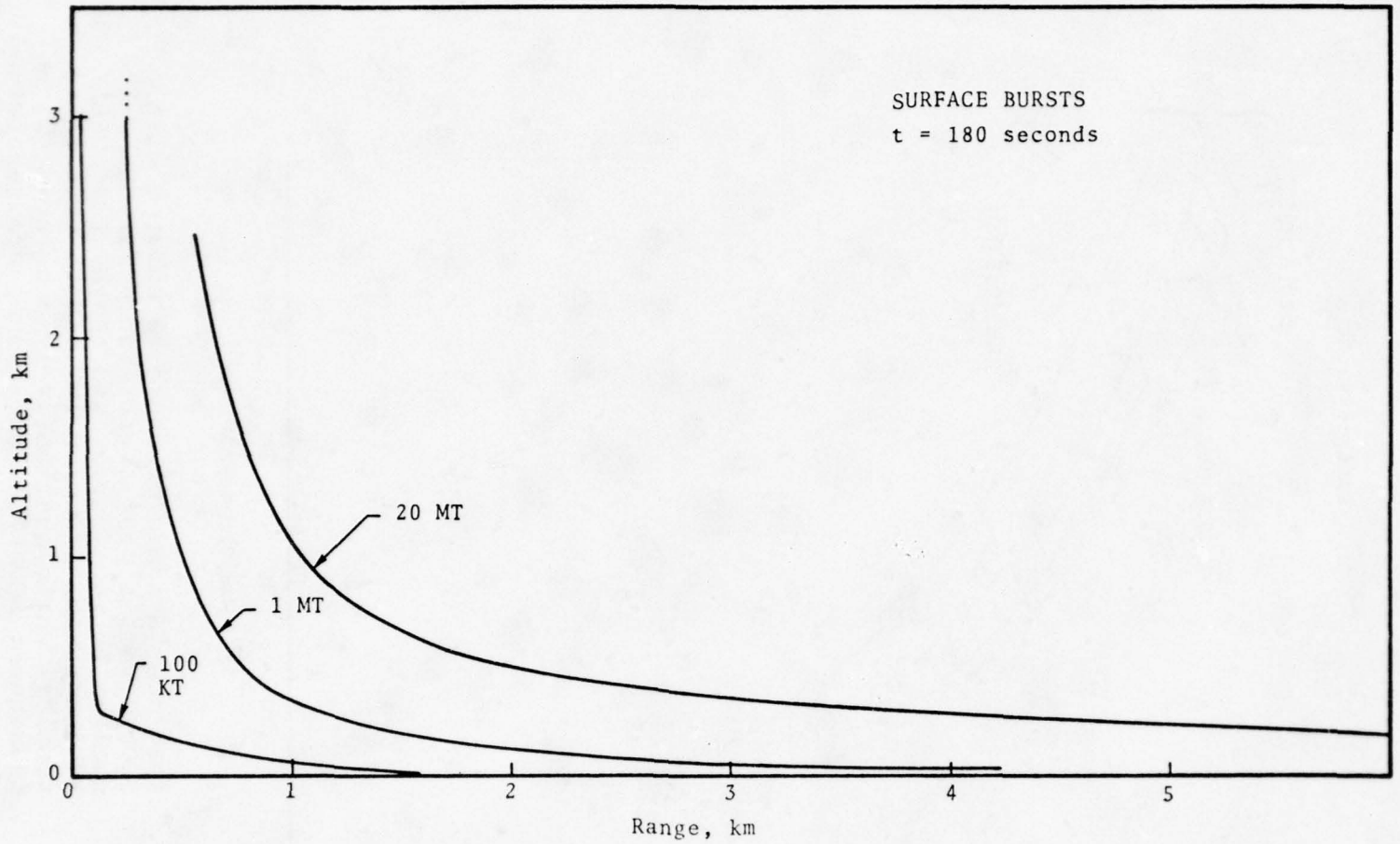

Figure 3.11. Near-surface SCOUR dust clouds at 180 seconds for 100 KT, 1 MT, and 20 MT. Note that these results, while qualitatively consistent with subsequent SCOUR2 calculations, are superseded by results published in References 3 and 4.

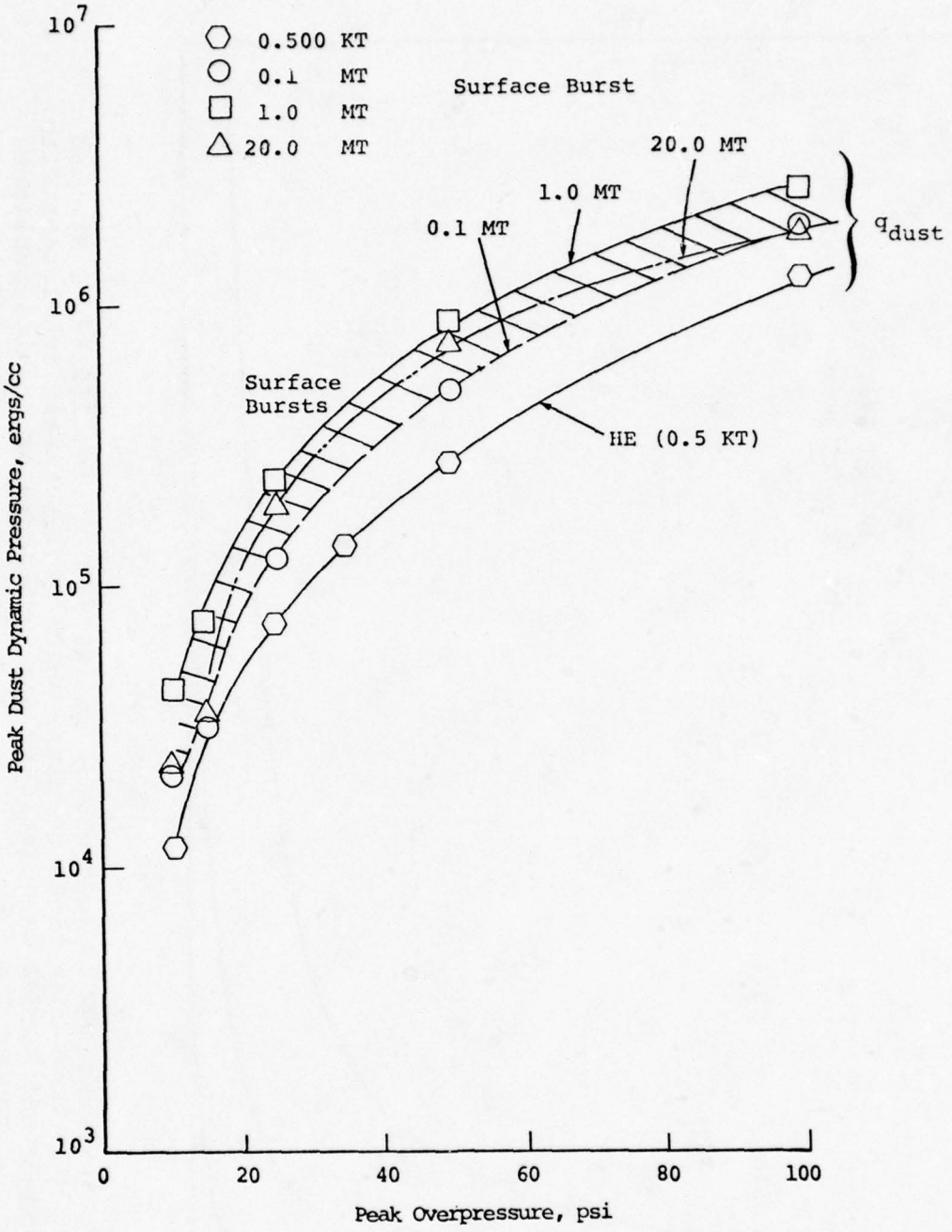

Figure 3.12. Peak dust dynamic pressure calculated with SCOUR2 versus peak overpressure for three nuclear surface bursts and the MIXED COMPANY HE detonation (Chapter IV). Note that these results, while qualitatively consistent with subsequent SCOUR2 calculations, are superseded by results published in References 3 and 4.

ground surface. These dust particles actually preceded the scouring of dust off the surface at a given radial location. When the scale of the SCOUR calculation is reduced to the one-half KT HE explosion, the high density dust is trapped in the boundary layer and does not reach the free stream velocities necessary to achieve the higher values of q_{dust}.

The total peak dynamic pressure loading in the non-interactive formulation of the nuclear surface burst dust storm is the sum of q_{dust} and q_{air}. These values are plotted versus overpressure in Figure 3.13. They are compared to the light dust and heavy dust total dynamic pressure taken from the current edition of DNA Report EM-1, Part I, "Capabilities of Nuclear Weapons," 1 July 1972. The basis for the latter curves is obscure. Presumably they are developed from a limited amount of dynamic pressure data obtained in actual above-ground nuclear explosions. In most cases, these were low HOB detonations, and DNA Report EM-1 dust predictions involve extrapolation of these data to surface bursts.

SCOUR2 gives lower dynamic pressure predictions at the higher overpressures, possibly due to the absence of crater ejecta in current SCOUR2 calculations. Dynamic pressures for a subsequent 36.6 KT, 350 ft HOB calculation were also compared to DNA Report EM-1 values (see Reference 3), and these indicated that the addition of neutron lofted dust to the region just under the blast significantly boosted the SCOUR2 predictions of q_{TOT}. The higher SCOUR2 dust loading and dynamic pressures at the lower overpressures ($p < 30$ psi) in Figure 3.13 may be attributable to lower (ideal surface) air dynamic pressures used in the derivation of the DNA curve.

The particle size distribution in the near-surface dust cloud varies with time and altitude. At early times the positive phase dust cloud closely adheres to the original in situ size distribution. However, at later times, the large particles

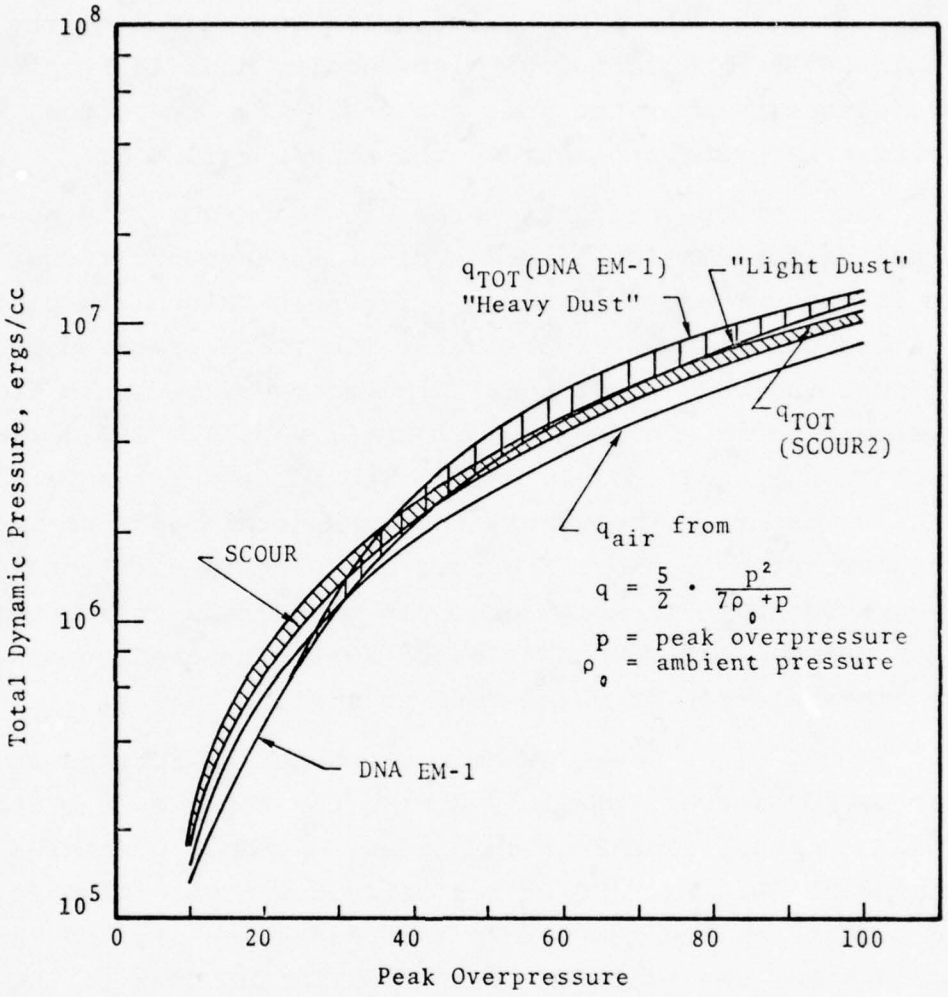

Figure 3.13. Peak total dynamic pressure versus peak overpressure as predicted by SCOUR2 and DNA EM-1 for nuclear surface burst. Note that these results, while qualitatively consistent with subsequent SCOUR2 calculations, are superseded by results published in References 3 and 4.

have fallen out and only particles with diameters less than 0.001 cm are left in the near-surface cloud. Results for a 1 MT surface burst are shown in Figure 3.14.

Peak dust concentrations in the positive phase range from 0.1×10^{-3} to 3×10^{-3} g/cc between the 0.5 psi and 100 psi overpressure location. In the negative phase, the more diffuse near-surface cloud consists of only the small size particulates ($d_p < 0.001$ cm) in concentrations between 1×10^{-5} g/cc and 2×10^{-4} g/cc.

The total mass flux of positive phase dust at the 50 psi overpressure station is plotted versus altitude in Figure 3.15. At each yield there is an altitude ($\tilde{Y}$) at which dust activity is most intense. Both the total mass flux and $\tilde{Y}$ increased with yield. Note that for the one-half KT HE calculation, intense dust activity is confined to altitudes less than 2 meters ($\tilde{Y}$ = 0.5 m). At multi-megaton yields, this is expanded to 25 meters ($\tilde{Y}$ = 7.5 m).

The peak dust impulse in the positive phase, $\int_{t_0}^{t^+} \rho_d u_d^2 dt$, scaled by $(W)^{1/3}$, is plotted as a function of peak overpressure in Figure 3.16 to illustrate that for nuclear surface bursts, dust impulse (like air impulse) can be scaled by the cube root of the yield ratio. This is because the peak dust dynamic pressure is almost independent of yield (see Figure 3.12) and the positive phase duration scales by $(W)^{1/3}$.

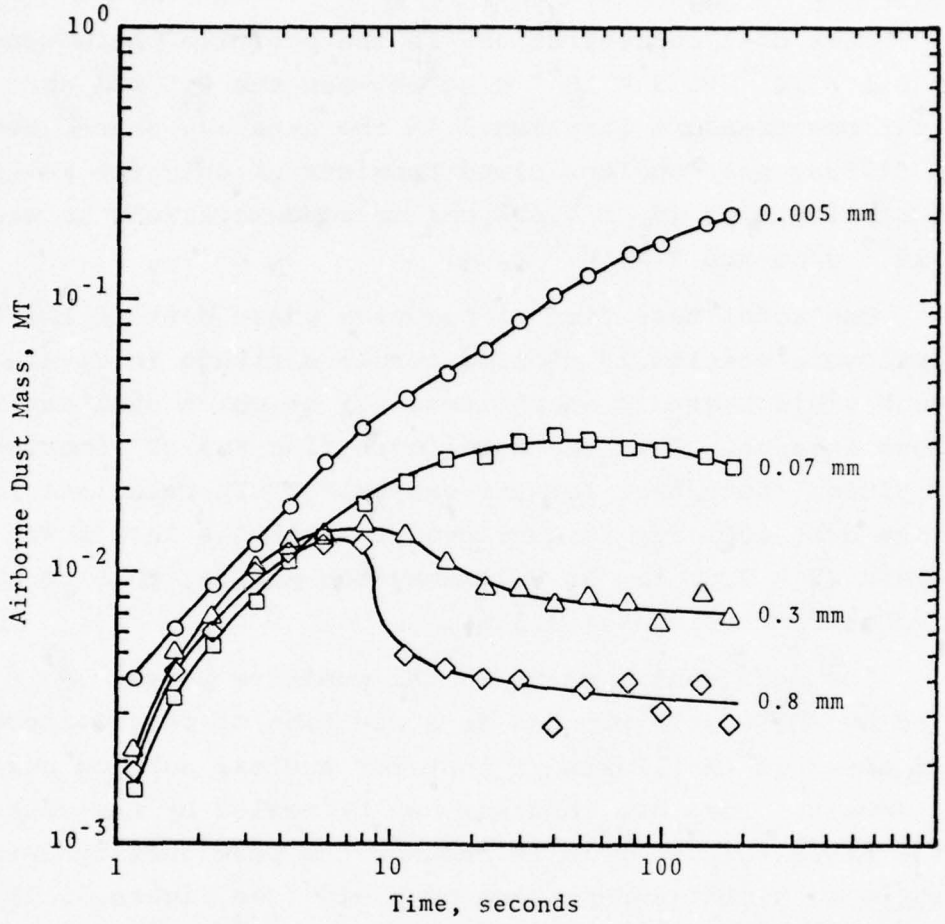

Figure 3.14. Airborne dust mass for each particle size in a SCOUR calculation of the air blast lofted dust cloud (1 MT yield). Note that these results, while qualitatively consistent with subsequent SCOUR2 calculations, are superseded by results published in References 3 and 4.

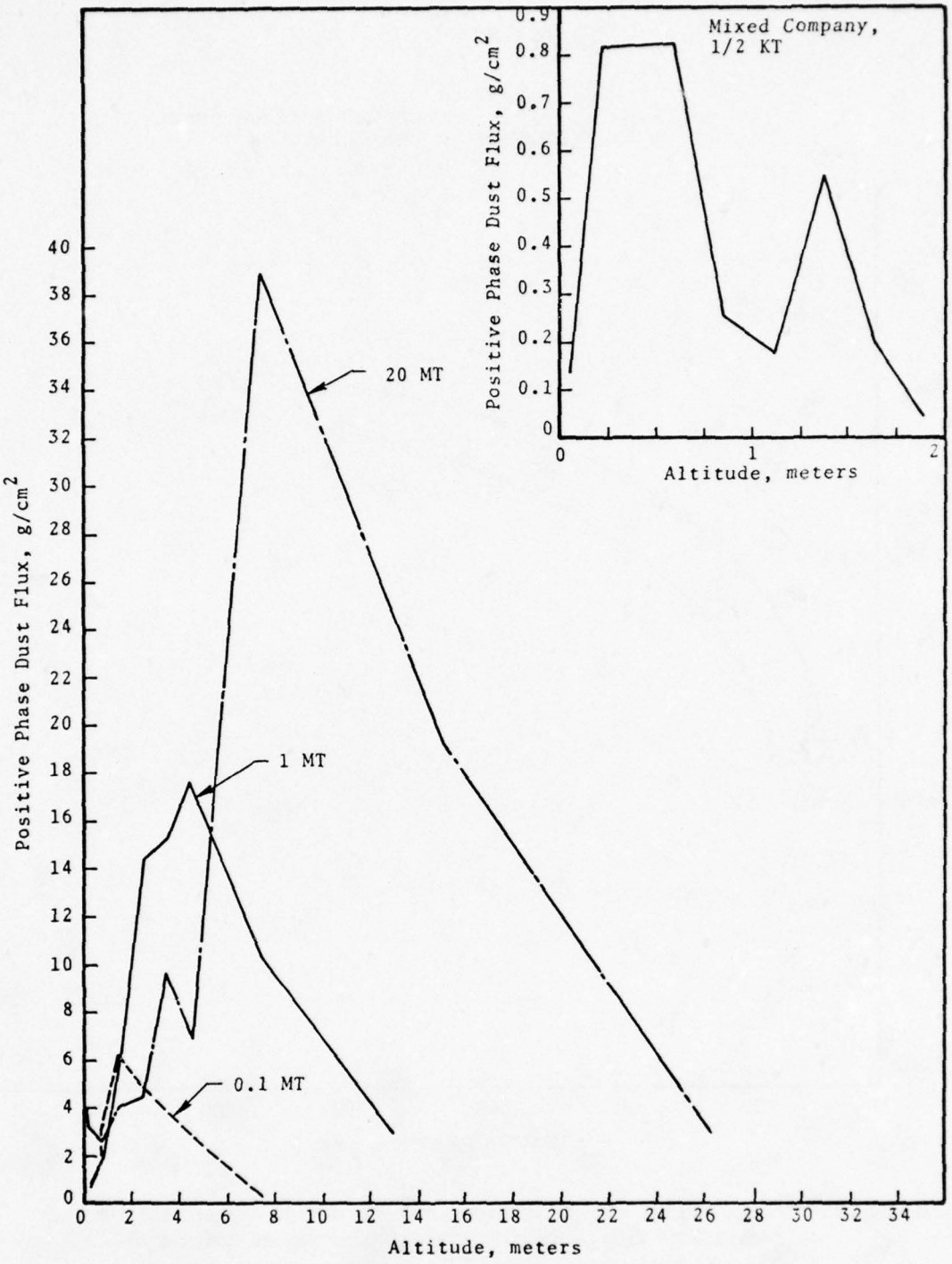

Figure 3.15. Positive phase dust mass flux profiles for three nuclear surface burst SCOUR calculations at 50 psi peak overpressure location. Inset gives profile from 500 ton HE SCOUR calculations discussed in Chapter IV. Note that these results, while qualitatively consistent with subsequent SCOUR2 calculations, are superseded by results published in References 3 and 4.

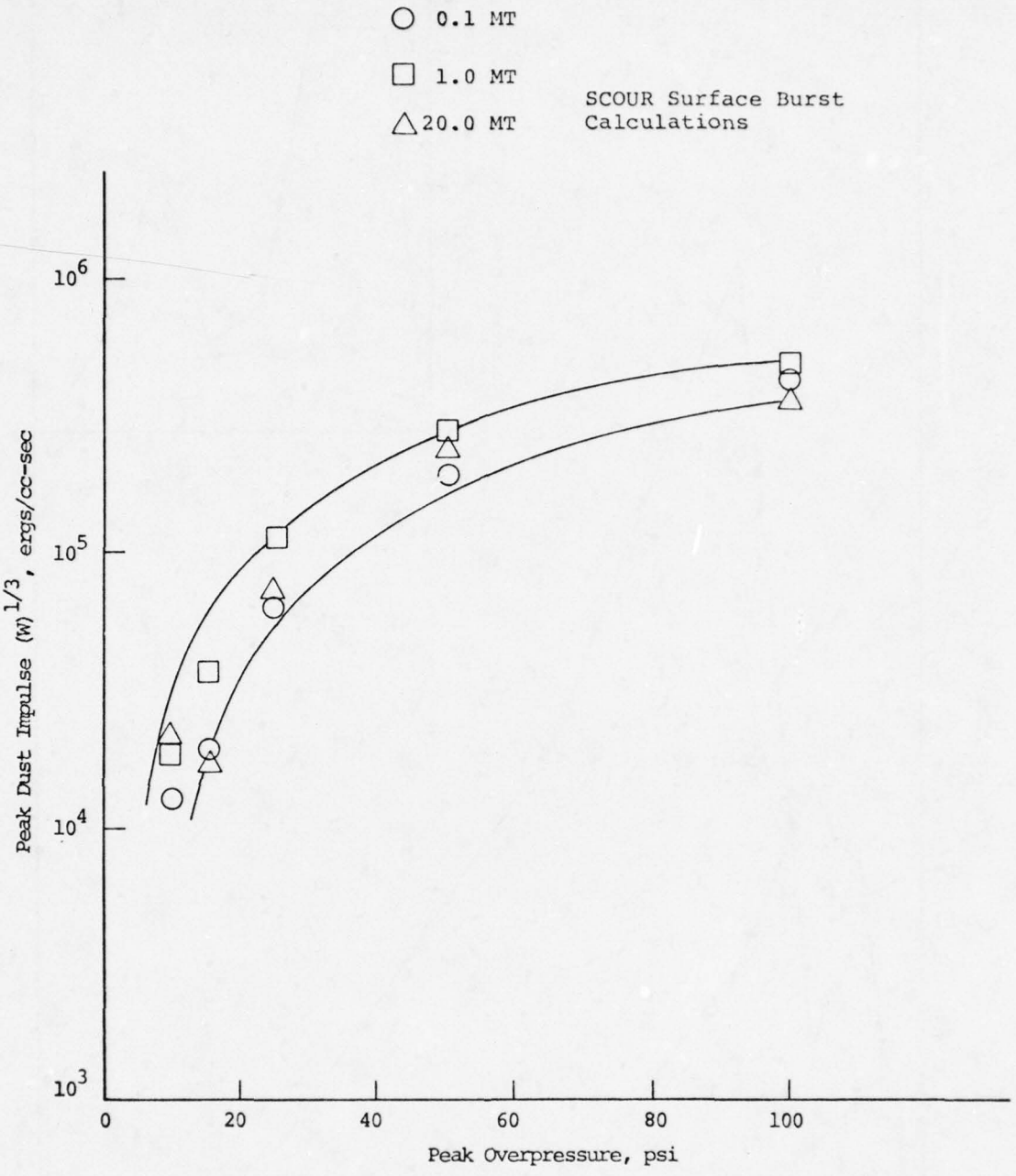

Figure 3.16. Peak dust impulse scaled by $W^{1/3}$ (W in MT) as a function of peak overpressure from three SCOUR calculations. Note that these results, while qualitatively consistent with subsequent SCOUR2 calculations, are superseded by results published in References 3 and 4.

IV. SCOUR CALCULATIONS OF BLAST WAVE DUST LOFTING EXPERIMENTS

4.1 INTRODUCTION

During the course of the S^3 effort to develop the SCOUR code, two major attempts were made to obtain blast wave dust storm data from large scale high explosive (HE) experimental detonations. Dust cloud measurements of cloud height and particulate concentration as a function of time were made at MIDDLE GUST, EVENT II[31] (100 tons of TNT) and MIXED COMPANY[32] (500 tons of TNT). Although the data recovered were incomplete and far from comprehensive, they do provide an experimental basis for comparison to SCOUR calculations.

In Reference 2, the previous and present diffusion models had been evaluated by comparing the results of calculations achieved with a special version of the SCOUR code designed for use with an idealized blast wave flow field. The focus was on the MIDDLE GUST results, and it was determined that the present diffusion model was adequate for the computation of the in situ dust cloud altitude versus time as well as the concentration of lofted particulates. (A "soil" of 5 mm diameter glass beads was used in the MIDDLE GUST experiments to determine particulate concentrations.) A set of calculations for MIXED COMPANY, using the newer diffusion model (discussed in Reference 28) were made shortly thereafter, and corroborated some preliminary (unpublished) results; i.e., without changing the SCOUR parameters from those used in the MIDDLE GUST calculations, the SCOUR model yielded a high degree of correlation to the experimental measurements of the in situ dust cloud.

These early SCOUR results were extremely encouraging, but due to the incomplete nature of the experimental results, it was only possible to conclude that SCOUR was "in the right ballpark". Moreover, it was realized at the end of the present

report period that a number of coding errors were present in the special version of the SCOUR code used in these calculations. While the errors were expected to have a minor effect on overall cloud characteristics, it was felt that they might exert a major influence on the SCOUR predictions for near-surface particulate concentrations, particularly in the negative phase. The corrections to the SCOUR code were as follows:

- Boundary layer transition – in the earlier versions of SCOUR, transition from the positive phase boundary layer to negative phase model was delayed by two time cycles. This was modified so that the negative phase boundary layer calculation is initiated immediately after a negative radial (inward) velocity is indicated for a given surface zone.
- Negative phase particle lofting – in the earliest version of SCOUR,[1] particles were ejected into the flow field at 90° to the horizontal. A later version[2] included a lofting model that ejected particles, randomly, between 10° and 90° to the horizontal. Due to a coding error (that has been corrected), the negative phase particles were ejected in opposition to the wind.
- Random number sequence – a coding error was inadvertently introduced to the SCOUR code (1974 version) whereby the random number sequence was automatically restarted whenever certain computer operations occurred during a calculation. This results in a bias in the random numbers, and was subsequently corrected for the SCOUR2 calculations.[3,4]

Our main concern, of course, was to determine if the tentative conclusions in References 2 and 28 were still justified; i.e., that the nominal SCOUR prescriptions for the mass

lofting coefficient, b_{ND} = 0.1, and the diffusion parameter, k' = 0.08, were adequate for the calculation of near-surface particulate concentrations as observed in the MIDDLE GUST II (5 mm glass beads) and MIXED COMPANY (in situ dust) particulate lofting experiments.

The MIXED COMPANY event was recalculated with SCOUR2 three times to evaluate the effect of using different values for the negative phase diffusion parameter. The results were slightly different than the earlier values and indicated that the nominal prescription was superior in the positive and early negative phases of the flow field (on the basis of comparisons to experiment).

Based on these results and some unanswered questions about the earlier MIDDLE GUST SCOUR calculations, the corrected SCOUR2 model was then used to recalculate the 5 mm diameter glass beads lofting experiment. These new results indicated that the nominal SCOUR mass lofting coefficient (b_{ND} = 0.1) was approximately half that required to match the experimental results. In addition, it was determined that the SCOUR deposition model may be primarily responsible for the overestimation of near-surface particulate concentrations at late times.

In this chapter, the results of these four sets of SCOUR calculations are presented in the following sequence: MIDDLE GUST II (1974), MIXED COMPANY (1974), MIXED COMPANY (1975), MIDDLE GUST II (1975). The MIDDLE GUST II (1974) results have been published in Reference 2, but are included in this chapter for ease of reference.

4.2 MIDDLE GUST (1974 CALCULATIONS)

The MIDDLE GUST event was a detonation of a 100 ton sphere of TNT located two sphere radii above the surface. An assortment of particulate lofting experiments were

conducted by a TRW research team.[31] These consisted of motion picture coverage of the early time rate of rise of the in situ dust cloud kicked up by the air shock at the 50 psi and 25 psi overpressure locations. In addition, 5 mm diameter beads were placed in prepared beds, 7 ft by 70 ft, that preceded the nominal 50 psi and 25 psi overpressure stations. Concentration histories of 5 mm glass beads at the 25 psi overpressure location were measured with a microwave attenuation system. Concentration data were not obtained at the 50 psi location.

The SCOUR dust cloud predictions require a hydro flow field input. An idealized prescription of the blast wave flow field was utilized, to avoid complications in the output of hydro calculations of HE detonations associated with the presence of reaction products. (Moreover, AFWL tapes of the HE calculations made available to S^3 do not cover the negative phase of the event.)

The input flow field, fully described in Appendix B, is similar to that used by Bannister.[33] Essentially, the predicted shock location, X_s, as a function of time t, has been fit by the following expression:

$$X_s \propto (t)^{0.525} \tag{4.1}$$

This gives the shock arrival time and peak (shock) flow conditions at a given radial location, X. This is combined with an idealized prescription of the positive phase and negative phase flow histories at X that require only the predicted positive phase duration as input. The air is assumed to be an ideal gas ($\gamma = 1.4$) and detonation products are not included in the flow field.

Prior to the detonation, the in situ soil was characterized as a sandy clay. It consisted primarily of fine grain

material. The measured particle size distribution is given in Figure 4.1. For SCOUR calculations, the following distribution was used:

Particle Size Range, mm	SCOUR Characteristic Particle Diameter, mm	Mass Fraction of Particle Size Class
$d \leq 0.030$	0.005	40%
$0.030 < d \leq 0.150$	0.005	20%
$0.150 < d \leq 0.400$	0.300	20%
$0.400 < d$	0.800	20%

4.2.1 In Situ Dust Cloud

The peak altitudes of particles in zones above the 50 psi and 25 psi overpressure locations are plotted in Figures 4.2 and 4.3. It is immediately apparent from these results that there is a consistent correlation at both locations between the observed cloud traces from the two cameras and the SCOUR cloud predictions. The smaller diameter particles (5 μ, 70 μ) rise at a rate intermediate between the two cloud rise curves taken from the two photographic records. At both locations, the 300 μ particles initially rise to heights greater than the observed cloud. Their rate of rise lessens, and by 40-80 milliseconds are at altitudes comparable to the smaller particles. The 0.8 mm particles, delayed by the time it takes to achieve lofting velocities, eventually outclimb all other particle sizes.

The concentration profiles at specific times in the calculation are plotted (as bar graphs) in Figures 4.4a-c. These are compared to cloud height indications from the photographic records. It is seen that if the SCOUR model is accurate, the HYCAM camera was blacked out by concentrations between 1×10^{-4} g/cc and 3×10^{-4} g/cc of the larger grain

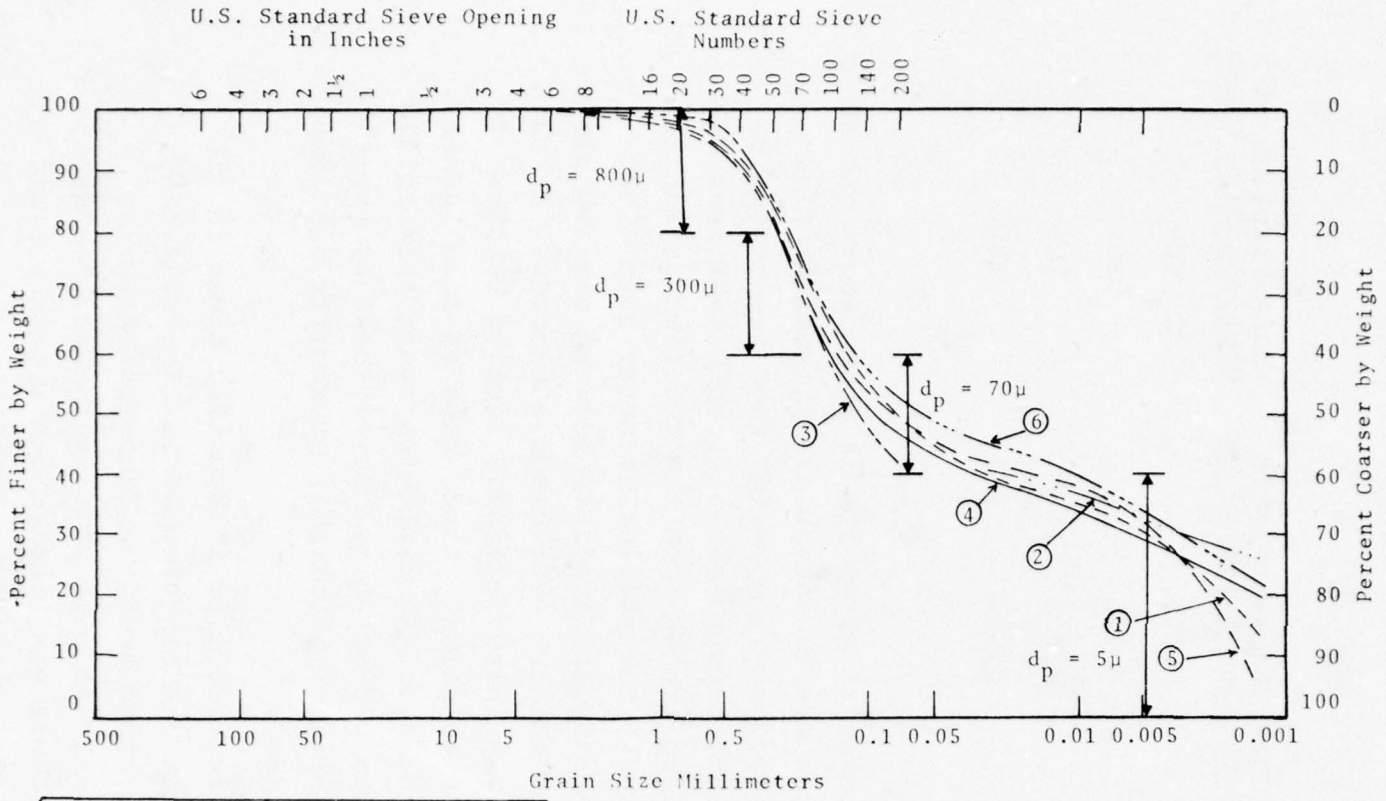

	Depth (ft)	Classification
①	0.0-2.0	Sandy Clay - - - - - -
②	0.5	Sandy Clay —·—
③	1.0	Sandy Clay — - - —
④	1.7	Clayey Sand ———
⑤	1.7	Sandy Clay —— ——
⑥	2.0	Sandy Clay — · - - · —

Figure 4.1. Particle distribution measured at MIDDLE GUST site.[31] Four particle sizes utilized in SCOUR calculation are shown.

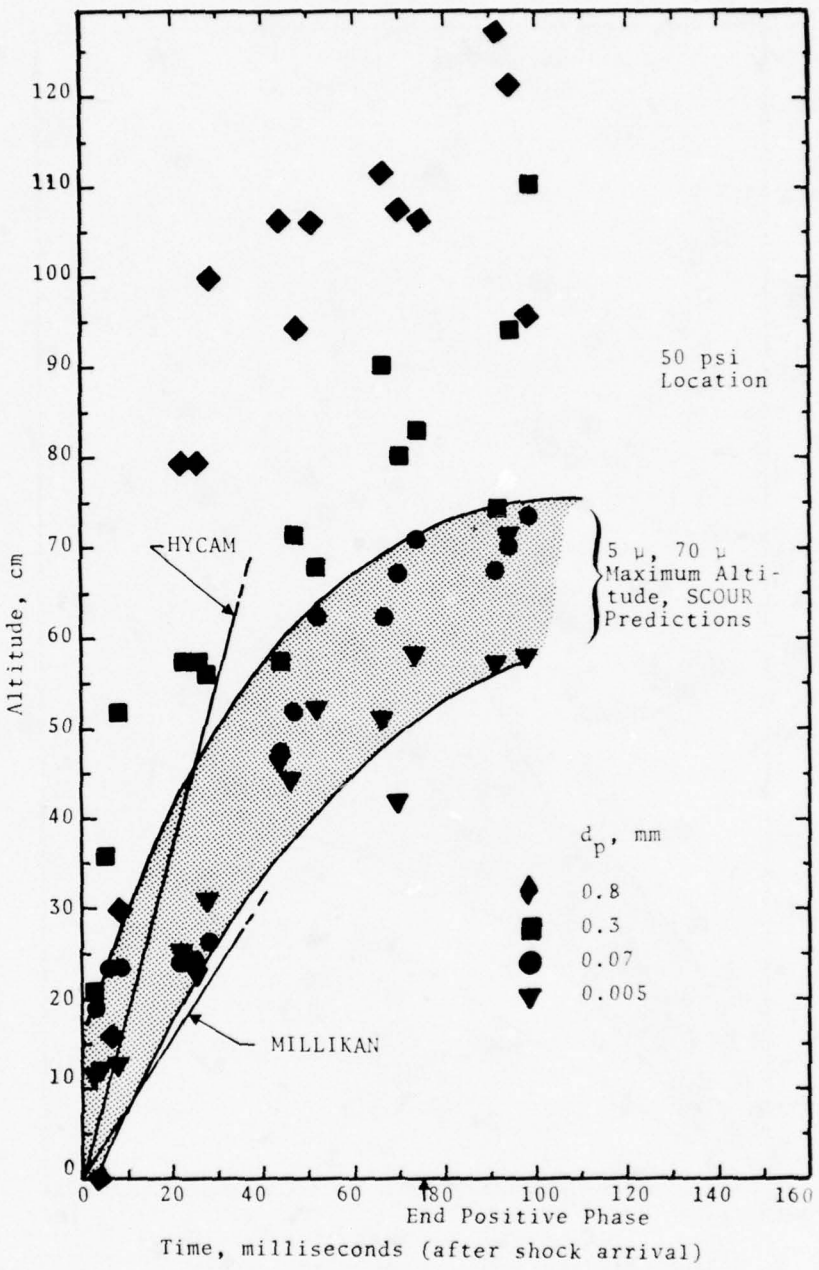

Figure 4.2. Peak altitudes of SCOUR (1974) particles above the 50 psi overpressure location (MIDDLE GUST).

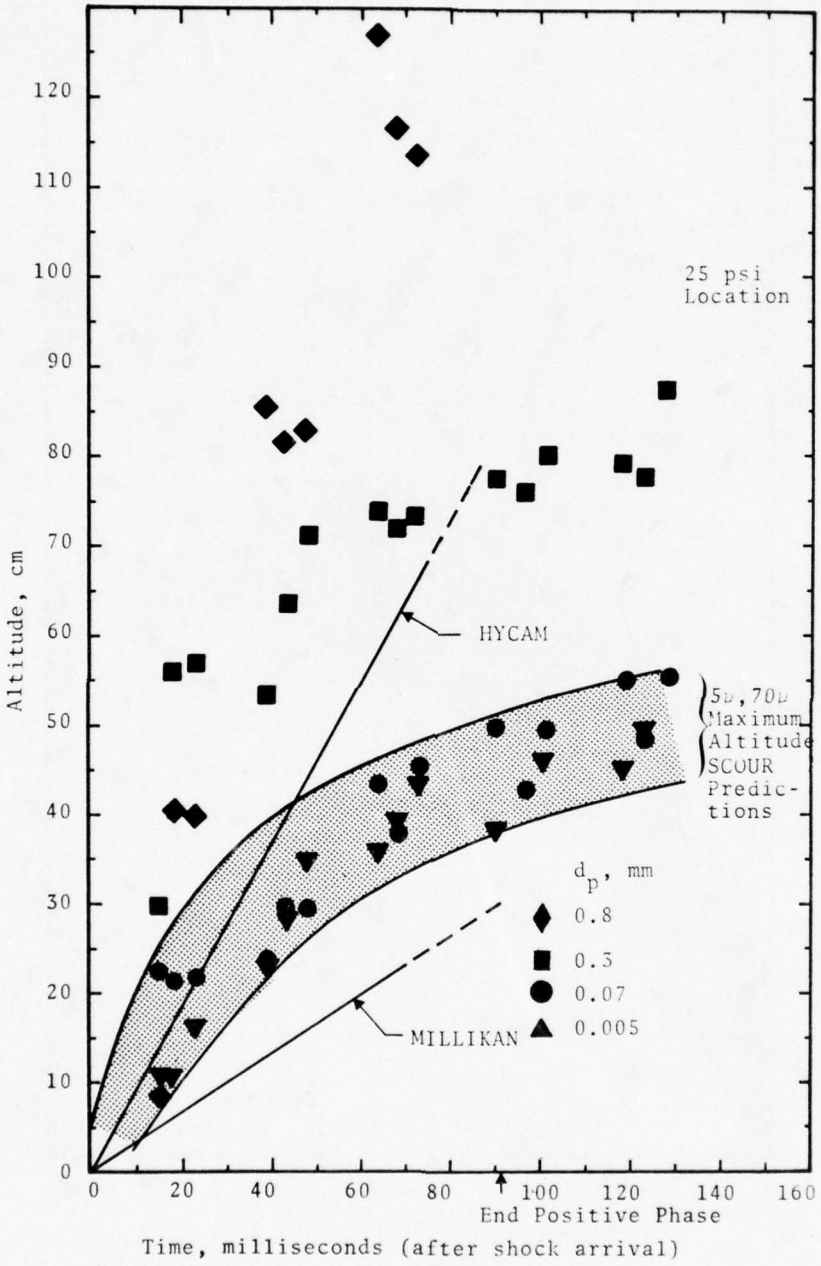

Figure 4.3. Peak altitudes of SCOUR (1974) particles above the 25 psi overpressure location (MIDDLE GUST).

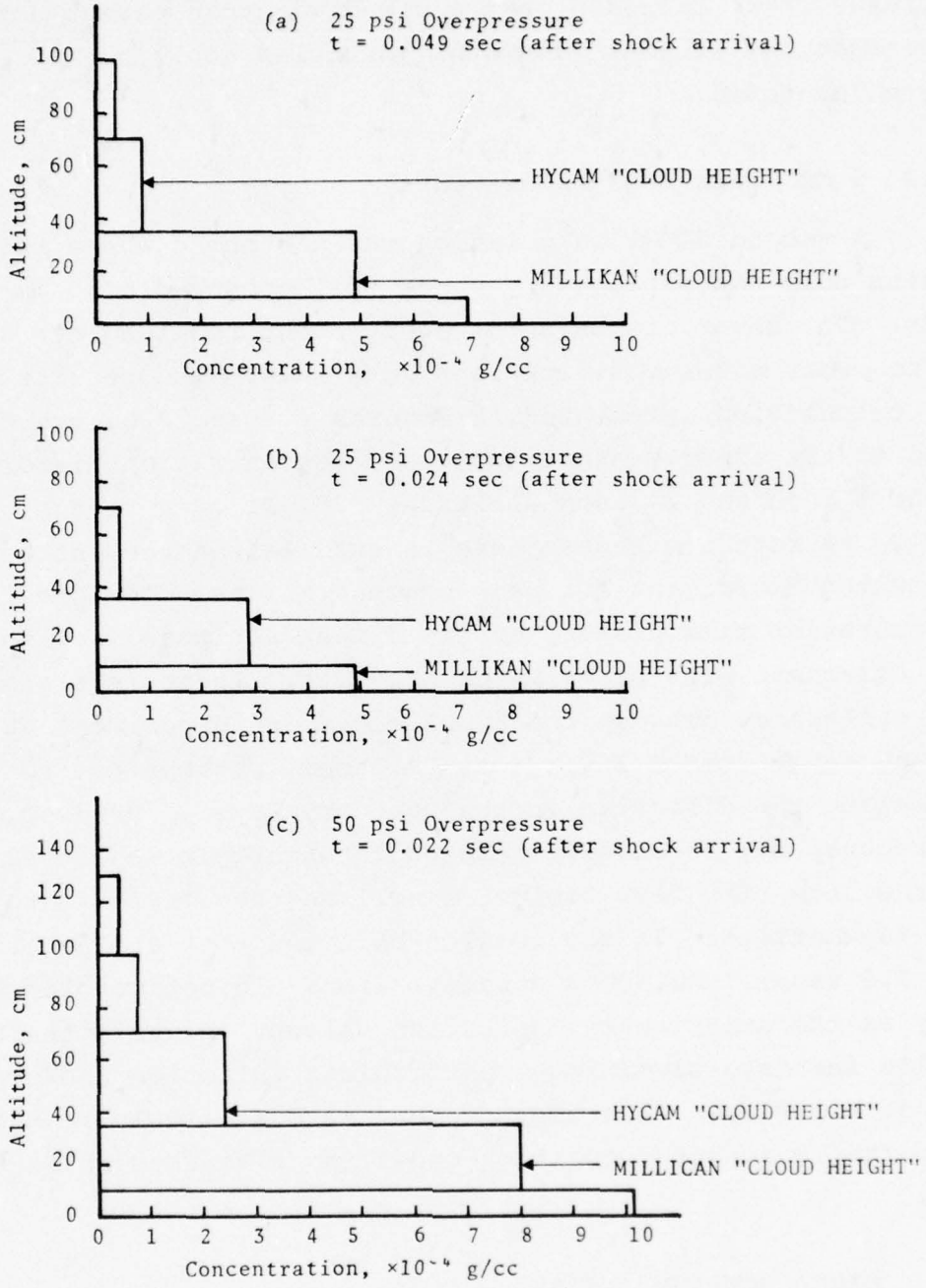

Figure 4.4. Dust concentration levels predicted by SCOUR (1974) for in situ MIDDLE GUST dust cloud.

particles. The Millikan camera cloud was transparent until concentrations of small diameter particles above 5×10^{-4} g/cc were encountered.

4.2.2 5 mm Glass Bead Experiments

A second SCOUR calculation was performed where the in situ soil was replaced by a new soil composed of 5 mm glass beads. The shear transmission coefficient remained set at 0.1, and no other model modifications were made. The results of this calculation, presented in Figures 4.5 and 4.6, are compared to the experimentally obtained concentration histories at the 6 inch and 24 inch altitudes (25 psi overpressure location). At both altitudes there is excellent agreement between theory and experiment for peak concentrations. The predicted concentration time history at the 6 inch altitude is also in good agreement with experimental results. There is a significant difference between the SCOUR cloud and experiment at the 24 inch height for 0.2 sec < t < 1.0 sec, perhaps due to underestimating the diffusion in the boundary layer. However, the discrepancy may be closely related to uncertainties in simulating the late time flow fields as well as the aftereffects of flow asymmetries. It should also be noted that at late times (t > 1.0 secs), the SCOUR concentrations did not monotonically decay as the experimental saltation values. Rather, the SCOUR results indicate significant particulate saltation and/or fallout activity. This disagreement is most likely related to the particle impact deposition model (as discussed in Section 4.5).

4.3 MIXED COMPANY (1974)

The MIXED COMPANY HE event had a spherical charge configuration of 500 tons of TNT, centered one radius above ground zero. Two primary measurements were made to study the dust

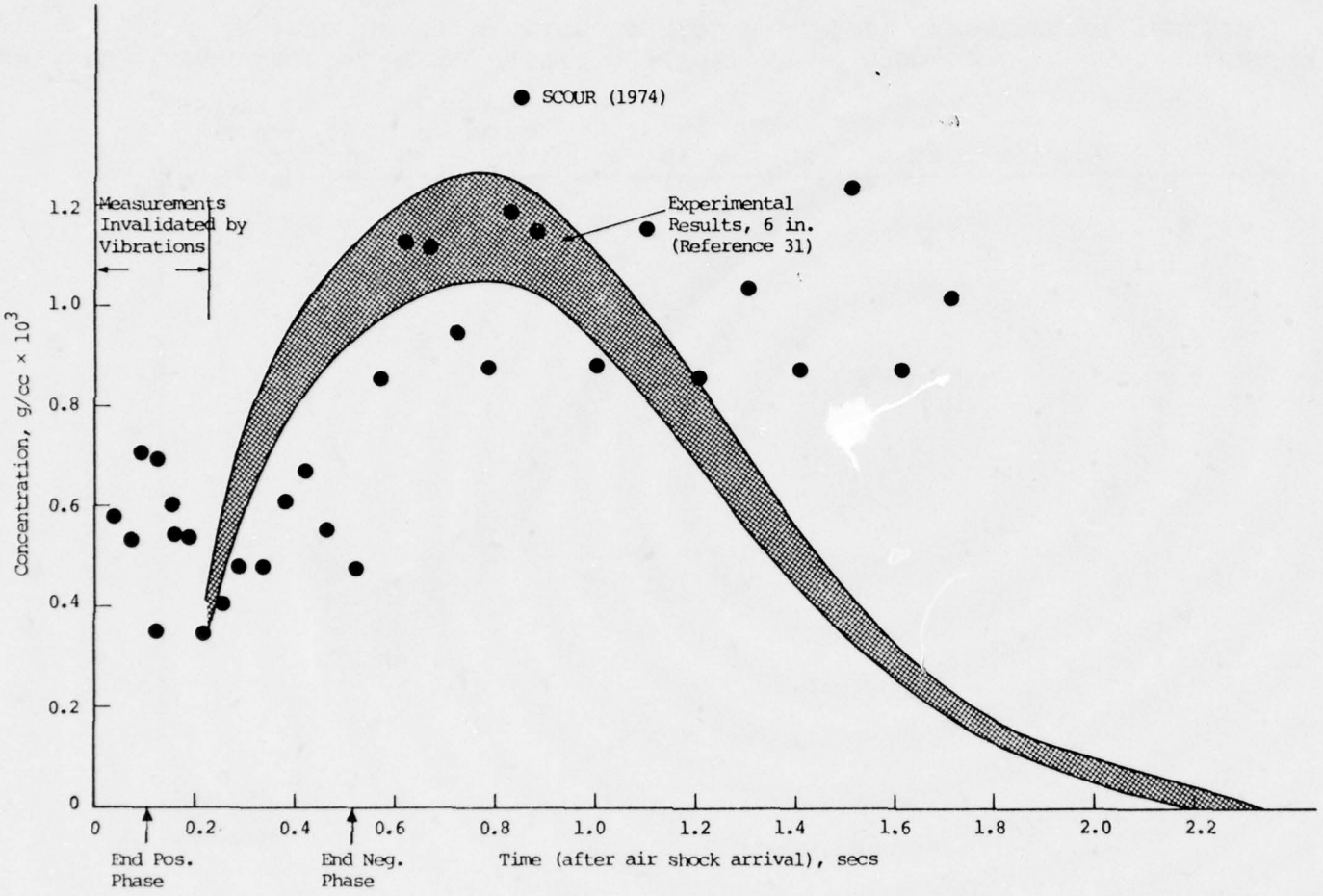

Figure 4.5. Comparison of SCOUR (1974) predictions of 5 mm bead concentrations at the 6 inch height station to MIDDLE GUST II experimental results.

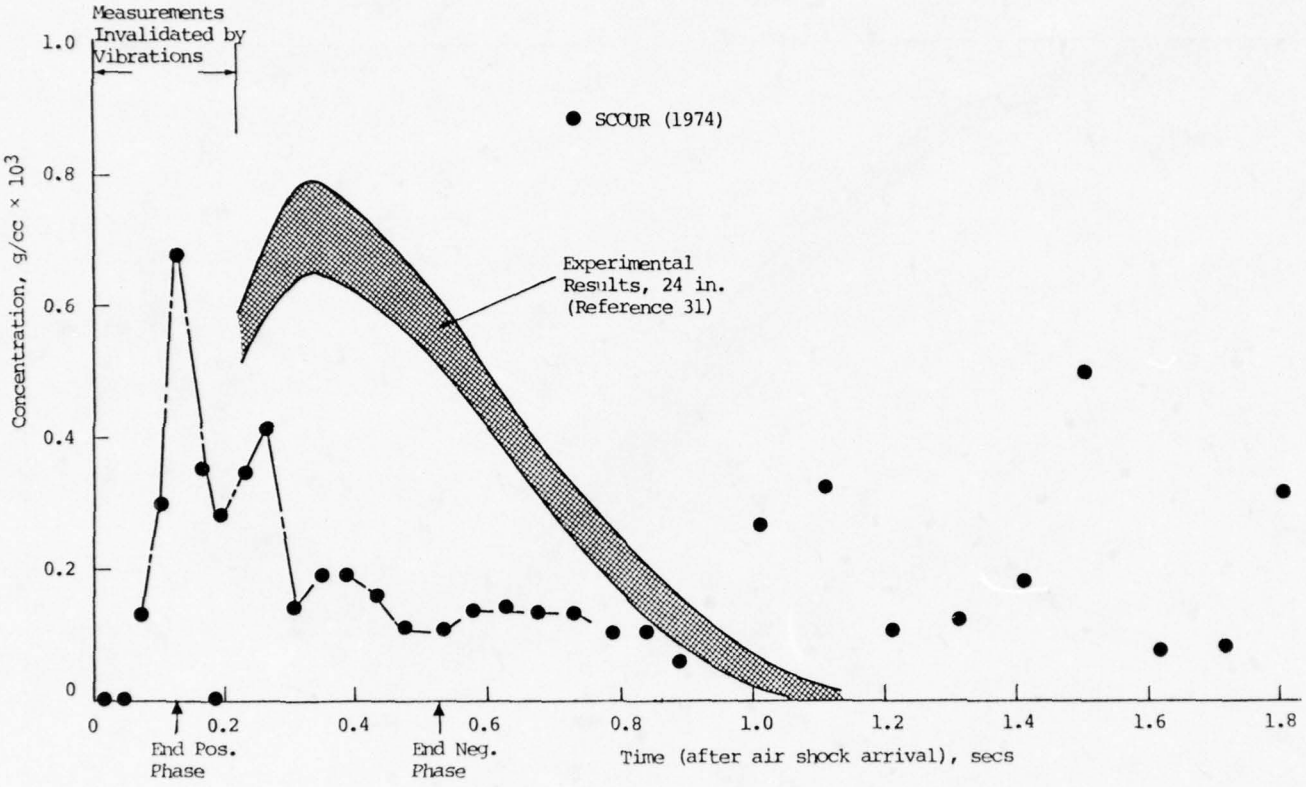

Figure 4.6. Comparison of SCOUR (1974) predictions of 5 mm bead concentrations at the 24 inch height station to MIDDLE GUST II experimental results.

lofting characteristics of the air blast wave. A concentration time history of the in situ dust cloud was measured with laser light extinction instrumentation at the 6 inch height of the 25 psi overpressure location. Motion picture coverage of the early time dust cloud was obtained at the 50 psi overpressure location. In addition, supplemental information was acquired at the 25 psi overpressure position from post-test examination of 7 foot high "greasy stakes" which collected dust impacting on the four flat faces of the stake. These experiments, performed by a TRW research team, are reported in Reference 32.

The "dust" at the MIXED COMPANY site was considerably modified from the original expectation of a silty soil similar to the MIDDLE GUST in situ dust. Due to previous snows, the soil was quite wet and cloddy at the time of the test. Interpretation of the laser light extinction data required that the in situ particle size distribution be deduced from the dust captured by the greasy stake. This distribution, indicated by the x's in Figure 4.7, was simplified into a four particle size in situ soil for the SCOUR calculation of the MIXED COMPANY dust cloud.

Particle Diameter	Mass Fraction
0.03 mm	30%
0.20 mm	30%
1.0 mm	20%
3.0 mm	20%

An idealized flow field was used to simulate the air blast wave passage and subsequent flow. It is a scaled version of the MIDDLE GUST flow field. Surface zones were 4.275 meters wide for this calculation (scaled from MIDDLE GUST by the cube root of the yield ratio, see Appendix B).

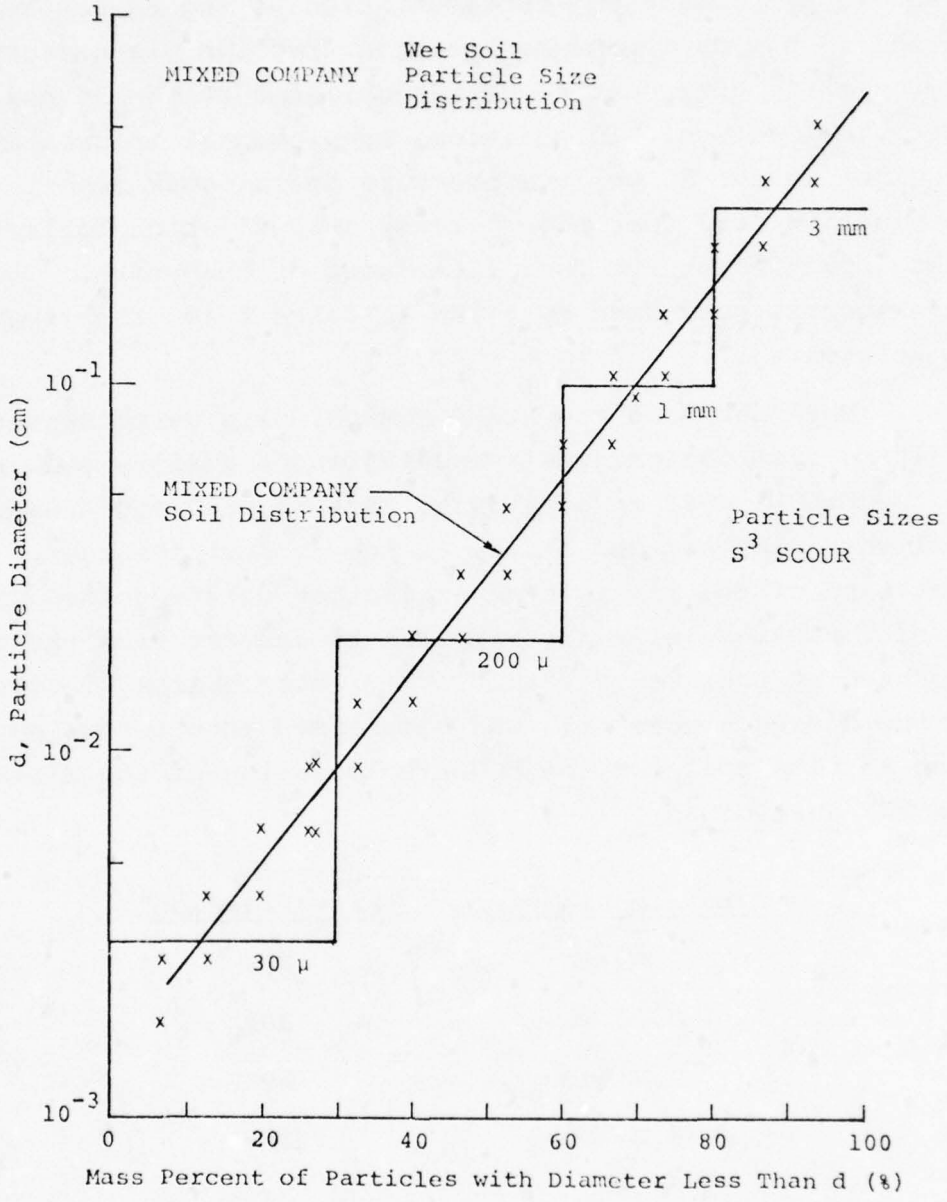

Figure 4.7. Particle sizes used in SCOUR simulation of MIXED COMPANY event compared to distribution used to reduce laser light extinction data[32].

4.3.1 In Situ Dust Concentration

SCOUR predictions of the dust concentration at the 6 inch height are compared with experimental results in Figure 4.8. Values at the 35 psi and 25 psi overpressure location are given to provide an indication of the spread in concentration data predicted by the SCOUR code for this HE event.

In general, the predictions with the standard SCOUR parameters are in good agreement with the experimental results ($\pm$ 1 $\times$ 10^4 g/cc). However, having data at only <u>one</u> altitude and at <u>one</u> overpressure location, does not provide adequate validation of the SCOUR model. The next figure (4.9) shows the SCOUR predictions for different values of the diffusion velocity parameter ($k' = 0.02$, 0.08, and 0.16). It is evident that the nominal prescription ($k' = 0.08$) matches the data best in the late time regime ($t > 0.5$ sec) but may be over-diffusing dust at early times.

To more appropriately validate the SCOUR model, dust <u>profile</u> information is required. Figure 4.10 compares the predicted dust concentrations between 35 cm and 70 cm above the original surface as a function of time for cases computed with different values of k'. Agreement with experiment in this altitudinal range (if data were available) would greatly strengthen the argument for a particular set of k' values. It would also provide greater insight into the applicability of the aerodynamic mass lofting prescription.

4.3.2 Dust Cloud Height

The dust cloud height versus time, measured with photographic techniques at the 50 psi overpressure location, is compared to the maximum particle altitudes predicted by SCOUR in Figure 4.11. The various symbols represent the different particle sizes used in the SCOUR calculation.

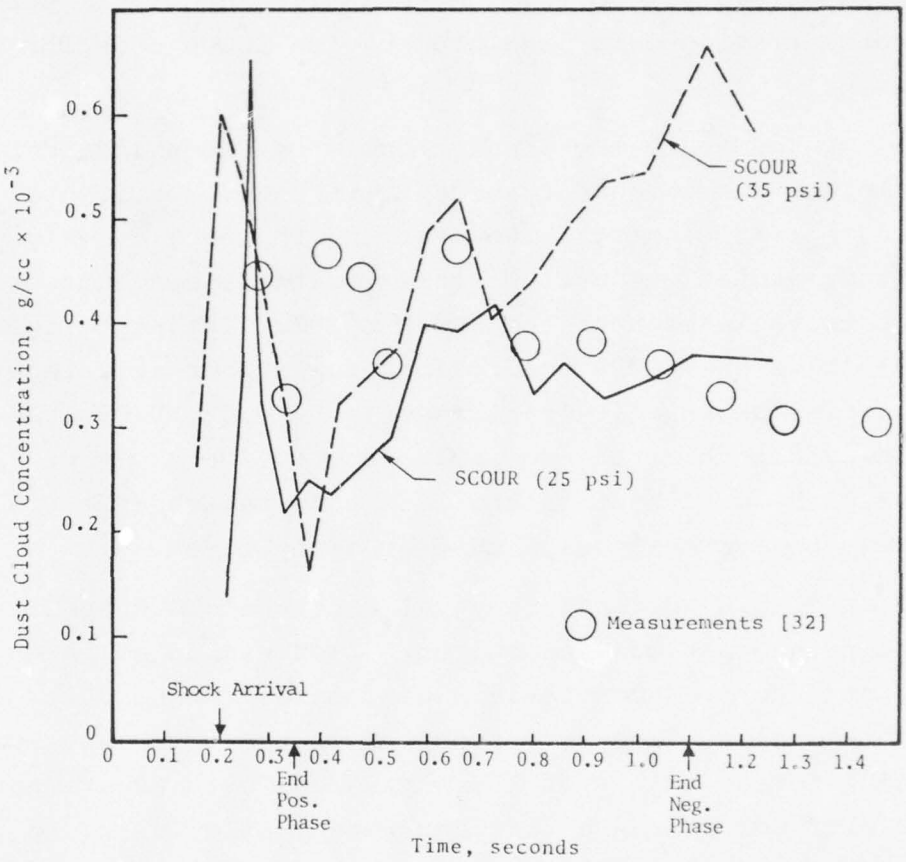

Figure 4.8. Comparison of calculated SCOUR (1974) dust concentrations at the 35 psi and 25 psi peak overpressure locations to MIXED COMPANY measurements[32] (at nominal 25 psi position).

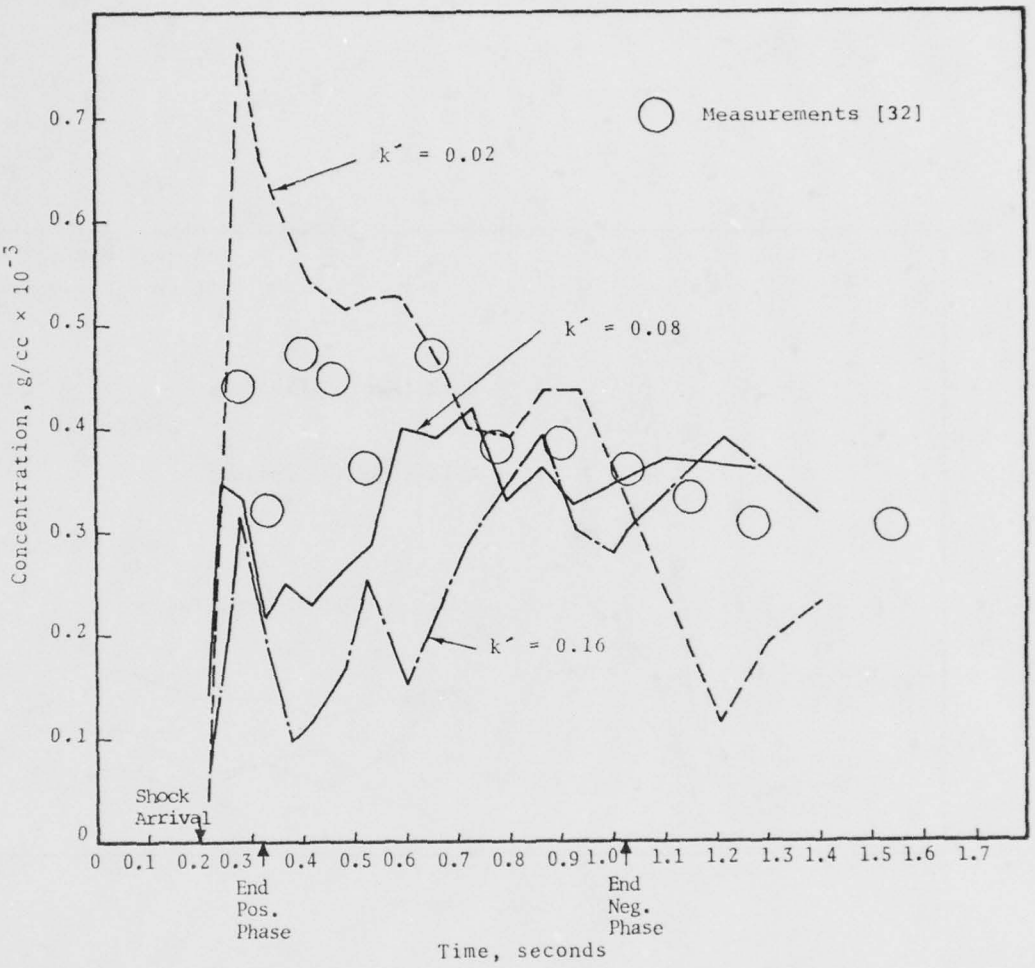

Figure 4.9. Comparison of SCOUR (1974) dust concentrations at the 25 psi overpressure location for three values of diffusion coefficient, k′, and the experimental observations made during MIXED COMPANY event.[32]

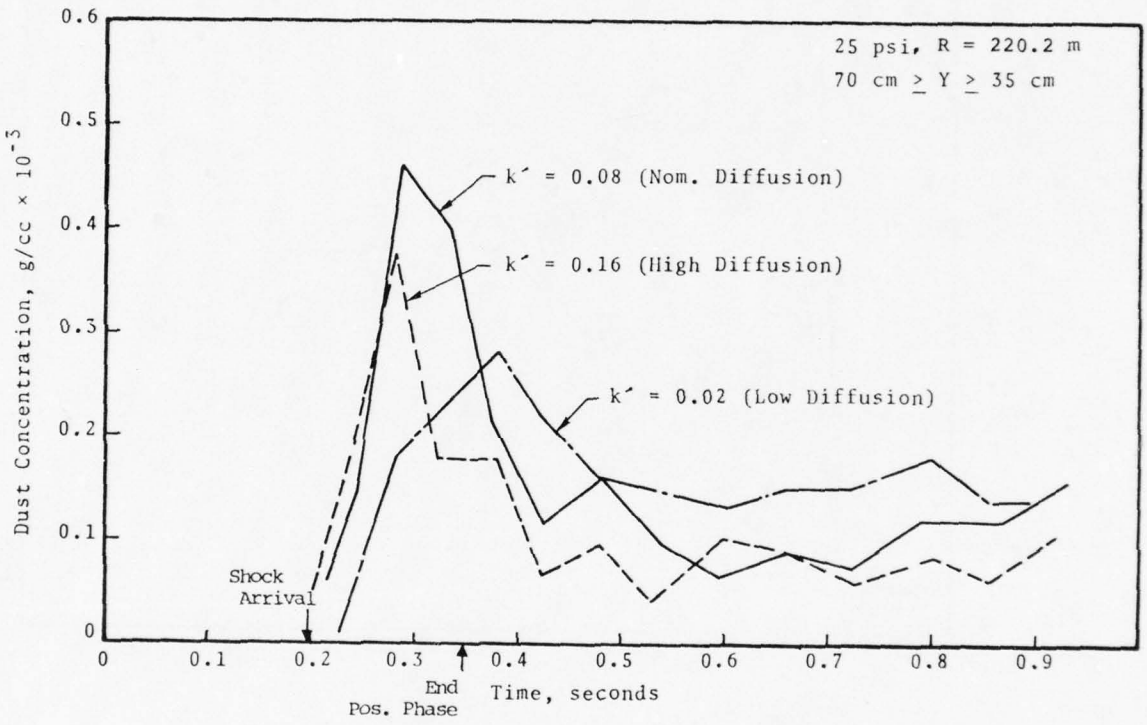

Figure 4.10. SCOUR (1974) predictions of dust concentration time histories between 35 cm and 70 cm above the ground surface at the 25 psi overpressure location for a 500 ton HE explosion, using three different diffusion coefficients.

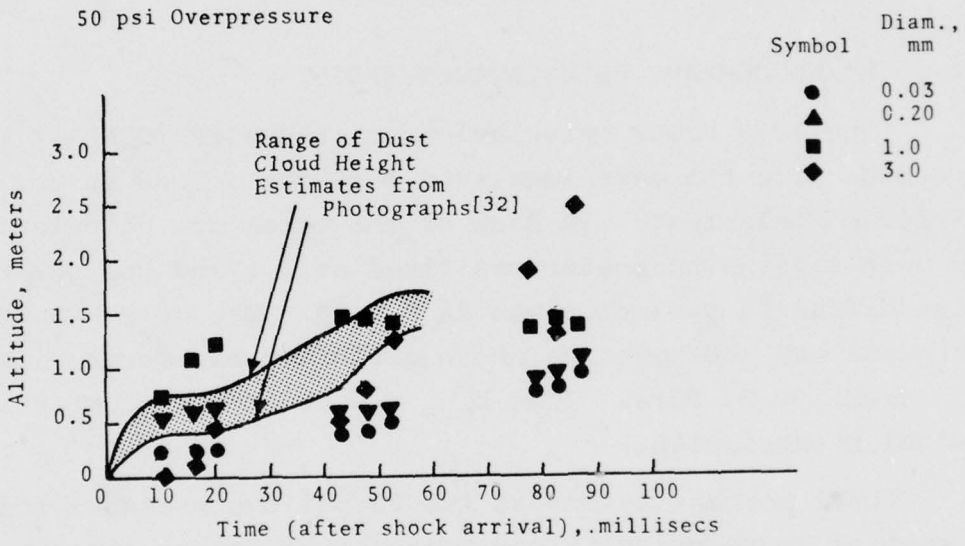

Figure 4.11. Maximum height of various size particles in SCOUR (1974) calculated dust cloud compared to photographic observations, MIXED COMPANY.[32]

From this comparison it is evident that the smaller particles (d_p = 0.03 mm, 0.20 mm) are embedded in the early time dust cloud while the larger particles (1 mm, 3 mm) indicate the outer periphery of the dust. Significantly, the standard k' prescription diffuses particles out to altitudes of one meter by the end of the positive phase, while reduced positive phase diffusion (k' = 0.02) limits the small particle altitudes to about 0.5 meter (plus a slower initial cloud rise). The greasy stakes experiment[32] indicated that the small diameter particles were concentrated throughout the bottom meter, giving supportive evidence for the higher diffusional rates behind the blast wave.

4.4 MIXED COMPANY CALCULATIONS (1975)

The 1975 SCOUR calculations of the MIXED COMPANY event were made with the same idealized flow field used in the earlier calculations. In each of the three new calculations, the mass lofting parameter was fixed at 0.1 and the positive phase diffusion parameter was k'_P = 0.08. The only change in each case was the negative phase diffusion parameter; i.e., k'_N = 0.02, 0.08, 0.16. (The $k'_{P,N}$ = 0.08 combination is the nominal prescription.)

Dust concentrations at the 25 psi overpressure location in each of these calculations are plotted versus time in Figure 4.12. They have been computed by averaging the dust concentration between 10 cm and 35 cm above the surface for three radial zones (213.7 m $\leq$ r $\leq$ 226.6 m). Also plotted in Figure 4.12 are the experimental measurements of dust concentration at a 6 inch altitude reported in Reference 32.

It is clear from the comparison of SCOUR predictions to the experimental results that SCOUR calculates dust concentrations that are in qualitative agreement with experiment for any value of k'_N. There are differences between the 1975

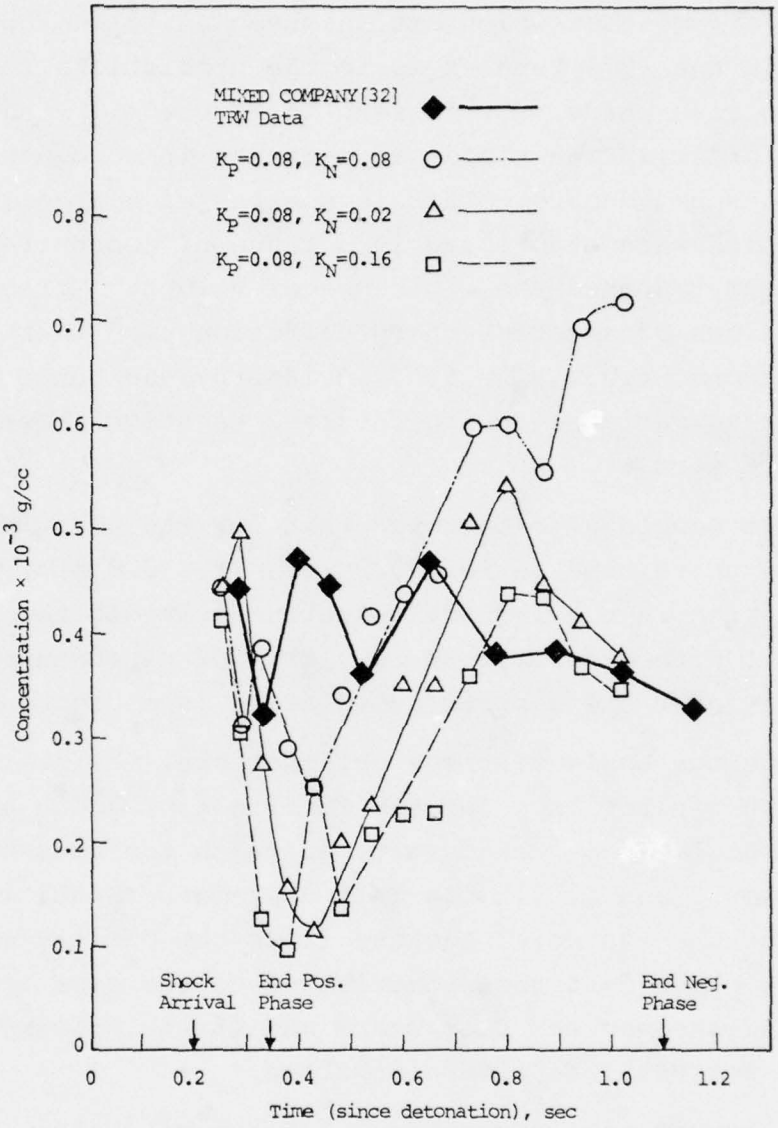

Figure 4.12. Dust concentrations between 10 cm and 35 cm above the original surface at the 25 psi overpressure location of the MIXED COMPANY event, computed with $k_P' = 0.08$ and three values of k_N' (SCOUR 1975). Results are compared to experimental observations made at 15.2 cm altitude.

nominal prescription results and those presented in Figure 4.9 (1974), most of which are inconsequential. The major change in the 1975 results is in the predictions for the late negative phase. It is seen in Figure 4.12 that the nominal prescription yields an increase in concentration as the wind speed decays. This is contrasted by the 1974 results which were stabilized in a range of concentrations that very nearly matched the experimental values. Moreover, the other values of negative phase diffusion used in the 1975 calculations, i.e., $k_N' = 0.02, 0.16$ provided better agreement with experiment during the late negative phase 0.6 sec $< t <$ 1.0 secs.

It should also be noted that for the positive-early negative phase time period, 0.2 sec $< t <$ 0.6 sec, the nominal prescription in the 1975 calculations provided the closest agreement with experimental results, and represented an improvement over the earlier calculation (see Figure 4.9).

On the basis of these calculations, the nominal prescription was retained for the final set of SCOUR surface burst calculations, the results of which are presented in References 3 and 4. It was felt that better positive phase agreement was essential because it is the positive-early negative phase dust that contributes to the most intense period of the nuclear dust storm and is the primary source of dust for the late time dust cloud.

However, the discrepancy between prediction and experiment at late times in the negative phase is a matter of concern because it indicates the possibility that the SCOUR model may be inadequate during this period. Here it should be stated that the ideal flow used in the SCOUR calculations does not include the effects of blast wave asymmetries, natural afterwinds, or excess turbulence in the decay process. All of these could play an important role in the suspension capacity of the late time dust flow field.

Another point that had not been previously considered was that the SCOUR model includes a dust deposition model that has not been validated. In SCOUR, particles that impact the surface are assumed to eject other particles of equal mass with roughly 10 percent of the impact momentum. If the ejected particle velocity would be less than that which is required for a particle to maintain saltation (as noted in Chapter II, see Figure 2.2), a new particle is not ejected and deposition occurs at the point of impact.

Examination of the impact data in the 1975 calculations reveals that deposition begins at about t = 0.75 secs after detonation. Thus, in the late negative phase we could anticipate that the SCOUR deposition model plays a major role in the near-surface dust concentration predictions. This is corroborated in the average concentration (at 17.5 cm) versus time plots for the three calculations in Figure 4.13. These differ from those presented in Figure 4.12 in that the concentrations from the bottom 10 cm have been averaged with those in the altitude range 10 cm to 35 m. The mean height (17.5 cm) is very close to the 15.2 cm altitude at which the experimental observations were made. After t = 0.55 second, the concentrations rise steadily, indicating the strong possibility that saltating particles in the near-surface region could be strongly influencing the near-surface dust concentrations. This may be an especially important effect in the MIXED COMPANY dust lofting results because the in situ soil was damp and cloddy. Thus, it is possible that late negative phase saltation was impeded by these surface conditions.

4.5 MIDDLE GUST II (1975)

The 1974 MIDDLE GUST SCOUR calculations, presented in Figures 4.2, 4.3, 4.4, and 4.5, indicated that the revised

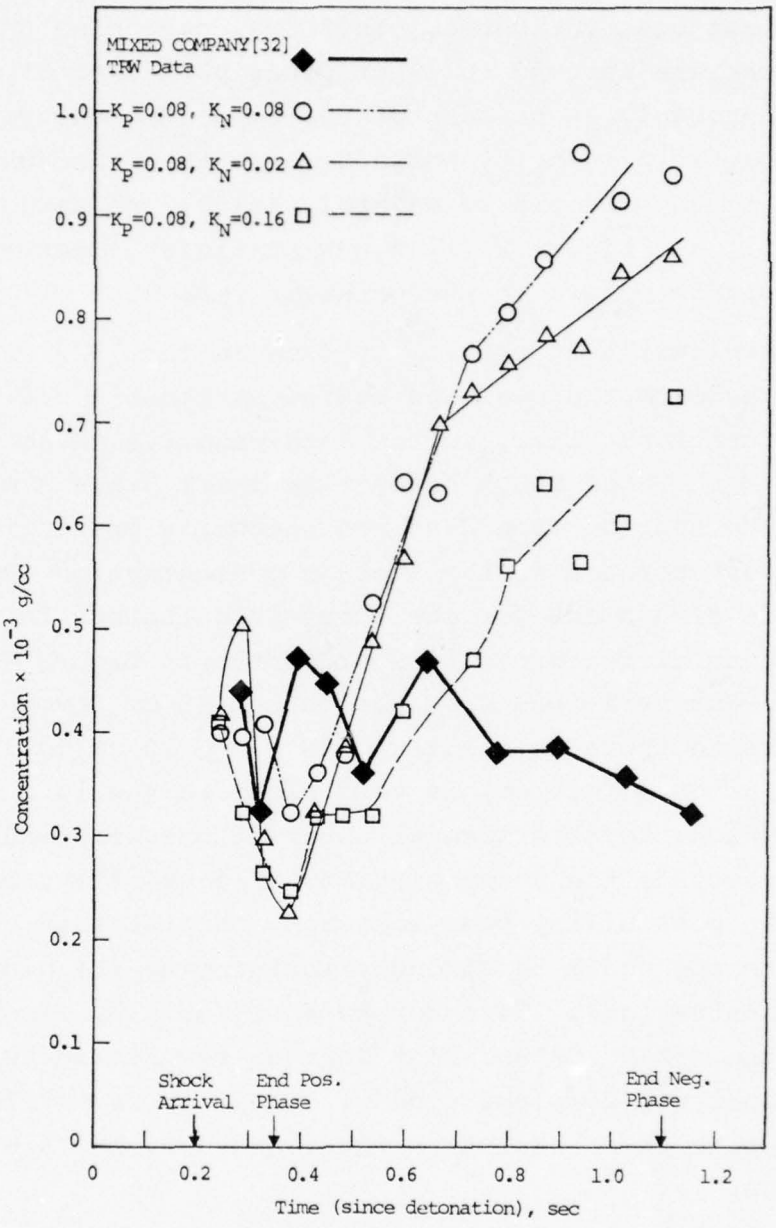

Figure 4.13. Dust concentrations between 0 and 35 cm above the original surface at the 25 psi overpressure location of the MIXED COMPANY event, computed with $k_P' = 0.08$ and three different values of k_N' (SCOUR 1975). Results are compared to experimental observations at 15.2 cm altitude.

SCOUR models for particulate lofting and diffusion (incorporated in SCOUR in 1973) provided an adequate correlation with the near-surface observations of the blast wave dust cloud rate of rise and the concentrations of 5 mm diameter glass beads that were lofted by the windstorm at the 25 psi overpressure location. However, the code deficiencies cited in Section 4.1 necessitated a recalculation of the event. In addition, the discrepancy between the late time SCOUR predictions of high bead concentrations (for t > 2 secs) and the near zero concentration readings of the experimental apparatus remained to be better understood. A second area of concern was that the problem setup for the 1974 calculations assumed a continuous bead surface that extended beyond the actual observation point used for comparison to experiment. This was in slight contrast to the experimental setup where bead concentrations were actually observed slightly downstream of the end of the bed.

Four SCOUR2 calculations were made to determine if the above-mentioned problem areas were important to the quantitative and qualitative nature of the SCOUR2 bead concentration predictions for the MIDDLE GUST II event. The particle ejection routine for the negative phase was corrected and particle ejection was limited to the radial extent of the two glass bead beds used in the experiment. Bead concentration was monitored at the surface zones near the end of the bed in three vertical bins.

Vertical Bin	Altitude Range	Mean Altitude
1	0 – 10 cm	5.0 cm
2	10 – 35 cm	22.5 cm
3	35 – 70 cm	52.5 cm

Each surface zone covered 2.5 meters in the radial direction. As observed in previous SCOUR calculations, it is necessary

to average over three radial zones to obtain relatively smooth curves for concentration. For the present calculations, SCOUR predictions were made by averaging over the last two zones in the glass bead bed and the first downstream "inactive" zone (radial zones 44-46).

The results of the first 1975 calculation were not nearly as satisfactory as those indicated in Figures 4.5 and 4.6. Concentrations in the bottom three vertical bins are compared in Figure 4.14 to the experimental measurements made at heights of 15 cm and 60 cm. The concentrations are approximately one-third the observed values, and do not decay significantly at late times. A second set of concentrations from the same calculation are plotted in Figure 4.15. In this case, the concentrations were computed by averaging over the last three radial zones of the bed (all "active" bead lofting zones). The concentrations are significantly higher, but still below the experimental values.

To improve SCOUR2 predictions for the "beads" experiments, the angle for particle ejection in the SCOUR mass lofting routine was limited to angles between 10° and 40°. The results for this second calculation are shown in Figure 4.16. This had the beneficial effect of raising bead concentrations without qualitatively changing the temporal history. Note that at the lower altitudes, the apparent (first) peak in concentration is predicted to occur at about 0.9 sec (0.78 sec after shock arrival). For the third vertical zone, the first peak occurs at about 0.5 sec (0.38 sec after shock arrival). Both of these are in excellent agreement with peak concentration times observed during MIDDLE GUST. A discrepancy in concentration magnitude still remains, however, and the monotonic decay of the experimental data beyond these times is not simulated.

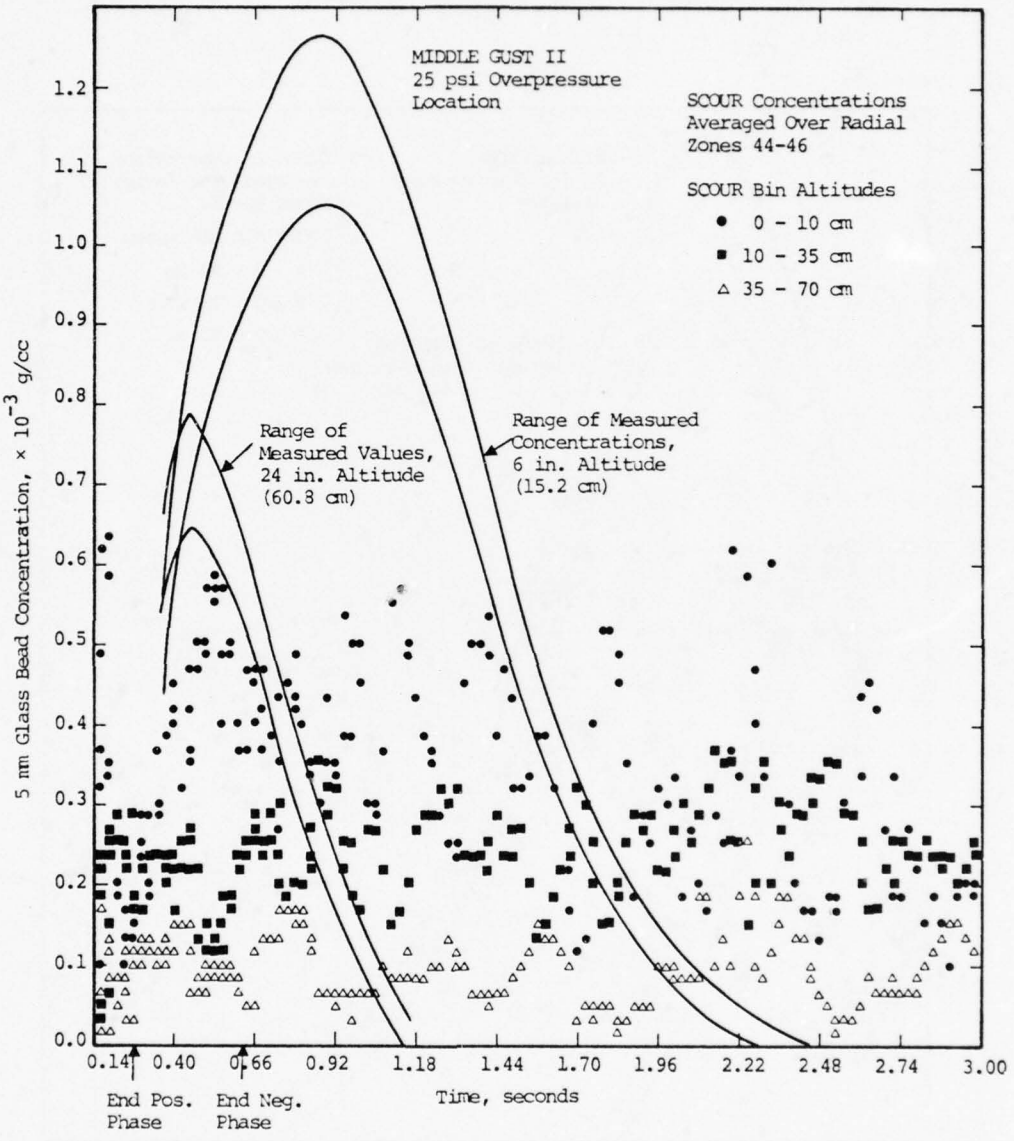

Figure 4.14. Results of first SCOUR2 (1975) calculation (using nominal prescription) compared to MIDDLE GUST II experimental results.[31]

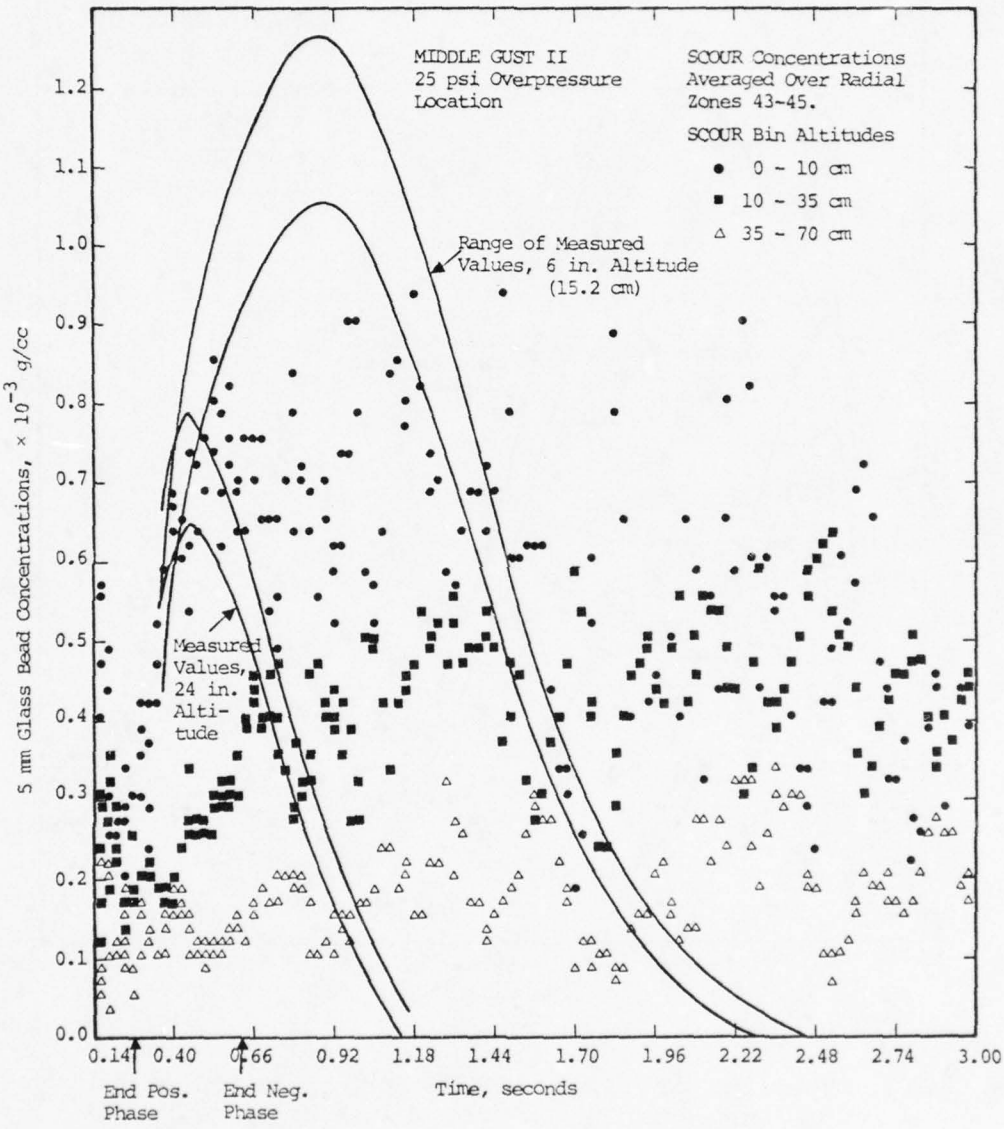

Figure 4.15. Results of first SCOUR2 (1975) calculation, using nominal parametric prescription but averaging over last three "active" surface zones, compared to MIDDLE GUST II experimental results.[31]

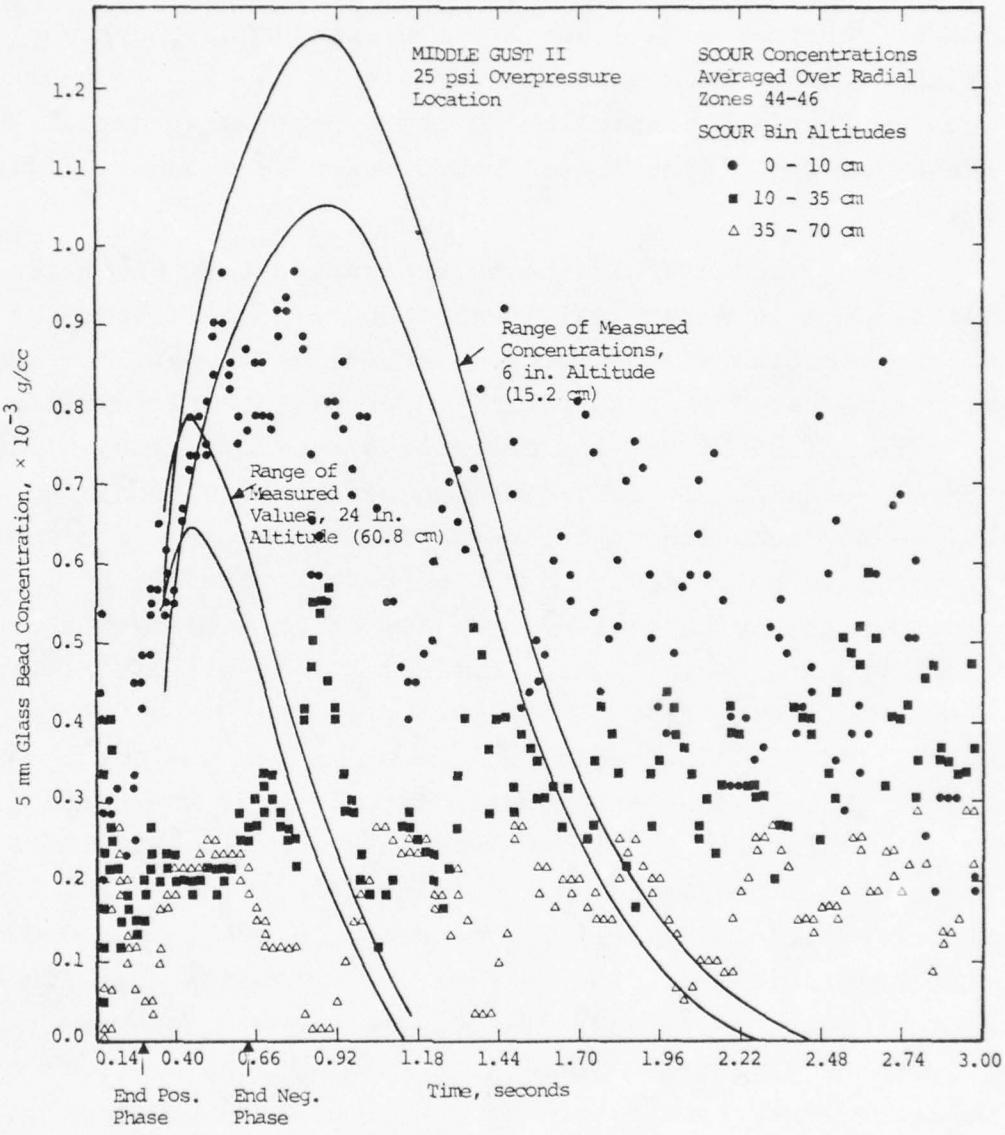

Figure 4.16. Results of second SCOUR2 (1975) calculation. The range of particle ejection angles was reduced to $10° \leq \theta \leq 40°$.

Since we are interested in concentrations at a 15 cm (6 inch) height, and the gradients in this region are quite high (as indicated by the large difference between concentrations in vertical bins 1 and 2), the average dust concentration throughout zones 1 and 2 ($0 \leq y \leq 35$ cm, $\bar{y} = 17.5$ cm) is a more appropriate comparison to the experimental data. This average for the "tight angle" calculation is shown in Figure 4.17.

The periodicity in the concentration time histories (most evident in Figure 4.17) was thought to be associated with the bouncing of particles. Inspection of particle impact data corroborated this suspicion. The 515 SCOUR2 particles that were lofted by the air shock underwent over 1500 impacts in three seconds. To determine the effect of eliminating particle bouncing from the SCOUR2 predictions, the minimum impact velocity necessary to eject a surface particle by a descending particle was raised by a factor of five over the nominal SCOUR prescription. This had the result of "killing" three out of every four SCOUR2 particles that impacted the ground. ("Killed" particles are deposited at the point of impact.) The concentration time histories for the three vertical zones with the impact modifications in this third SCOUR2 calculation are compared to the experimental results in Figures 4.18 and 4.19. The decrease in particle bouncing led to predictions of time to peak concentration that are in agreement with the experimental observations. However, the magnitude of glass bead particle concentrations predicted by SCOUR2 are lower by a factor of three, and the decay to zero concentration is too rapid.

In the subsequent fourth SCOUR2 calculation, the momentum transmission coefficient between impacting and (to be) ejected particles was increased from 0.1 to 0.7. This results in more particle impact lofting as well as a more energetic

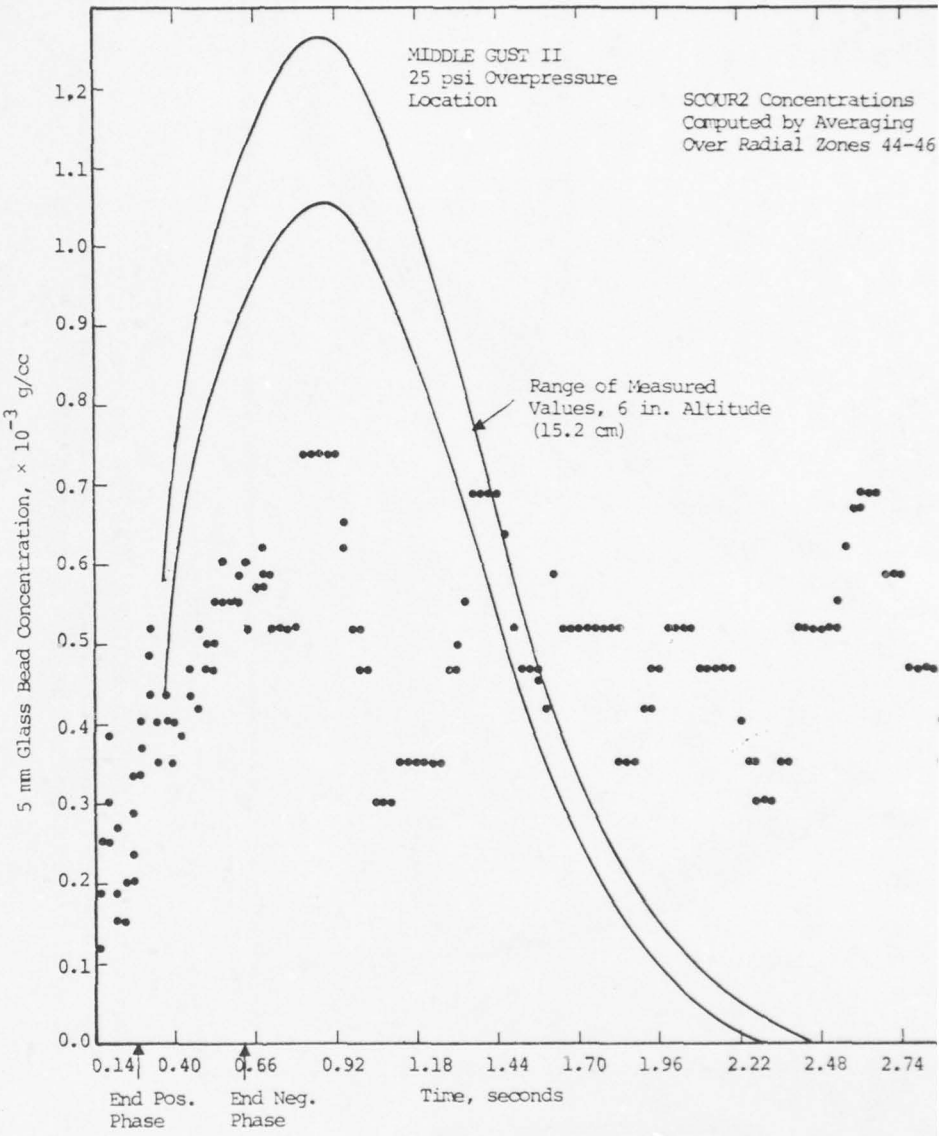

Figure 4.17. Results of second SCOUR2 (1975) calculation using $10° \leq \theta \leq 40°$ and averaging the concentration between 0 cm and 35 cm.

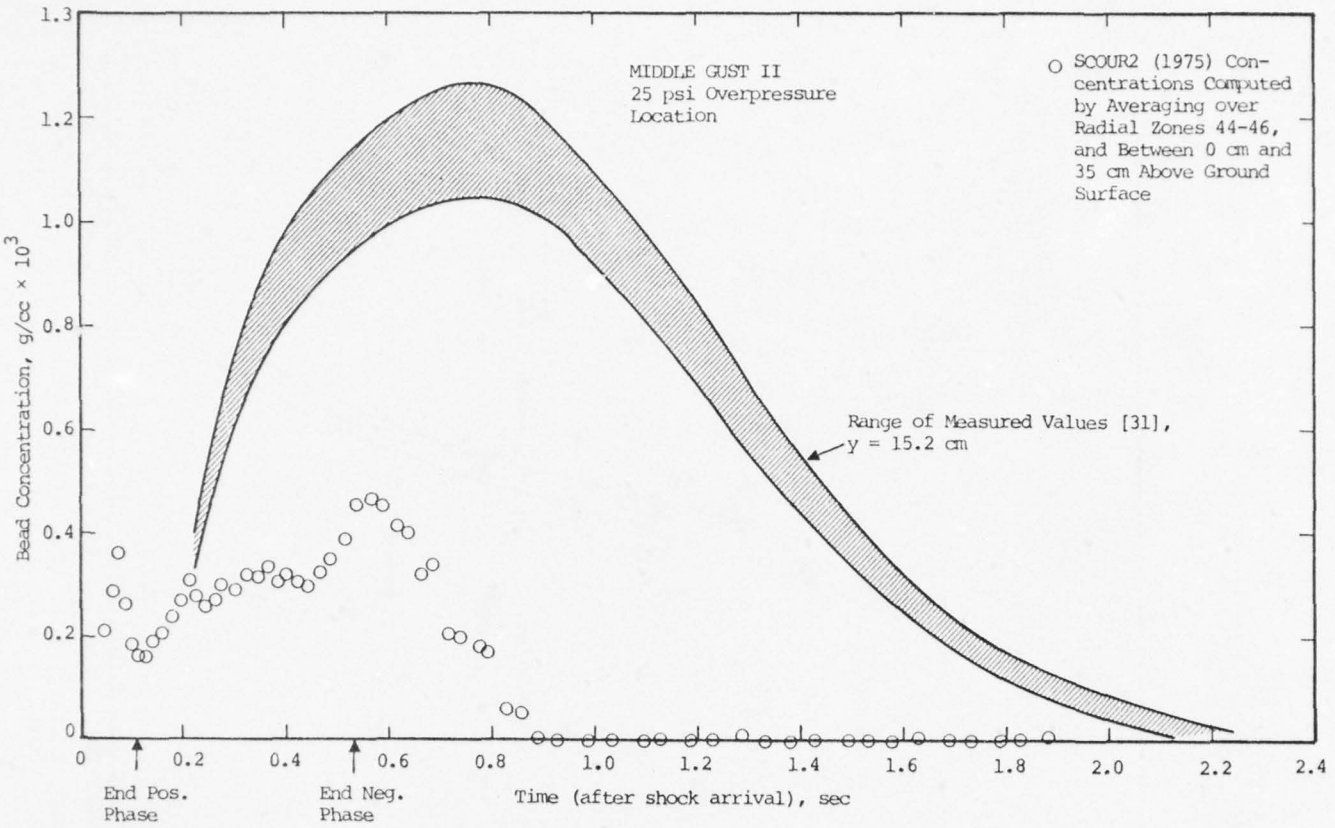

Figure 4.18. Results of the third SCOUR2 (1975) calculation, $\bar{y}$ = 17.5 cm, using $10° \leq \theta \leq 40°$ and multiplying the minimum impact velocity to loft an additional particle by a factor of five.

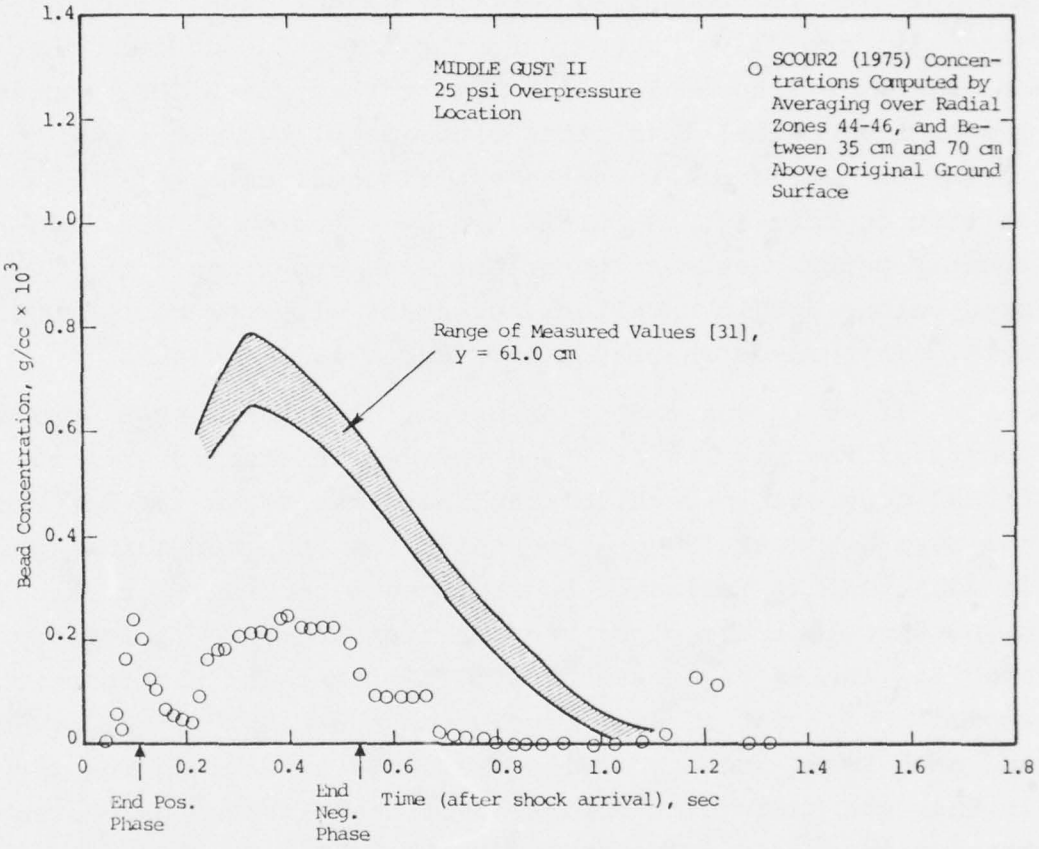

Figure 4.19. Results of the third SCOUR2 (1975) calculation, $\bar{y}$ = 52.5 cm, using $10° \leq \theta \leq 40°$ and multiplying the minimum impact velocity to loft an additional particle by a factor of five.

saltation layer near the surface. The SCOUR2 concentrations at $\bar{y}$ = 17.5 cm and $\bar{y}$ = 52.5 cm are compared to experimental results in Figures 4.20 and 4.21. The SCOUR2 concentrations averaged over the three "live" bed zones (zones 43-45) are also plotted for comparison to the nominal case (zones 44-46) (the last two "live" zones, and the first "dead" zone just downstream of the bed). It is clear that the SCOUR2 concentrations are still lower than experiment, but the time variations are similar to the experimental data. If the mass lofting coefficient is multiplied by a factor of 2.3 (to roughly match peak concentrations with experiment) the SCOUR2 predictions are in excellent agreement with the MIDDLE GUST data. This is demonstrated in Figures 4.22 and 4.23.

If we accept the experimental data for MIDDLE GUST as accurate, the results of these parametric studies with the SCOUR2 code are indicative that the glass beads surface medium was more susceptible to aerodynamic lofting than actual soil. In addition, as indicated by shock tube studies, our calculations show that the glass bead particles may be limited to ejection angles of less than 40°. It is clear that particle impact conditions strongly influence the bead "cloud" dynamics and need to be more carefully studied. An encouraging result is that the basic time variation of the glass beads concentration is predicted by the SCOUR2 calculations. Hence, it appears that the dynamics of "bead" lofting processes can be well represented by the SCOUR2 code models and numerical procedures.

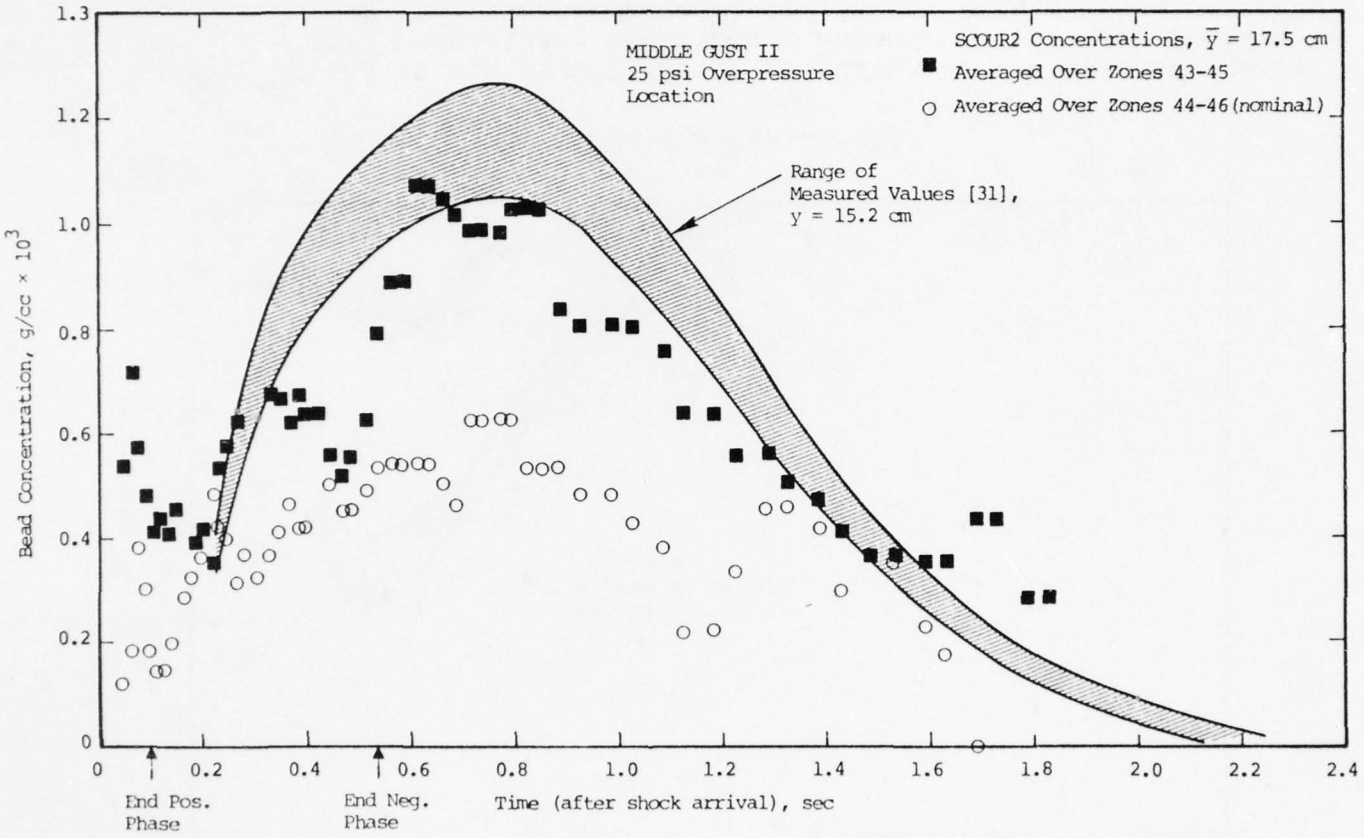

Figure 4.20. Results of the fourth SCOUR2 (1975) calculation, $\bar{y}$ = 17.5 cm, using $10° \leq \theta \leq 40°$, multiplying the minimum impact velocity for lofting by a factor of five, and increasing the impact momentum transmission coefficient from 0.1 to 0.7.

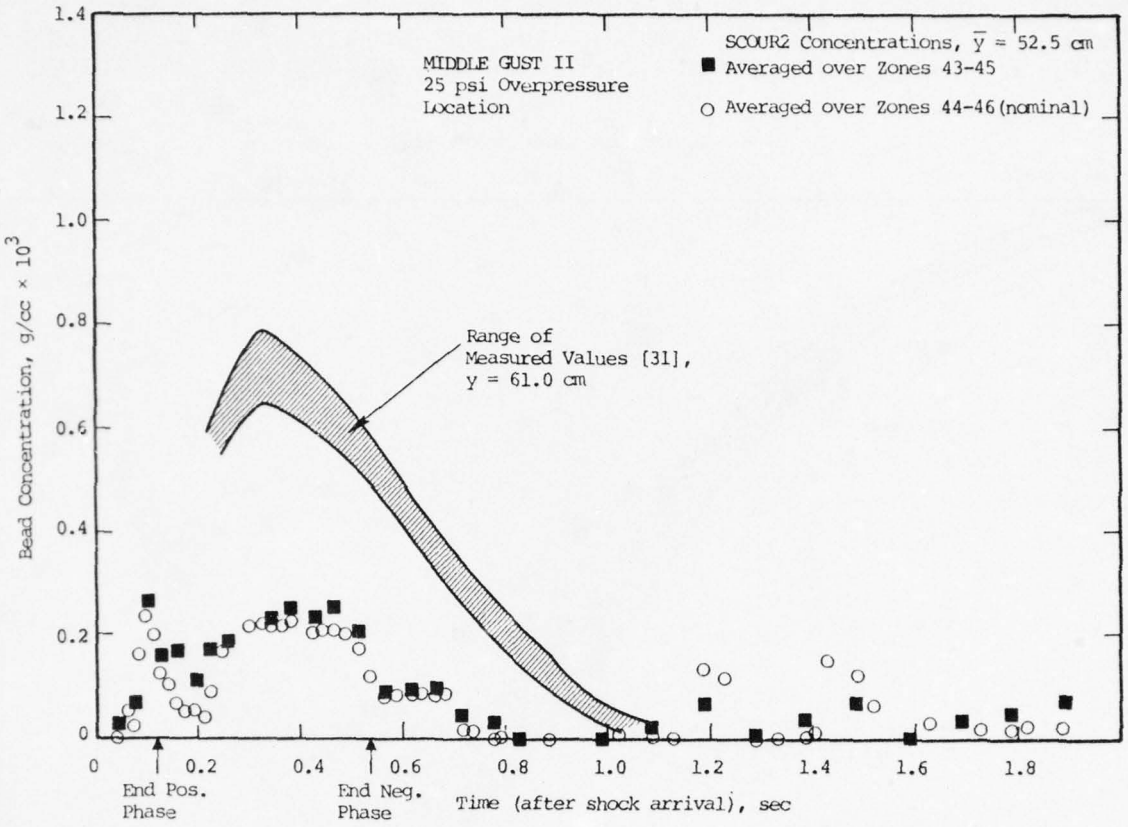

Figure 4.21. Results of the fourth SCOUR2 (1975) calculation, $\bar{y}$ = 52.5 cm, using $10° \leq \theta \leq 40°$, multiplying the minimum impact velocity for lofting by a factor of five, and increasing the impact momentum transmission coefficient from 0.1 to 0.7.

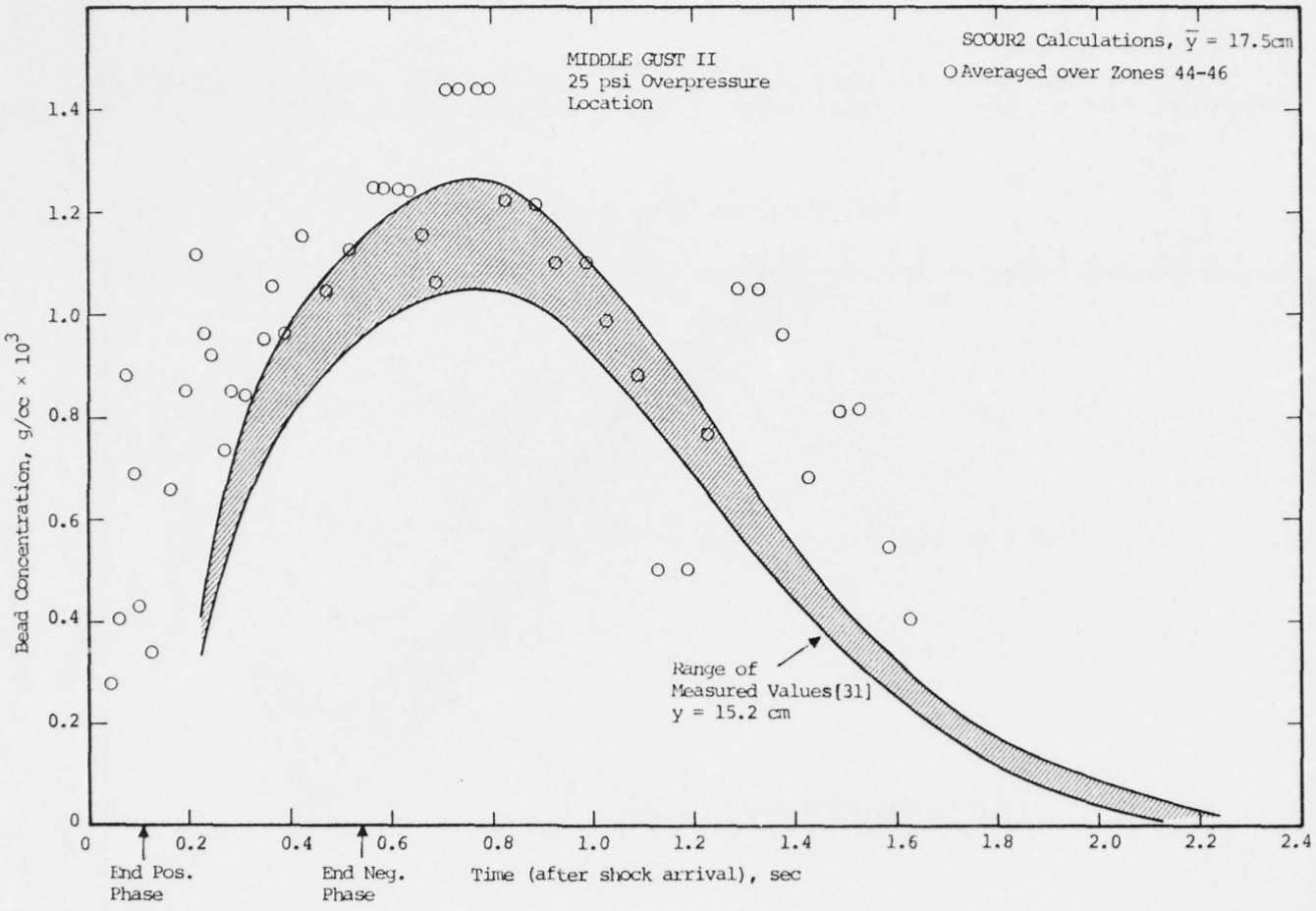

Figure 4.22. Results of the fourth SCOUR2 (1975) calculation, $\bar{y}$ = 17.5 cm, modified by increasing the aerodynamic lofting coefficient from 0.1 to 0.23.

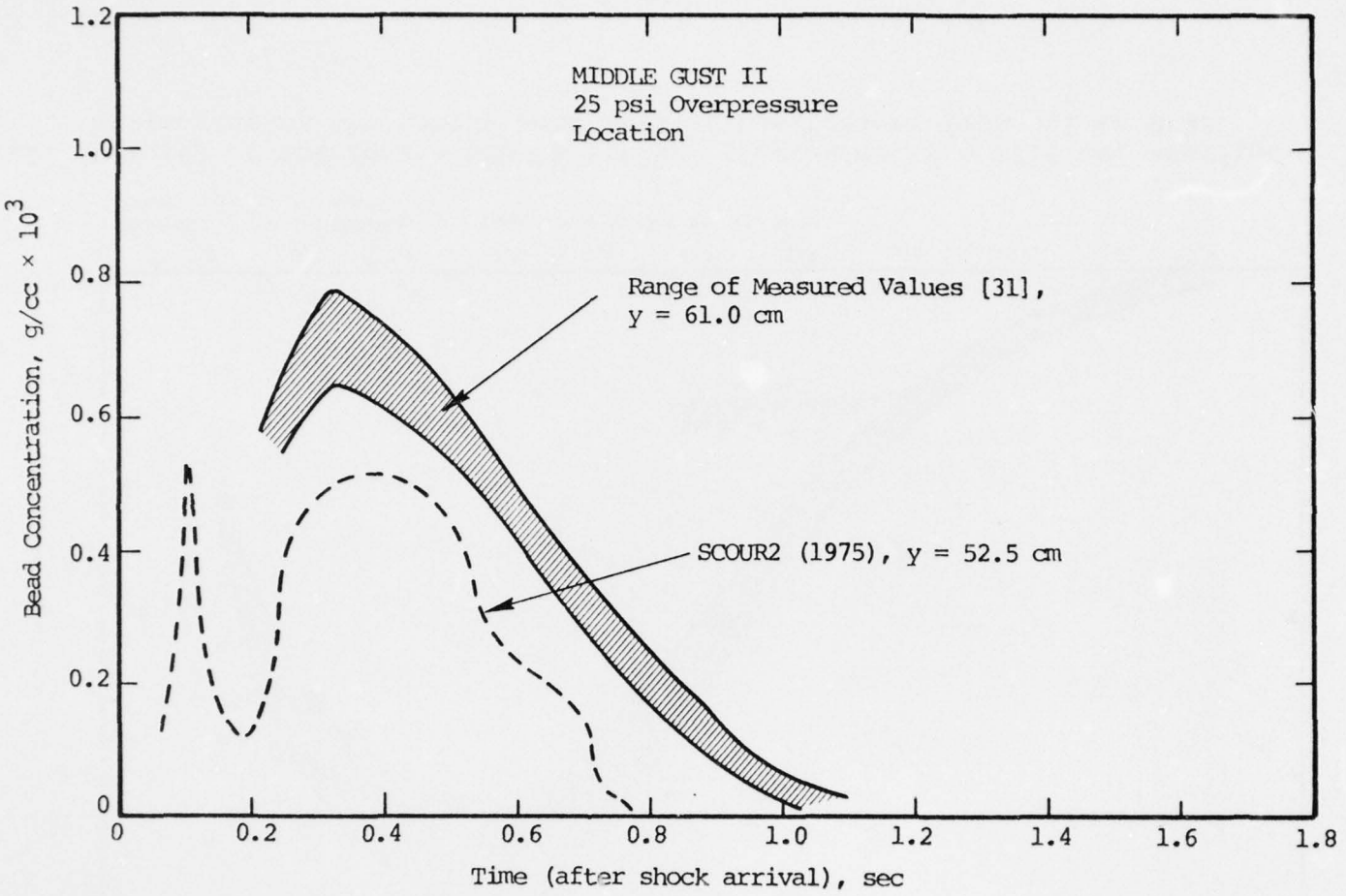

Figure 4.23. Results of the fourth SCOUR2 (1975) calculation, $\bar{y}$ = 52.5 cm, modified by increasing the aerodynamic lofting coefficient from 0.1 to 0.23.

V. S^3 FLUIDIZED BED CALCULATIONS OF THE REVERSE PERCOLATION PROCESS

5.1 INTRODUCTION AND SUMMARY

It was recognized early in dust lofting research that a possible mechanism for dust blowoff from the surface was the so-called reverse percolation process.[8] The passage of a high pressure, air blast-wave pulse over the surface of a porous soil could lead to the pressurization of air trapped in the pores. As the overpressure decreases above the soil, the (high pressure) trapped air would flow upwards through the soil matrix (i.e., reverse percolation), entraining soil particles if there was a strong enough pressure gradient.

Reverse percolation was observed in a series of simple experiments performed by Shock Hydrodynamics in 1973.[8] In these tests, a 20 cm diameter column of packed sand (650 μm diameter (mean), 33 percent porous) was exposed to surface overpressures that corresponded to the 100 psi overpressure environment for a 1 MT surface burst. Significant fluidization and upward motion of the near-surface sand was observed, and a large fraction of the 180 cm long column was set in motion.

In an earlier report,[2] S^3 performed a simplified analysis of the reverse percolation process at low overpressures and determined that it was possible to fluidize the surface particulates, but the flow velocity was too small to actually eject particles into the positive phase air flow. It was believed, however, that additional research should be performed on the degree to which near-surface, porous layers could be fluidized and/or ejected into the negative phase air flow.

Relevant to the dust lofting problem, S^3 had initiated the research and development of a new computer code, FLUB (FLUidized Bed code). This work was originally performed in

S^3's IR&D program.[10,34] The intent was to better understand the dynamics of fluidized beds, and to develop advanced numerical codes that could be used to study fluidized bed problems. The FLUB code, described in the next section (5.2) has been used to calculate the fluidized bed dynamics observed in the shock tube experiments[11] and to make some preliminary estimates of the porous soil response at a high overpressure position under nuclear surface burst conditions.

The FLUB results, described in Sections 5.3 and 5.4, demonstrate that the air trapped in pores of the soil matrix will fluidize porous, strengthless soils down to depths of tens of centimeters. Large quantities of dust can be given positive vertical velocities. If the simplified model and assumptions that underlie the application of the FLUB code are valid, large quantities of dust will be given small (but finite) positive vertical velocities. Thus, the reverse percolation effect could dramatically alter the air flow/surface interface conditions from that generally assumed for aerodynamic lofting. Namely, the low lying saltation layer would be replaced by a fluidized bed with much higher particulate concentrations. Presumably, the mass entrainment at the air flow/fluidized soil interface would still be proportional to the shear at the interface, and the shear may still be modeled by a rough wall shear law (as in SCOUR2). Thus, the simple models for mass lofting and shear presently in SCOUR2 may be an appropriate formulation/conceptualization for entrainment from fluidized beds, but the parameters may require reevaluation.

Although the FLUB calculations provide significant insight to a potential problem area in the SCOUR code formulation, this line of study and model development was not further explored in the S^3 study. The chief reason was that a thorough understanding of the reverse percolation process would involve

a far more definitive treatment of soil models than that possible within the scope of the SCOUR2 development program. Such an effort would include porosity, saturation, strength effects, and soil matrix analyses. Ultimately, this would involve parametric code calculations to gauge model sensitivity and additional experimentation to validate model "numbers".

Secondly, the reverse percolation process is significant only in the negative phase of the blast wave flow field, over a limited range and time. The SCOUR2 model for aerodynamic scouring by the positive phase blast wave would not be significantly affected, hence positive phase dust loads on structures would not be affected. Taking this into account, and realizing that a soil matrix with small but finite cohesion would seriously reduce the reverse percolation lofting potential, this topic was given a lower priority than the popcorning due to thermal radiation and neutron absorption by groundwater.[3,4]

5.2 FLUB

The FLUB code was originally developed to solve the governing equations for an unsteady, chemically inert gas-fluidized bed in one space dimension. These equations, developed within the framework of the Theory of Interacting Continua (TINC), express the principles of conservation of mass and momentum for both components (solid particles and interstitial gas) of the mixture. Derivations of these equations can be found in Garg.[34] S^3 is in the process of extending the methodology to two space dimensions, including chemical reactions, energy transfer, and multiple species.[35]

In the original version of FLUB, the fluid is treated as an ideal gas, which may be either isothermal or isentropic. The solid is considered to consist of a large number of

uniform-size spherical particles; this collection of particles behaves like a Newtonian fluid with bulk and shear "viscosities" which may depend in an arbitrary way upon the local solid concentration. Each individual particle is treated as an incompressible sphere, but, in the aggregate, the particles may be pressurized if the local packing density exceeds a preset value. The solid and fluid phases are coupled through a friction law which approaches Stokes law in the thin-mixture limit and which approximates flow through a porous matrix at high packing densities. The effective "permeability" as a function of porosity was matched to data collected by Jackson[36] in the porosity range 0.4-0.5, as well as to Stokes law.

The numerical procedure employs rather elaborate implicit iterative techniques to solve the highly nonlinear (and occasionally singular) system of equations which results from using realistic constitutive relations in the fundamental governing equations. The scheme is basically a finite difference procedure in both the space and time domains. Simultaneous use of an Eulerian and a Lagrangian grid permits free surfaces to be accurately delineated. The Lagrangian features in no way depend on the ordering of the Lagrangian nodes, so that the scheme may be readily generalized to multidimensional geometries without restrictions upon grid distortion.

5.2.1 Fundamental Relations

The field equations developed by Garg[34] for the one-dimensional case may be expressed as follows:

1. Conservation of Solid Mass:

$$\frac{\partial \theta}{\partial t} + \frac{\partial}{\partial x} (\theta u) = 0 \qquad (5.1)$$

2. Conservation of Gas Mass:

$$\frac{\partial}{\partial t}\left[(1-\theta)\rho_f\right] + \frac{\partial}{\partial x}\left[(1-\theta)\rho_f u_f\right] = 0 \tag{5.2}$$

3. Conservation of Solid Momentum:

$$\frac{\partial}{\partial t}(\theta u) + \frac{\partial}{\partial x}(\theta uu) = \theta g - \frac{\partial}{\partial x}(\theta f) - \frac{1}{\rho_s}\frac{\partial P}{\partial x} + \frac{\partial}{\partial x}\left[\frac{\left(\lambda + \frac{4}{3}\mu\right)}{\rho_s}\frac{\partial u}{\partial x}\right] \tag{5.3}$$

4. Conservation of Gas Momentum:

$$u_f = u - \frac{k(\theta)}{(1-\theta)\eta_f}\frac{\partial P}{\partial x} \tag{5.4}$$

Here, ρ_s = solid density (a constant)

$\theta = 1 - \phi$ = 1 - porosity

ρ_f = gas density

u = solid velocity

u_f = gas velocity

λ, μ = "viscosity" coefficients for solid (depend on θ)

η_f = gas viscosity

g = gravity acceleration

P = gas pressure (interstitial)

θf = solid kinematic pressure

k = solid permeability (depends on θ and the nature of the particulate)

The gas is taken as polytropic, so:

$$P = (\gamma-1)C_V T\,\rho_f \tag{5.5}$$

where

C_V = specific heat at constant volume

T = gas temperature

γ = ratio of specific heats for gas.

Two forms of gas thermodynamics will be considered:

Isothermal, in which case:

$$T = T_0 = \text{const} \tag{5.6a}$$

so that the equation of state becomes

$$P = (\gamma-1)C_V T_0 \rho_f \tag{5.7a}$$

and

Adiabatic, in which case:

$$T = T_0 (\rho_f/\rho_{f0})^{\gamma-1} \tag{5.6b}$$

so that

$$P = (\gamma-1)C_V T_0 \left(\frac{\rho_f}{\rho_{f0}}\right)^{\gamma-1} \rho_f \tag{5.7b}$$

Here, T_0 and ρ_{f0} are the reference state designating the particular isentrope under consideration.

The gas viscosity is taken as proportional to absolute temperature, so

$$\eta_f = \eta_{f0}(T/T_0).$$

Thus, for the isothermal case,

$$\eta_f = \eta_{f0} \tag{5.8a}$$

AD-A050 114 SYSTEMS SCIENCE AND SOFTWARE LA JOLLA CALIF F/G 18/3
NEAR-SURFACE NUCLEAR DUST CLOUD STUDIES.(U)
JAN 77 J W KIRSCH DNA001-73-C-0128
UNCLASSIFIED SSS-R-76-2828 DNA-4332F NL

2 OF 2
AD A050 114

END
DATE FILMED
3-78
DDC

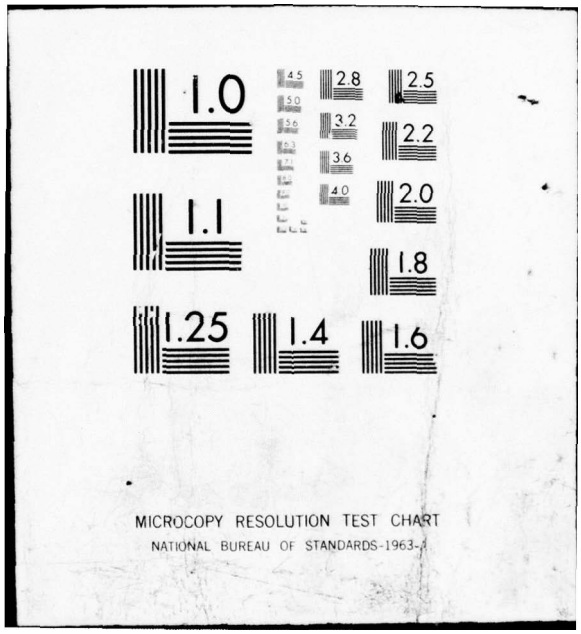
1.0
1.1
1.25
1.4
1.6
1.8
2.0
2.2
2.5
2.8
3.2
3.6
4.0
4.5
5.0
5.6
MICROCOPY RESOLUTION TEST CHART
NATIONAL BUREAU OF STANDARDS-1963-A

and for the adiabatic case

$$\eta_f = \eta_{f0}(\rho_f/\rho_{f0})^{\gamma-1} \tag{5.8b}$$

The kinematic solid pressure θf is expressed in the following mathematical form:

$$\theta f = \frac{a^2}{2}(\theta-\theta_0)^2 \text{ for } \theta > \theta_0$$
$$= 0 \quad \text{otherwise} \tag{5.9}$$

where a and θ_0 are specified constants.

The ratio of the permeability (k) to the square of the solid particle radius is simply a function of θ:

$$\kappa(\theta) = k/r_0^2 \ . \tag{5.10}$$

The following form has been found to fit available data for spherical particles in the γ-range 0.4 to 0.5,[36] and also matches Stokes law in the limit as θ approaches zero:

$$\kappa(\theta) = \frac{2}{9}\frac{1-\theta}{\theta} \times \exp\left[(-4.093 + 0.3625[1-\theta])\left(\frac{\theta}{1-\theta}\right)^{1/3}\right] \tag{5.11}$$

(see Figure 5.1). For the solid viscosity terms, it is convenient to define:

$$\nu(\theta) = \left|\lambda + \frac{4}{3}\mu\right| /\rho_s \tag{5.12}$$

and to use the form:

$$\nu(\theta) = \nu_0 \times \left(\frac{\theta}{\theta_0}\right) \tag{5.13}$$

where $\nu_0 = \left(\lambda_0 + \frac{4}{3}\mu_0\right)/(\rho_s)$ = the kinematic viscosity measured at $\theta = \theta_0$.

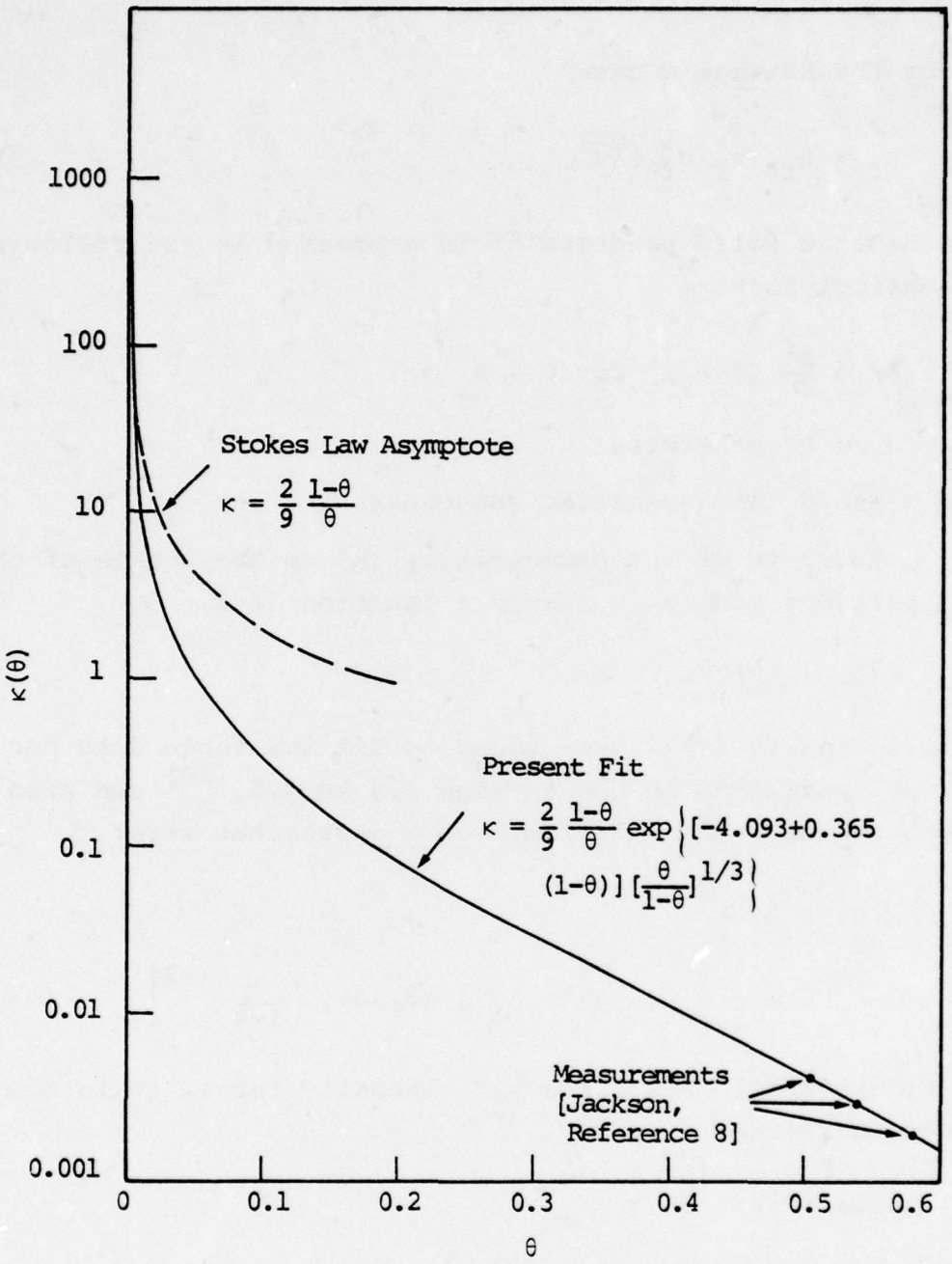

Figure 5.1. Dimensionless permeability ($\kappa = k/r_0^2$) as a function of porosity ($=1-\theta$) fitted to Stokes Law and Jackson [36] data.

5.2.2 Boundary Conditions

The system of equations is to be solved on the region $0 \leq x \leq X$. The walls are considered impenetrable by solid particles, so:

$$u = 0 \text{ at } x = 0, X \tag{5.14}$$

For the gas motion, two options are available. If the boundary is considered impermeable, the requirement is:

$u_f = 0$ at the boundary, or, using (5.4) and (5.14),

$$\frac{\partial P}{\partial x} = 0 \text{ at the boundary } (x = 0 \text{ or } X) \tag{5.15}$$

If, on the other hand, the boundary represents a screen or filter through which the gas can pass, the condition is:

$$P = P_B(t) \text{ at the boundary} \tag{5.16}$$

where $P_B(t)$ is a specified boundary gas pressure which may vary with time.

5.2.3 Transformed Relations

It is useful to use the above determinate expression (Eqs. (5.5)-(5.13)) to rewrite the fundamental field equations in a convenient way. The solid mass relation is unchanged:

$$\frac{\partial \theta}{\partial t} + \frac{\partial}{\partial x}(\theta u) = 0 \tag{5.17}$$

For the gas mass conservation constraint (5.2), we first use (5.4) to eliminate explicit dependence on u_f:

$$\frac{\partial}{\partial t}[(1-\theta)\rho_f] + \frac{\partial}{\partial x}[(1-\theta)\rho_f u] = \frac{\partial}{\partial x}\left[\frac{k}{\eta_f}\rho_f \frac{\partial P}{\partial x}\right] \tag{5.18}$$

If the gas is isothermal, Eqs. (5.7a) and (5.8a) yield for the term on the right:

$$\frac{\partial}{\partial x}\left[\frac{k}{\eta_{f0}}\,(\gamma-1)C_V T_0 \rho_f \frac{\partial \rho_f}{\partial x}\right] \tag{5.19a}$$

In the adiabatic case, the term is (using 5.7b and 5.8b):

$$\frac{\partial}{\partial x}\left[\frac{k}{\eta_{f0}}\,(\gamma-1)C_V T_0 \left(\frac{\rho_{f0}}{\rho_f}\right)^{\gamma-1} \rho_f \frac{\partial}{\partial x}\left\{\rho_f \left(\frac{\rho_f}{\rho_{f0}}\right)^{\gamma-1}\right\}\right] \tag{5.19b}$$

Using a little algebra, it is possible to show that this becomes:

$$\frac{\partial}{\partial t}\left[(1-\theta)\rho_f\right] + \frac{\partial}{\partial x}\left[(1-\theta)\rho_f u\right] = \frac{\partial}{\partial x}\left[\frac{\alpha}{2}\,\gamma^{\delta}\,\frac{\partial}{\partial x}\left(\rho_f^2\right)\right] \tag{5.20}$$

where

$$\alpha \equiv (\gamma-1)C_V T_0 \frac{k(\theta, r_0)}{\eta_{f0}} = \frac{(\gamma-1)C_V T_0 r_0^2}{\eta_{f0}} \times \kappa(\theta) \tag{5.21}$$

and where

$$\begin{aligned} \delta &= 0 \text{ for the isothermal case} \\ &= 1 \text{ for the adiabatic case.} \end{aligned} \tag{5.22}$$

The solid momentum equation may now be written:

$$\frac{\partial(\theta u)}{\partial t} + \frac{\partial}{\partial x}(\theta u u) = \theta g - \frac{\partial}{\partial x}(\theta f) - K\left[\gamma\left(\frac{\rho_f}{\rho_{f0}}\right)^{\gamma-1}\right]^{\delta} \frac{\partial \rho_f}{\partial x} + \frac{\partial}{\partial x}\left[\nu \frac{\partial u}{\partial x}\right] \tag{5.23}$$

where $K \equiv (\gamma-1)C_V T_0/\rho_s = \text{const.}$ (5.24)

and where, as before,

$\delta = 0$ for the isothermal case

$= 1$ for the adiabatic case.

The boundary conditions are, on solid velocity (Eq. (5.23))

$$u = 0 \text{ at } x = 0, X \tag{5.25}$$

At boundaries which are impermeable to gas, the condition on Eq. (5.20) is just:

$$\frac{\partial}{\partial x} (\rho_f^2) = 0 \text{ at the boundary} \tag{5.26}$$

At "prescribed gas pressure" (permeable) boundaries, the condition is

$$\rho_f^2 = \left[\frac{P_B(t)}{(\gamma-1)C_V T_0} \right]^{2\left(1-\delta\left[\frac{\gamma-1}{\gamma}\right]\right)} \times \rho_{f0}^{2\delta \frac{(\gamma-1)}{\gamma}} \tag{5.27}$$

5.2.4 Summary of Principle Equations

To repeat, the entire system is now reduced to the following:

1. Solid mass conservation:

$$\frac{\partial \theta}{\partial t} + \frac{\partial}{\partial x} (\theta u) = 0 \tag{5.28}$$

2. Gas mass conservation:

$$\frac{\partial}{\partial t} [(1-\theta)\rho_f] + \frac{\partial}{\partial x} [(1-\theta)\rho_f u] = \gamma^{\delta} \frac{\partial}{\partial x}\left[\frac{\alpha}{2} \frac{\partial}{\partial x} \left(\rho_f^2\right)\right] \tag{5.29}$$

3. Momentum conservation:

$$\frac{\partial}{\partial t}(\theta u) + \frac{\partial}{\partial x}(\theta u u) = \theta g - \frac{\partial}{\partial x}(\theta f) - K\left[\gamma\left(\frac{\rho_f}{\rho_{f0}}\right)^{\gamma-1}\right]^{\delta} \frac{\partial \rho_f}{\partial x} + \frac{\partial}{\partial x}\left[\nu \frac{\partial u}{\partial x}\right] \quad (5.30)$$

where

θ = 1 - porosity

u = solid velocity

ρ_f = gas interstitial density

g = gravity acceleration

$\alpha = \kappa(\theta) \times (\gamma-1) C_V T_0 r_0^2 / \eta_{f0}$

γ = ratio of specific heats

$\theta f = \frac{a^2}{2}(\theta-\theta_0)^2$ for $\theta > \theta_0$

$= 0$ for $\theta \leq \theta_0$

$K = (\gamma-1) C_V T_0 / \rho_s$

$\nu = \frac{1}{\rho_s}\left(\lambda_0 + \frac{4}{3}\mu_0\right) \times (\theta/\theta_0)$

$\delta = 0$ for isothermal gas

$= 1$ for adiabatic gas

C_V = gas constant volume specific heat

T_0 = standard gas temperature

ρ_{f0} = standard gas density (at T_0)

η_{f0} = standard gas viscosity (at T_0)

r_0 = solid particle radius

ρ_s = solid particle density

λ_0, μ_0 = solid "viscosity coefficients" at $\theta = \theta_0$

$$\kappa(\theta) = \frac{2(1-\theta)}{9\theta} \exp\left[(-4.093 + 0.3625[1-\theta])\left(\frac{\theta}{1-\theta}\right)^{1/3}\right]$$

Thus, to specify a problem, the following must be provided:

Gas Properties: δ, γ, C_V, T_0, η_{f0}, ρ_{f0}

Solid Properties: ρ_s, θ_0, a^2, λ_0, μ_0, r_0

Domain: g, length of domain (X)

Boundary Conditions: $P_L(t)$ and/or $P_R(t)$ (gas pressures at $x = 0$, $x = X$), or specification of impermeable boundary

Initial Conditions: Distributions of $\theta(x)$, $u(x)$, $\rho_f(x)$ at $t = 0$

5.3 FLUB CALCULATIONS — SAND COLUMN EXPERIMENTS (100 psi *OVERPRESSURE*)

When the blast wave from an explosion passes over a porous permeable land surface, compressed air will be driven into the soil and will diffuse to greater and greater depths as time goes on. Once the above-surface blast pressure declines, this air will begin to flow back upward, out of the soil. If the soil is loose and the blast pressure sufficiently great, this "surface breathing" may carry considerable amounts of solid material aloft as the compressed air rushes out of the pores. This process has been termed "reverse percolation" by Zernow, et al.[8]

To evaluate this effect, Zernow, et al. conducted a series of small-scale experiments in which a vertical shock tube was used to generate a long-period, 100 psi (6.8 atm) overpressure air shock. This shock impinged from above upon

a vertical tube partially filled with sand; the diameter of the sand column was 8 inches (20 cm) and its height was about 71 inches (180 cm). Measurements were made of the variation with time of the position of the sand surface and of the interstitial gas pressure time-history at various depths below the original sand surface level. These experiments were carried out with various shock wave periods and with various "batches" of sand characterized by different particle sizes. In most of the experiments, the bottom of the sand column was "partially vented"; small holes in the bottom of the tube containing the sand were provided to allow restricted air passage. A few experiments were also performed with these holes blocked off ("unvented") so as to completely prohibit air motion at the bottom of the bed. The observed sand lofting was much greater in the latter case.

This experimental configuration was treated using the original FLUB one-dimensional code, both to test the code and to gain insight into the important mechanisms operative in the sand-lofting process. Two complete calculations were made. These correspond to tests using the "1.36 inch diameter orifice" and "Batch II Standard Sand" (see Zernow, et al.).[8] The experimental air-pressure-versus-time history at the surface was fit with the following function:

$$P(0,t) = 1 + 6.8\, f(t) \exp(-t/0.21 \text{ sec})$$

where $P(0,t)$ is the absolute pressure at the surface in atmospheres, and

$$f(t) = 1 \qquad (t < 0.55 \text{ sec})$$

$$= 1 - 4\,(t-0.55) \qquad (0.55 \text{ sec} \leq t \leq 0.8 \text{ sec})$$

$$= 0 \qquad (t > 0.8 \text{ sec})$$

This corresponds to a surface burst of 1.0 MT. The sand bed was represented by 72 Eulerian zones, each of height 2.5 cm for a total height of 180 cm; an additional 28 empty zones were provided above the bed to permit up to 70 cm of sand lofting before material strikes the upper mesh boundary. A total of 360 Lagrangian nodes were used to follow sand motion.

The air was treated as an adiabatic, $\gamma = 1.4$ ideal gas; the pressure/volume relation was the isentrope reached by ambient air shocked to 6.8 atm. The increase in air viscosity with temperature was taken into account. Most of the essential sand properties are available in Zernow, et al.; the crystal density was 2.4 g/cm^3, the initial porosity (ϕ_0) was taken as uniform throughout the bed and equal to 0.33, and the particle diameter (required by the code for permeability calculations) was taken as 650 microns, which is given by Zernow, et al. as the mean particle size for "Batch II Standard Sand". The bulk pressure in the sand was taken as

$$P_{SB} = 3\left(1 - \frac{\phi}{\phi_0}\right)^2 \times 10^5 \text{ atm for } \phi < \phi_0 = 0.33$$

$$= 0 \text{ for } \phi > \phi_0$$

(where ϕ = porosity) which agrees reasonably well with the experimental measurements over the pressure range of interest. Zernow, et al. did not measure the intrinsic viscosity of the sand bed; for the calculation, the viscosity was taken as zero. Preliminary calculations showed the results to be insensitive to reasonable values of the parameter.

Two cases were run; the first treated the bottom of the computing region as completely impermeable, corresponding to the experimental "unvented" case. The second allowed complete air mobility at the bottom of the mesh, so that the gas pressure there remained at one atmosphere throughout the calculation. This "fully vented" calculation was intended to simulate

the "partially vented" experimental case, but of course is not quite the same thing. Exact simulation of the experimental boundary conditions would have involved a fair amount of code development, and was therefore not attempted.

The height-versus-time of the surfaces of the sand columns computed by the FLUB code are compared with measurements in Figure 5.2. The early "precursor" cloud in the experimental measurements is associated with high frequency noise in the incident pressure signal resulting from shock reverberations in the apparatus as Zernow, et al. have demonstrated experimentally. Measured peak heights for the partially vented case varied between 16 and 19 cm; the computed result for the fully vented case was 15.93 cm. For the unvented case, the experiments were unable to determine peak height, but it was known to be > 35 cm; the computed peak height was 46.58 cm. The agreement is seen to be quite good, particularly in view of the experimental test-to-test variations and the inability of the code to exactly simulate the lower boundary condition for the vented case. Interstitial gas-pressure histories at depths of zero, 84 and 146 cm are shown in Figure 5.3. For comparison, the experimental results for the partially vented case are listed below (no results were presented by Zernow, et al. for the unvented case):

	Depth	
	84 cm	146 cm
Peak gas pressure (atm)	1.34 - 1.71	∿0.6
Time of peak (sec)	0.22 - 0.23	∿0.3

Again, agreement is good.

The total mass of sand above the pretest surface per unit area as computed by the code is shown as a function of time for each case in Figure 5.4. As can be seen, the unvented case lofts substantially more material.

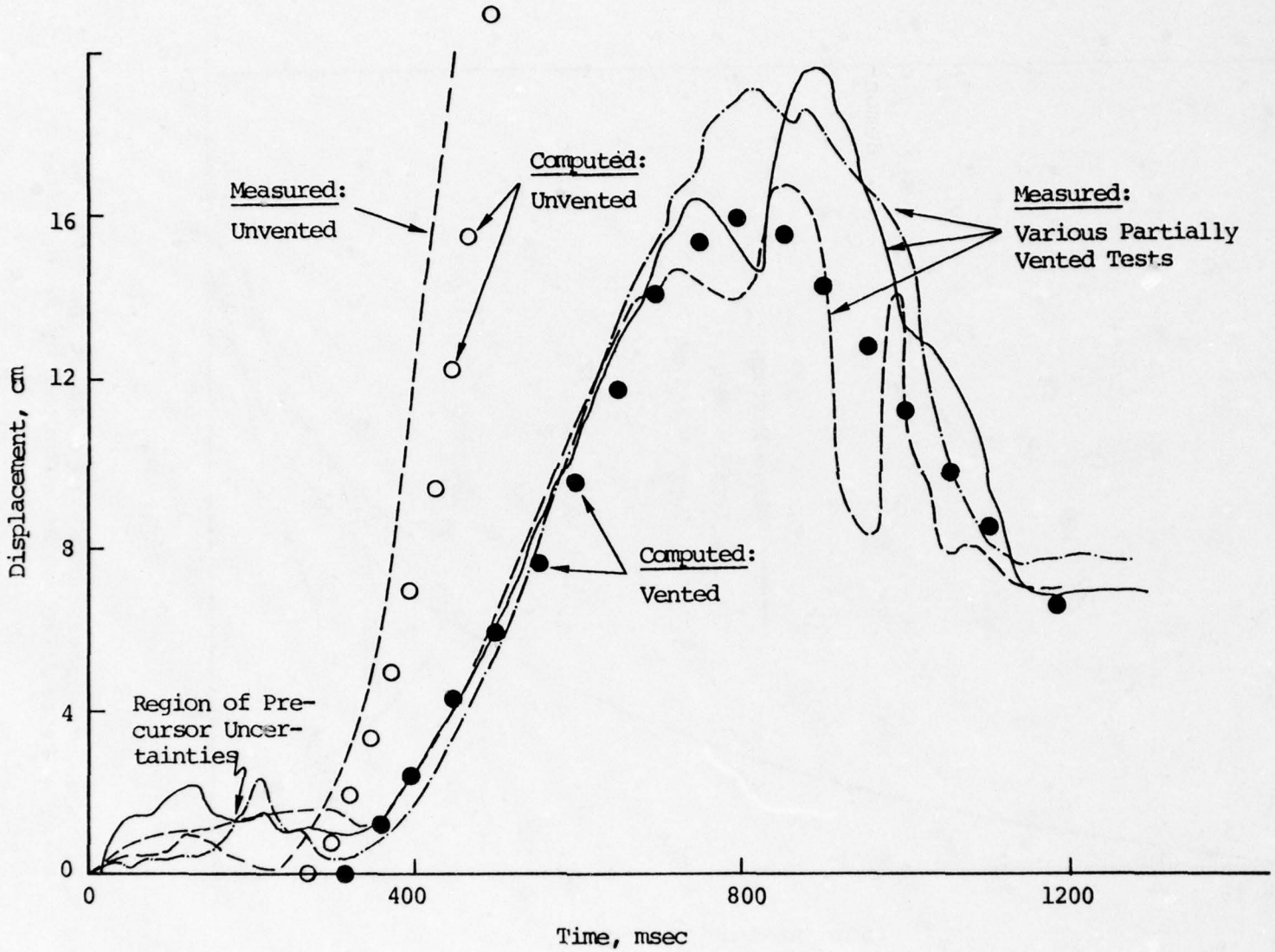

Figure 5.2. Surface displacement versus time – comparison between data of Zernow, et al. [8] and FLUB computations.

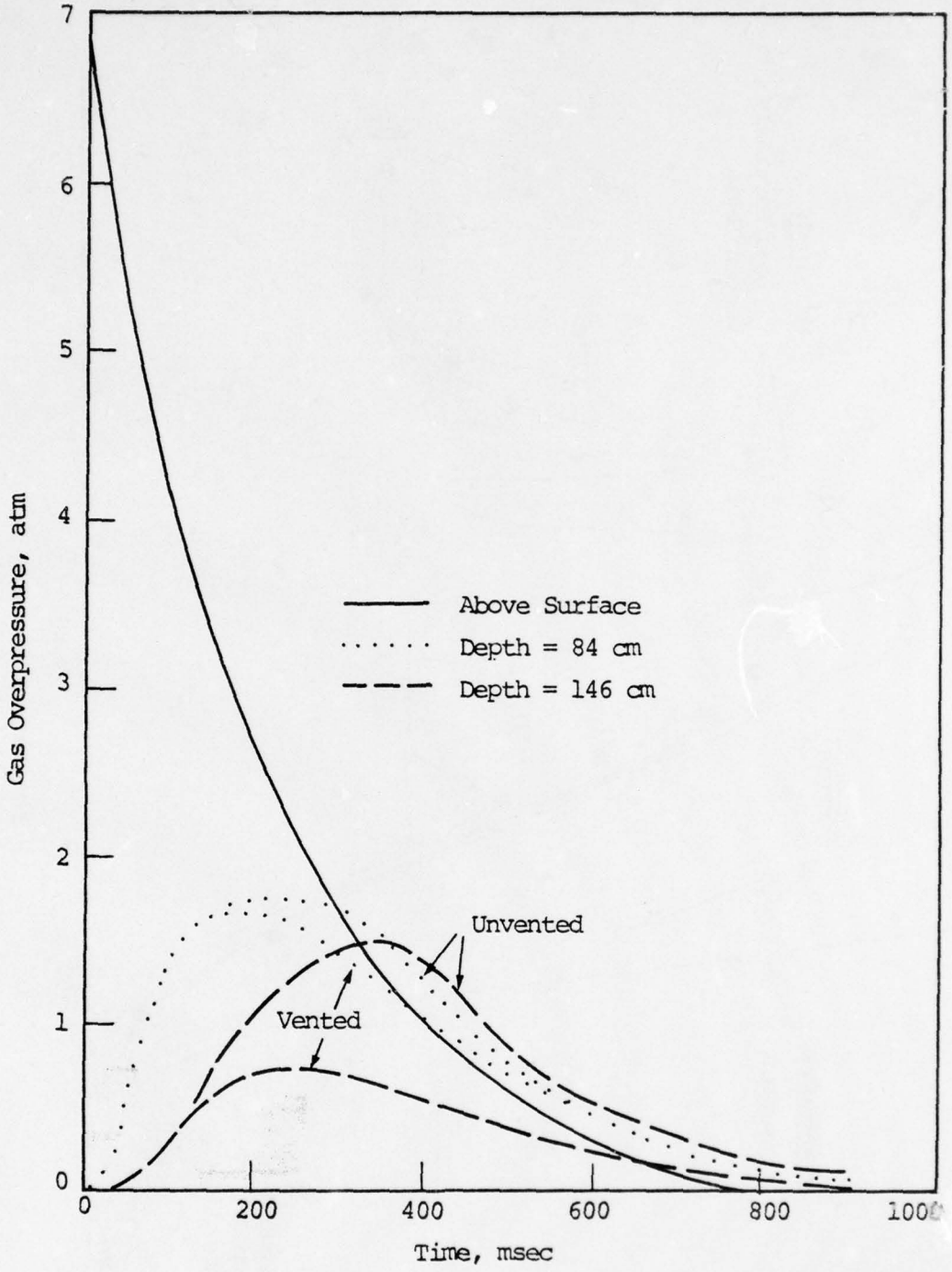

Figure 5.3. Gas overpressure versus time at surface and z = 84 and 146 cm as computed by FLUB code.

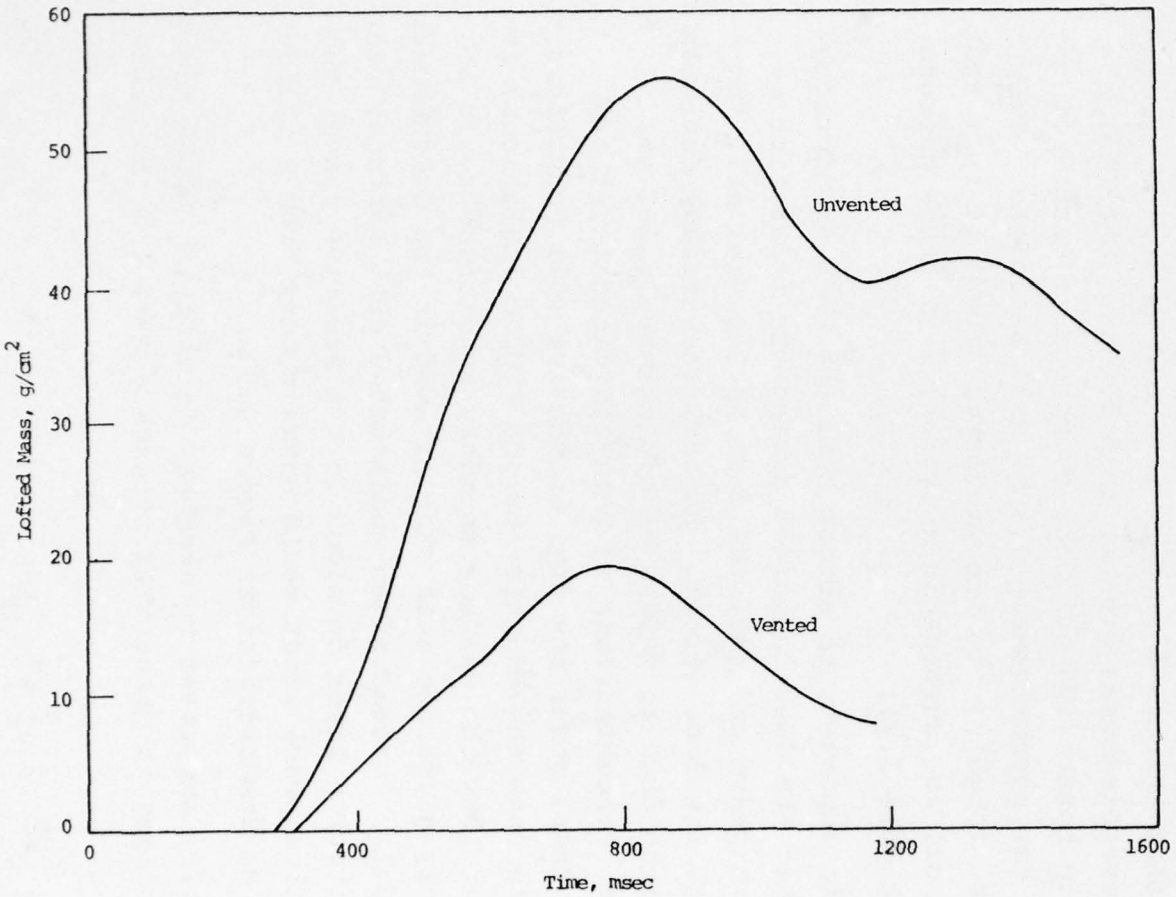

Figure 5.4. Total solid mass aloft versus time as computed by FLUB code.

5.3.1 Remarks

Based on the results in Figure 5.4, it would be reasonable to assume that at least 10 g/cm^2 would be available for entrainment in the negative phase afterwinds. If we assume that this is a representative mass lofting potential, for overpressures greater than 100 psi, then for a 1 MT surface burst (100 psi peak overpressure occurs at a range of 1 km) approximately 0.3 MT will be lofted. This corresponds, roughly, to the predicted amount of dust that is sheared off the surface in a typical 1 MT SCOUR calculation (see Figure 3.9).

It is important to stress that the FLUB predictions indicate that the dust is lofted during the transition to the negative phase and that the dust is not violently "popcorned" into the free stream. Rather, the surface dust has been fluidized down to depths of approximately 200 cm. Typical dust concentrations in this fluidized layer are 0.5 g/cc. Thus, under the dry, incohesive soil conditions evaluated in both the experiments and FLUB calculations, it would appear that the surface boundary conditions could be significantly different than that assumed in the SCOUR shear lofting model. Instead of an undisturbed dust surface, over which a saltation layer develops in the negative phase, the early negative phase winds would entrain dust from a fluidized layer as demonstrated in Figure 5.5.

Equally important to remember is that the SCOUR model for dust lofting is quantified through a mass lofting relation

$$\dot{M}_p = \frac{b_{ND}}{V_0} (\rho_a u_*^2 - \tau_{th}) dA_i \qquad (5.31)$$

where M_p is the aerodynamic lofting rate of dust from the particulate surface and the shear ($\rho_a u_*^2$) is determined by a

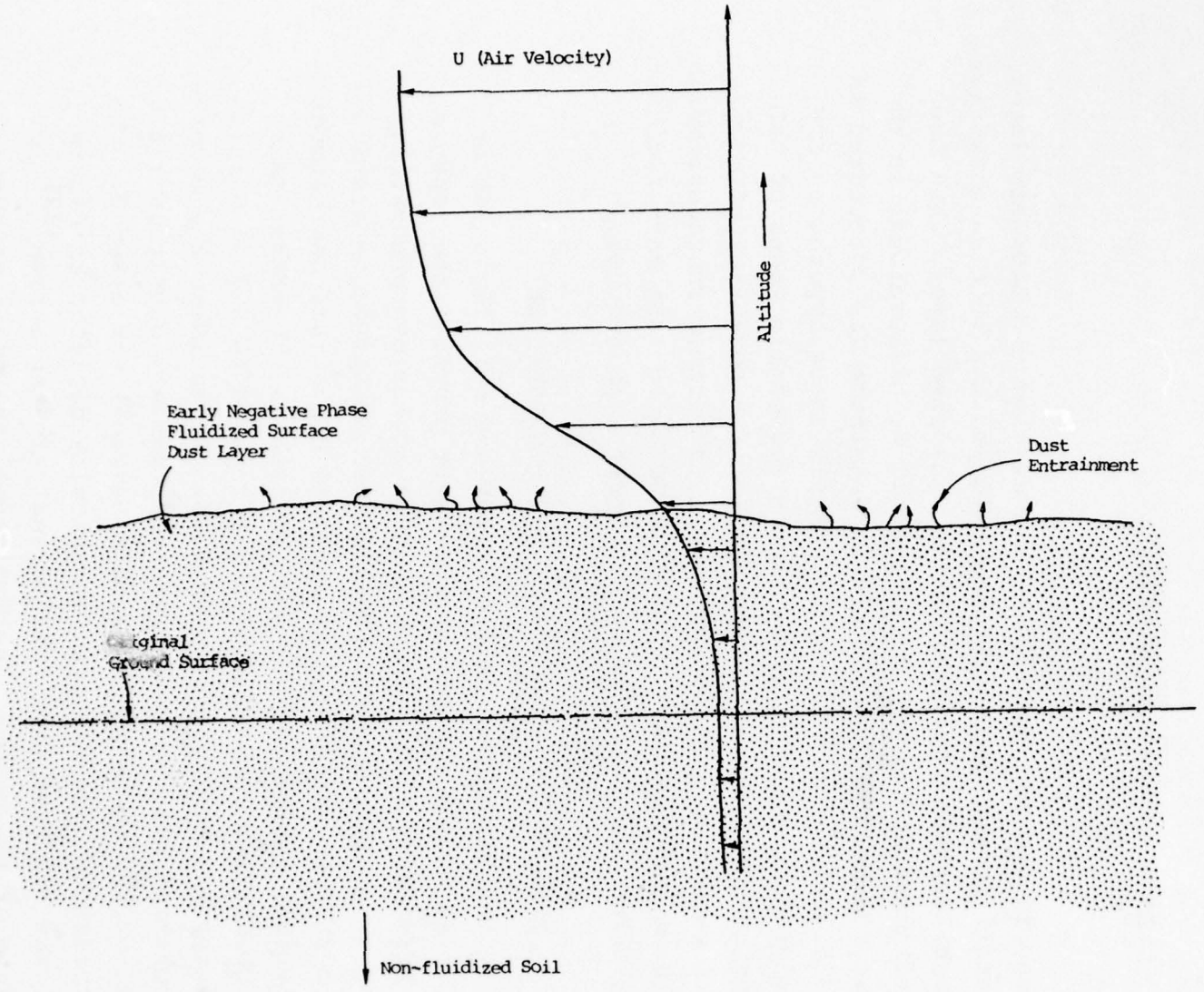

Figure 5.5. Schematic of new air-soil interface that results if surface soil is fluidized during reverse percolation.

rough-wall shear law for the so-called "perfectly rough" flow regime,

$$\frac{u_*}{U_e} = \frac{0.707}{\left(2.87 + 0.7 \ln \frac{x}{k_s}\right)} \tag{5.32}$$

Hence, if one may continue to assume that the boundary layer is still in the perfectly rough regime, and that an effective (rough) surface is buried in the fluidized layer, then the entrainment at the surface may still be proportional to the shear at the fluidized layer-air interface (as postulated in Eq. (5.31)). The SCOUR model, if all these hypotheses are appropriate, would still provide a reasonable means of calculating the negative phase mass lofting potential of nuclear blast wave flow fields. Presently, a minimum roughness height of 10 cm has been incorporated in SCOUR to take this fluidization effect (and surface modulations) into account.

5.4 FLUB CALCULATION – 1100 PSI OVERPRESSURE

The surprising degree of surface soil fluidization predicted at the 100 psi overpressure provided the impetus for additional FLUB calculations at higher overpressures. A representative case is the 1100 psi overpressure station for a 36.6 KT detonation at a 350 ft HOB. This corresponds to typical yields and HOB for NTS events. To better match NTS conditions, particle size was reduced to 0.1 mm particle diameter and soil porosity to 0.25. To maximize the reverse percolation effect, the "unvented" boundary condition (at a depth of 180 cm below the ground surface) was assumed. The overpressure time history, graphically depicted in Figure 5.6, was computed from Brode's analytic expression[37] for a range of 165 meters. As indicated, the positive phase is complete 0.3 seconds after air shock arrival. All other

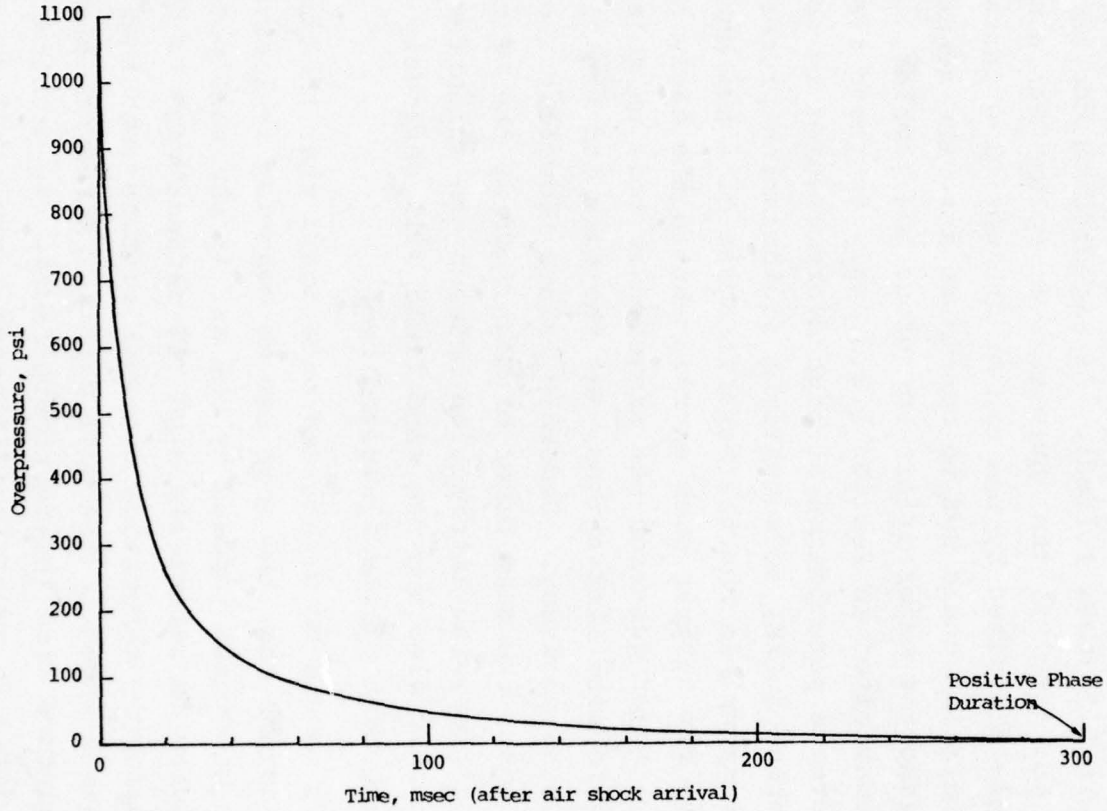

Figure 5.6. Overpressure time history at the 1100 psi overpressure station for a 36.6 KT detonation at 300 ft HOB, from Brode. [37]

aspects of the calculation were identical to the parameters and grid used in the preceding 100 psi test case.

The results for this FLUB calculation are presented in Figure 5.7 (soil altitude), Figure 5.8 (blowoff velocity), and Figure 5.9 (mass lofted). As expected on the basis of the 100 psi results, the unvented soil column was almost completely fluidized by the end of the positive phase, and the calculation could not be continued into the negative phase without a major effort to rezone the problem. The conclusions cited in Section 5.3.3 apply to these results; i.e., reverse percolation at high overpressures in cohesionless, porous soils, is actually a fluidization process that may be responsible for the establishment of a new boundary condition for surface dust entrainment in the early negative phase. A major question not answered in this calculation, due to grid size limitations, was the time for the fluidization process to decay. Secondly, since blowoff velocities are, at most, the same order of magnitude as the near-surface air velocities, the interaction between the subsurface (percolation) air flow and the wind field will seriously affect the development of the fluidized bed.

It should be emphasized once again that the present results assume that the soil has no cohesion (relative to the pressure gradients imposed by the air in the soil pores); that the porosity is relatively high (25 percent) and is distributed uniformly throughout the soil surface; and that there are no shock waves in the soil matrix. Moreover, because of the surface wind interaction effects, the problem should be considered in two space dimension. Nevertheless, these preliminary results give evidence that the general problem of (air) boundary layer interaction with a fluidized surface layer should be more closely studied.

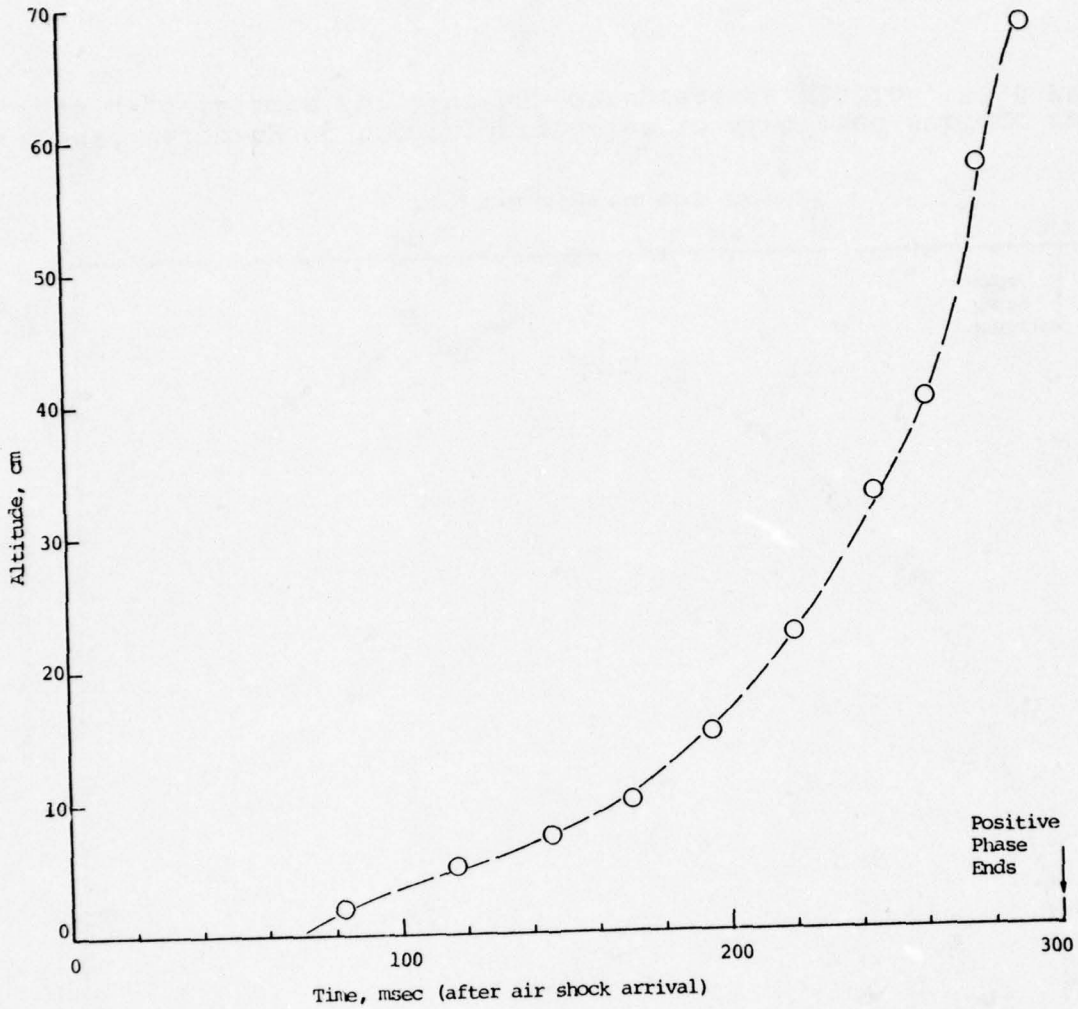

Figure 5.7. Maximum altitude of fluidized soil particles above the original ground surface, from FLUB calculations for 1100 psi overpressure station, 36.6 KT at 300 ft HOB.

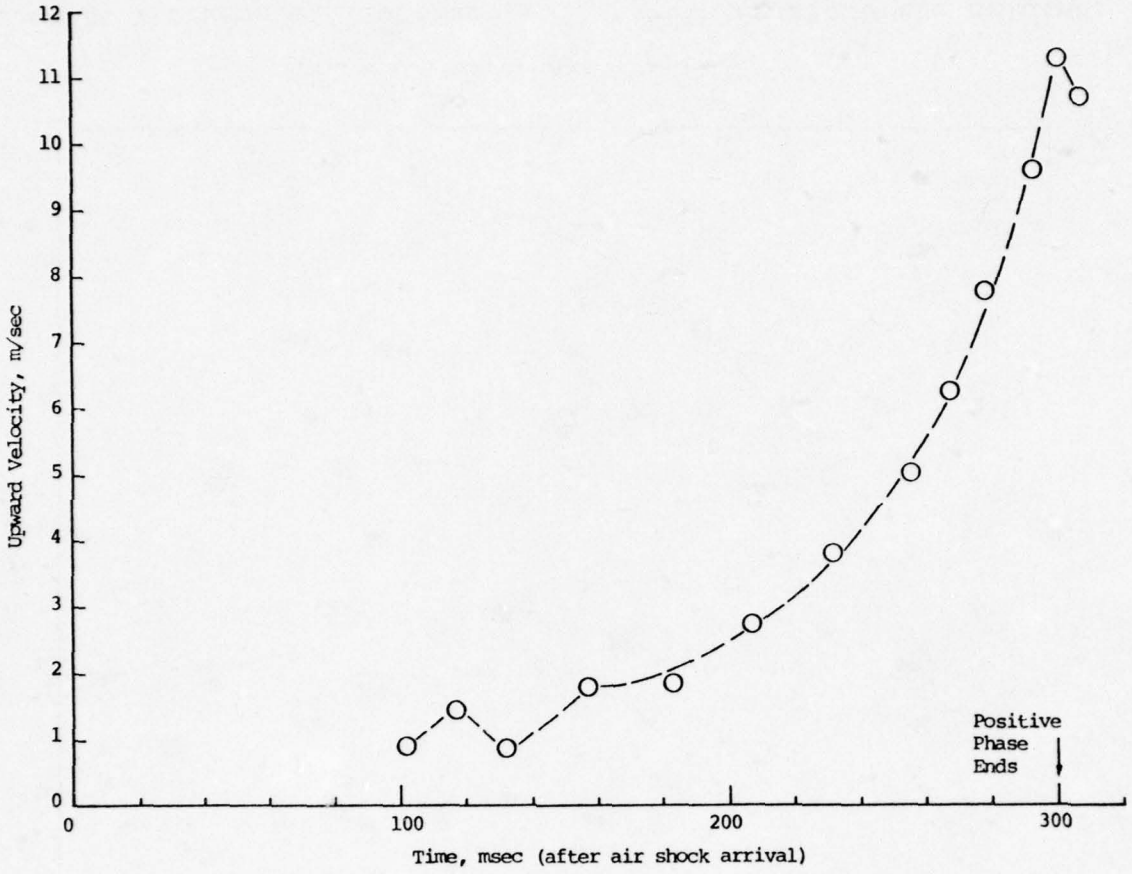

Figure 5.8. Upward velocity of topmost particles in fluidized surface region, from FLUB calculations for 1100 psi overpressure station, 36.6 KT at 300 ft HOB.

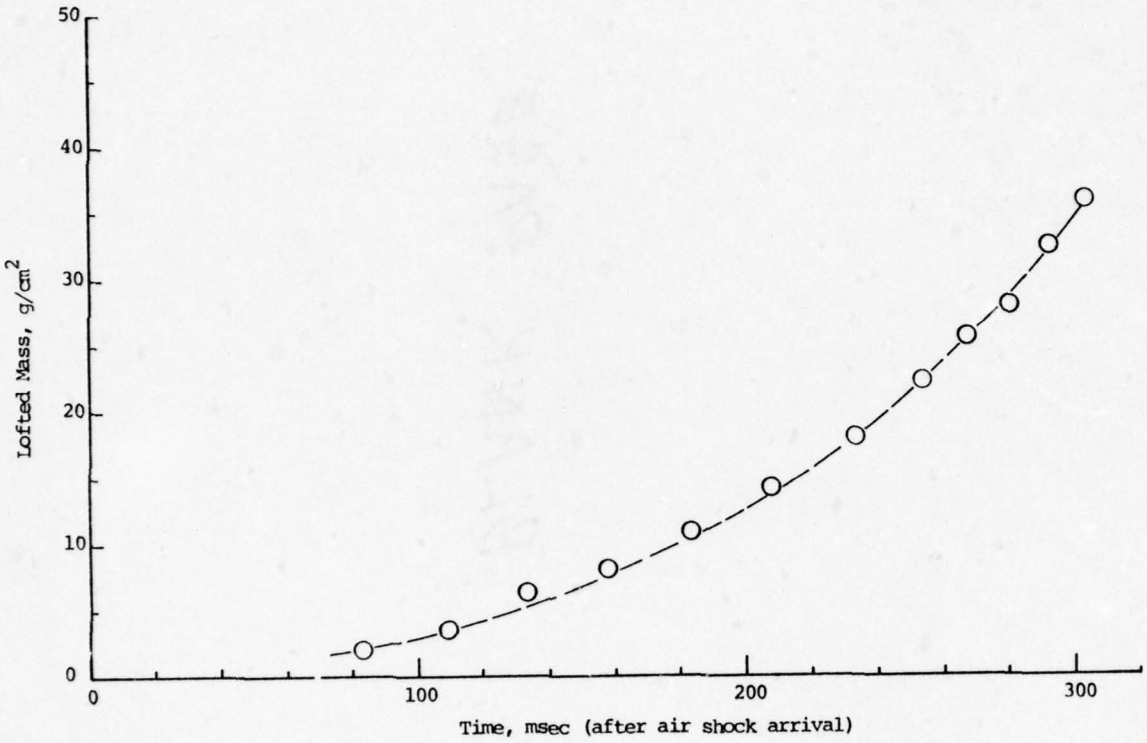

Figure 5.9. Mass of dust in fluidized surface layer above the original surface, from FLUB calculations for 1100 psi overpressure station, 36.6 KT at 300 ft HOB.

VI. REFERENCES

1. Kirsch, J. W., and J. E. Welch, "Dust Lofting Capabilities of Air Blast Wave Flow Fields," Systems, Science and Software Final Report. (Unpublished)

2. Kirsch, J. W., P. L. Anderson, and J. E. Welch, "The Dust Lofting Capacity of Surface Burst Air Blast Wave Flow Fields," Systems, Science and Software Final Report. (Unpublished)

3. Kirsch, J. W., M. H. Rice, P. L. Anderson, and E. W. Sims, "The Near-Surface Nuclear Dust Cloud," Systems, Science and Software Final Report, SSS-R-76-2818, DNA 3879F, Contract No. DNA 001-74-C-0190, December 1975.

4. Kirsch, J. W., M. H. Rice, P. L. Anderson, and E. W. Sims, "The Near-Surface Nuclear Dust Cloud," Systems, Science and Software Final Report, SSS-R-76-2827, DNA 3962F, Contract No. DNA 001-75-C-0198, April 1976.

5. Horrocks, M. J., B. H. Lieu, and R. W. Roig, "Effects of Dust Clouds on Microwave Communications," General Research Corporation, CR-1-416, WGRC 73-3247, for Defense Communications Agency under Contract DCA 100-73-C-0030.

6. Mansfield, J. E., W. M. Layson, R. T. Liner, and J. T. Powers, "HOB Effects on Dust Lofting Mechanisms," Science Applications, Inc., February 1975. (Unpublished)

7. Kirsch, J. W., letter dated 1 November 1973, to Mr. Steve Gutsche, Mission Research Corporation, Santa Barbara, California. Enclosures of surface burst dust cloud concentrations for input to GRC calculations with HARC code.

8. Zernow, L., N. Louie, W. H. Andersen, and P. A. Blatz, "An Experimental Study of the 'Reverse Percolation' Lofting Process in a Sand Medium," Shock Hydrodynamics Division of Whittaker Corporation Report No. DNA 3210F, November 16, 1973.

9. Scott, R. F., and Hon-Yim Ko, "Transient Rocket Engine Gas Flow in Soil," AIAA Journal, Vol. 6, No. 2, pp. 258-264.

10. Pritchett, J. W., "FLUB: A Numerical Procedure for Treating Dense Gas Particulate Mixture Dynamics," Volume 1, Systems, Science and Software Internal Report SSS-IR-74-2113, March 1974.

11. Pritchett, J. W., "Theoretical Calculations of Sand Lofting Due to Reverse Percolation," Systems, Science and Software Internal Report SSS-IR-74-2091, February 1974.

12. Owen, P. R., "Saltation of Uniform Grains in Air," J. Fluid Mechanics, Vol. 20, Part 2, pp. 225-242, 1964.

13. Layson, M. W., "Nuclear Surface Burst Debris and System Vulnerability," General Research Corporation, August 1969. (Unpublished)

14. Banister, J. R., and R. J. Emrich, "Preliminary Investigation of Dust Raised by Blast Waves (Operation Greasy Stake)," Sandia Report SC-3610-TR, Sandia Corporation, Albuquerque, New Mexico, January 3, 1955.

15. Gordon, M., et al., "Dust Density Versus Time and Distance in the Shock Wave," Army Chemical Warfare Laboratories, Project 1.13, WT-1113 (Operation Teapot), June 21, 1957.

16. Mansfield, J. E., et al., "Physical Mechanisms for Dust Generation by MIRV Weapons," Science Applications, Inc., September 1972. (Unpublished)

17. Hartenbaum, B., "Lofting of Particulates by a High Speed Wind," Applied Theory, Inc., September 1971, prepared for DNA under Contract DASA 01-70-C-0041, DNA-2737.

18. Carpenter, H. J., et al., "Blast Wave Boundary Layer Measurements," TRW Systems Group, AFWL-TR-73-211 (MIDDLE GUST, Event IV), March 1974.

19. Crawford, D. R., V. Quan, and J. T. Ohrenberger, "Blast Wave Turbulent Boundary Layers," Final Report, DNA 2768F, February 1972.

20. Mirels, H., "Boundary Layer Behind Shock or Thin Expansion Wave Moving into Stationary Fluid," NACA TN 3712, May 1956.

21. Ausherman, D. R., "Initial Dust Lofting: Shock Tube Experiments," TRW Systems Group, Redondo Beach, Ca., DNA 3162F, 11 September 1973.

22. Bagnold, R. A., The Physics of Blown Sand And Desert Dunes, Methuen and Company, Ltd., London, 1941.

23. Weinberger, R. K., and G. L. Adlon, "Particle Dislodgement and Entrainment by a Low Density Airstream Flowing Over a Surface," NASA CR 1119254, 6 August 1971.

24. Seebaugh, W. R., and J. A. Shannon, "Comparison of Recent Calculations of Sweep-up Dust Cloud Geometry with Nevada Test Site Photographic Data," memorandum, 14 March 1973, Science Applications, Inc.

25. Shannon, J., "Preshock Thermal Layer Formation and Dust Lofting by Nuclear Bursts," Science Applications, Inc. Report 73-549-AR, 8 October 1973.

26. Shannon, J., "Nuclear Precursor Phenomenology and Sweep-up Cloud Development," Science Applications, Inc. Progress Report SAI-73-585-AR, prepared for DNA under Contract DNA 001-74-C-0080, 31 December 1973.

27. Ganong, G. P., and W. A. Whitaker, "The Nuclear Blast Precursor," Air Force Weapons Laboratory, Kirtland Air Force Base, New Mexico, March 1969. (Unpublished)

28. Kirsch, J. W., "Dust Sweep-up Calculations using the SCOUR Code," Systems, Science and Software Topical Report, June 1973. (Unpublished)

29. McGahan, J. T., E. M. Diamond, W. M. Layson, J. A. Shannon, and W. R. Thomson, "The Modeling of Nuclear Clouds," General Research Corporation, Arlington, Virginia, DASA 2626, March 1971.

30. "Capabilities of Nuclear Weapons," Report DNA EM-1, Part I, Headquarters, DNA, Washington, D. C., July 1972. (Unpublished)

31. Freeman, D. E., A. H. Gibbs, P. Lieberman, P. Molmud, and P. J. O'Neill, "Dynamic Dust Measurements, MIDDLE GUST, Event II," TRW Systems Group, DNA 2882F, March 1, 1972.

32. Leech, J., P. Lieberman, J. P. O'Neill, A. H. Gibbs, and S. A. Pollack, "MIDDLE NORTH SERIES, MIXED COMPANY Event, Dynamic Dust Measurements," POR-6611, Project LN124, TRW Systems Group, Redondo Beach, Ca., Contract No. DNA 001-72-0188, 25 July 1973.

33. Banister, J. R., and R. J. Emrich, "Preliminary Investigation of Dust Raised by Blast Waves (Operation Greasy Stake)," Sandia Corporation Report SC-3610-TR, Albuquerque, New Mexico, January 3, 1955.

34. Garg, S. K., "Dynamics of Gas-Fluidized Beds," Systems, Science and Software Report SSS-IR-74-2097, February 1974.

35. Blake, T. R., S. K. Garg, H. B. Levine, and J. W. Pritchett, "Computer Modeling of Coal Gasification Reactors, Year 1," Systems, Science and Software Report SSS-R-76-2967, July 1976.

36. Jackson, R., "Fluid Mechanical Theory," Chapter 3 of Fluidization, J. F. Davidson and D. Harrison, eds., Academic Press, New York, 1971.

37. Brode, H. L., "Height of Burst Effects at High Overpressures," Rand Corporation Report RM-6301, DASA 2506, July 1970.

APPENDIX A

SCOUR2 INPUT

Card input for SCOUR2 contains the basic parameters necessary for a SCOUR calculation. All units are cgs.

1. RUN Parameters

CYCLE	= cycle to begin on.
TDUMP	= time to begin on.
YIELD	= yield in megatons.
HOB	= height of burst.
WC	= soil water content, mass fraction.
TND	= time to end on.

2. EDIT Parameters

NPRINT	= scale factor cycles between zone prints.
NDUMP	= scale factor cycles between restart tape dumps.
NPPRT	= scale factor cycles between particle prints.
NCPRT	= scale factor cycles between printer plots.

3. GRID Parameters

IMAX	= number of horizontal zones.
JMAX	= number of vertical zones.
DXZ	= zone width (constant in radial direction).
DYZ	= scaling factor for concentration (printer plots).
KEMAX	= scale factor for kinetic energy printer plots.
PEMAX	= scale factor for potential energy printer plots.
TEMAX	= scale factor for total energy printer plots.

DPMAX = scale factor for dynamic pressure printer plots.

CCMAX = scale factor for concentration ratio printer plots.

DPCMAX = scale factor for dynamic pressure ratio printer plots.

RHSOIL = density of soil.

RHOP = crystal density of soil particles.

GRAV = acceleration due to gravity (positive is downward).

GAMMA = time integration coefficient, shock lofting integral at shock front.

XSTART = range of first zone beyond crater.

4. No. of particles = number of particle sizes in the calculation.

Initial random number = initial number for random number subroutine.

5. PARTICLE Parameters

RCHAR = characteristic particle radius for which the roughness height (HBAR(I)) is calculated (positive phase).

RCHARN = RCHAR (negative phase).

RADZ(ND) = particle radius (for each size particle).

IFRONT = flag for creating first particle of size ND at shock front (0 = no, 1 = yes).

6. MASS LOFTING Parameters

DBAR = minimum roughness height.

FACN = boundary layer diffusion parameter for the negative phase.

FACP = boundary layer diffusion parameter for the positive phase.

SMALLA = fraction of mass of shock lofted SCOUR particle necessary to create wind-lofted SCOUR particle.

DELMAX = maximum altitude of the boundary layer.

ALPHA(ND) = scale factor in prescription of particle ejection velocity, particle size ND.

SMALLB(ND) = mass fraction of particle size ND.

XLAM(ND) = mass lofting coefficient of particle size ND.

7. CRATER LOFTING Parameters

PLM = mass represented by SCOUR crater particles.

RCR = crater radius.

DCR = crater depth.

FCRM = fraction of crater mass to be ejected.

YLOAD = maximum ejection altitude of crater particles at TDUMP.

VBAR = crater particle ejection velocity.

8. GLAB = alphanumeric label for the run.

SCOUR2 OUTPUT

1. Printout of the Input Parameters (Typical)

```
RUN PARAMETERS
     YIELD=  1.000+00
       HOB=  0.000
        WC=  0.000
       TND=  1.800+02

EDIT PARAMETERS
    NPRINT=    10
    NDUMP=    10
    NPPRT=    10
    NCPRT=    10

GRID PARAMETERS
      IMAX=    75
      JMAX=    20
       DXZ=  5.000+03
       DYZ=  1.000-03
     KEMAX=  1.000-03
     PEMAX=  1.000-03
     TEMAX=  1.000-03
     DPMAX=  1.000+05
     CCMAX=  1.000-03
    DPCMAX=  1.000+05
    RHSOIL=  1.800+00
      RHOP=  2.500+00
      GRAV=  9.800+02
     GAMMA=  1.000+00
    XSTART=  1.750+04
     ANGLE=  1.000+00

NO. OF PARTICLES=     1
INITIAL RANDOM NUMBER=           1

PARTICLE PARAMETERS
     RCHAR=  3.500-03
    RCHARN=  4.000-02
      RADZ=  5.000-03
    IFRONT=         1

MASS LOFTING PARAMETERS

      DBAR=  1.000+01
      FACN=  8.000-02
      FACP=  8.000-02
    SMALLA=  2.000-01
    DELMAX=  1.750+04
     ALPHA=  1.000+00
    SMALLB=  4.000-01
      XLAM=  1.000-01
```

```
APPLE 27

        CRATER LOFTING PARAMETERS
              PLM=  1.000+08
              RCR=  1.750+04
              DCR=  8.750+03
             FCRM=  2.000-02
            YLOAD=  1.000+02
             VBAR=  1.000+04

        CRATER LOFTING:     CRATER MASS= 9.4708+11     NO. OF PRELOADED PARTICLES=  189
```

Crater mass is the mass of dust that occupied the crater. The number of preloaded particles refers to the number of SCOUR2 particles used to represent the fraction of the crater mass that is to be tracked in the SCOUR2 calculation. The APPLE27 is the alphanumeric label for this particular run. Note that in this calculation only one particle size (radius = 5×10^{-3} cm) was assumed for the soil, and that since RCHAR, RCHARN were specified as different values, the characteristic roughness height ($\bar{h}$) was not dependent on the particle altitudes ($\bar{h}$ = DBAR). Furthermore, the radius of the crater particles is missing from this printout. It will be included in subsequent SCOUR2 input printouts.

2. Boundary Layer Information

APPLE 27

T= 3.0393+00 XS= 2.4919+05

I	UZ	DELTA	HBAR	VDIFF	USTAR	RHOZ	VZ	EDEPTH	SUMTOTSUM
2	1.8801+04	4.8370+02	1.0000+01	6.6131+00	2.0589+03	3.9240-06	1.4353+04	2.3746-02	2.6856+07
3	1.5501+04	4.2876+02	1.0000+01	4.9409+00	1.6937+03	3.7786-06	-1.3965+04	1.8454-02	2.6089+07
4	-1.0982+04	3.8113+02	1.0000+01	3.1827+00	1.2321+03	3.8792-06	-1.5358+04	2.9301-02	4.9708+07
5	-1.1174+04	3.2287+02	1.0000+01	2.8072+00	1.2968+03	4.1241-06	4.5200+03	3.7545-02	7.4309+07
6	-2.1728+03	9.5257+01	1.0000+01	1.6490-01	3.1061+02	4.2652-06	5.8111+03	2.2804-02	5.1582+07
7	2.6963+03	1.1130+02	1.0000+01	2.4495-01	3.7401+02	4.3901-06	4.4288+03	2.9969-02	7.6263+07
8	1.5783+03	7.5904+01	1.0000+01	1.0024-01	2.3630+02	4.8882-06	3.2414+03	4.7051-02	1.3303+08
9	2.3064+02	2.1701+01	1.0000+01	4.2956-03	4.8300+01	5.8394-06	2.6665+03	5.2210-02	1.6238+08
10	8.4230+01	1.0969+01	1.0000+01	8.1395-04	2.0753+01	7.4431-06	1.6165+03	6.4656-02	2.1937+08
11	-1.4774+03	7.2465+01	1.0000+01	9.6874-02	2.2339+02	9.9741-06	6.5896+02	4.6529-02	1.7103+08
12	-1.6151+03	9.0437+01	1.0000+01	1.3586-01	2.3054+02	1.5332-05	3.6501+02	2.9612-02	1.1801+08
13	-1.9389+03	8.7809+01	1.0000+01	1.6290-01	2.8170+02	2.2000-05	3.8517+02	7.5746-02	3.2125+08
14	-8.4725+02	4.9445+01	1.0000+01	4.1268-02	1.3974+02	2.8650-05	3.0646+02	5.7454-02	2.5992+08
15	-3.4440+02	6.5181+03	1.0000+01	2.2787+00	2.5198+01	3.6469-05	2.2719+02	6.9124-02	3.3225+08
16	-1.9934+02	1.7500+04	1.0000+01	3.6524+00	1.4618+01	5.0399-05	1.5329+02	9.1482-02	4.6559+08
17	-8.2499+02	1.0579+04	1.0000+01	9.4336+00	6.0637+01	6.7873-05	1.1514+02	9.5849-02	5.1492+08
18	-6.1736+02	1.7500+04	1.0000+01	1.2069+01	4.5486+01	8.5558-05	1.3110+02	5.6080-02	3.1712+08
19	7.1370+02	1.7500+04	1.0000+01	1.4491+01	5.2736+01	1.0843-04	1.4565+02	8.6426-02	5.1317+08
20	7.3529+02	1.7500+04	1.0000+01	1.5408+01	5.4450+01	1.4015-04	8.7983+01	7.0434-02	4.3812+08
21	8.8667+02	1.7500+04	1.0000+01	1.9272+01	6.5837+01	1.8113-04	8.4845+01	9.2593-02	6.0214+08
22	1.3211+03	1.7500+04	1.0000+01	2.9825+01	9.8365+01	2.3198-04	8.1955+01	8.5502-02	5.8021+08
23	1.6133+03	1.7500+04	1.0000+01	3.7891+01	1.2048+02	2.9251-04	7.6398+01	7.6601-02	5.4146+08
24	1.9308+03	1.7500+04	1.0000+01	4.7248+01	1.4462+02	3.6005-04	6.8260+01	6.5947-02	4.8460+08
25	2.2400+03	1.7500+04	1.0000+01	5.7214+01	1.6832+02	4.3235-04	6.4783+01	1.0087-01	7.7003+08
26	2.5820+03	1.3501+04	1.0000+01	5.3209+01	1.9467+02	5.0710-04	6.1871+01	6.1792-02	4.8920+08
27	2.9392+03	9.9608+03	1.0000+01	4.6832+01	2.2238+02	5.8232-04	9.4902+01	3.8581-02	3.1635+08
28	3.3115+03	7.4913+03	1.0000+01	4.1684+01	2.5147+02	6.5620-04	5.7736+01	9.1681-02	7.7767+0
29	3.7110+03	5.6846+03	1.0000+01	3.7328+01	2.8291+02	7.2732-04	5.7289+01	5.7068-02	5.0021+08
30	4.1546+03	4.3119+03	1.0000+01	3.3476+01	3.1803+02	7.9573-04	5.7346+01	6.6354-02	6.0036+08
31	4.6037+03	3.3278+03	1.0000+01	3.0329+01	3.5396+02	8.6023-04	5.7973+01	4.5448-02	4.2406+08
32	5.0783+03	2.5823+03	1.0000+01	2.7600+01	3.9228+02	9.2127-04	6.1123+01	9.6350-02	9.2624+08
33	5.6166+03	1.9845+03	1.0000+01	2.5040+01	4.3604+02	9.8013-04	6.2515+01	5.7992-02	5.7369+08
34	6.2294+03	1.5078+03	1.0000+01	2.2626+01	4.8622+02	1.0377-03	6.5813+01	6.3336-02	6.4469+08
35	6.8779+03	1.1474+03	1.0000+01	2.0491+01	5.3996+02	1.0928-03	7.1174+01	2.6724-02	2.7958+08
36	7.5599+03	8.7303+02	1.0000+01	1.8585+01	5.9727+02	1.1469-03	7.3373+01	4.1525-02	4.4615+08
37	8.2775+03	6.6214+02	1.0000+01	1.6857+01	6.5851+02	1.2007-03	7.9400+01	5.8299-02	6.4287+08
38	9.0327+03	4.9895+02	1.0000+01	1.5270+01	7.2411+02	1.2546-03	8.7210+01	5.0108-02	5.6671+08
39	9.8324+03	3.7178+02	1.0000+01	1.3787+01	7.9478+02	1.3094-03	9.0282+01	5.7950-02	6.7179+08
40	1.0681+04	2.7257+02	1.0000+01	1.2381+01	8.7199+02	1.3658-03	9.3220+01	6.5963-02	7.8332+08
41	1.1561+04	1.9813+02	1.0000+01	1.1054+01	9.5436+02	1.4237-03	1.0308+02	3.4936-02	4.2475+08
42	1.2419+04	1.3857+02	1.0000+01	9.8266+00	1.0386+03	1.4813-03	1.0695+02	2.6336-02	3.2764+08
43	1.3248+04	9.5145+01	1.0000+01	8.6852+00	1.1255+03	1.5382-03	1.1135+02	4.2250-02	5.3756+08
44	1.4207+04	6.1139+01	1.0000+01	7.5443+00	1.2309+03	1.6010-03	1.1918+02	3.3017-02	4.2942+08
45	1.5609+04	3.4341+01	1.0000+01	6.2962+00	1.3882+03	1.6850-03	1.2428+02	6.9507-03	9.2368+07
46	1.7442+04	1.5693+01	1.0000+01	4.9646+00	1.6130+03	1.7944-03	1.3466+02	1.2718-02	1.7261+08
47	1.8533+04	5.0930+00	1.0000+01	3.7553+00	1.8467+03	1.8765-03	1.3807+02	1.2975-02	1.7976+08
48	0.0000	0.0000	1.0000+01	0.0000	0.0000	0.0000	0.0000	0.0000	0.0000
49	0.0000	0.0000	1.0000+01	0.0000	0.0000	0.0000	0.0000	0.0000	0.0000
50	0.0000	0.0000	1.0000+01	0.0000	0.0000	0.0000	0.0000	0.0000	0.0000
51	0.0000	0.0000	1.0000+01	0.0000	0.0000	0.0000	0.0000	0.0000	0.0000

T = time (sec).
XS = shock front (cm).
UZ(I) - horizontal velocity of air at center of zone i (cm/sec).
DELTA(I) - boundary layer height for zone i (cm).
HBAR(I) - average height of particles in zone i (cm).
VDIFF(I) - extra diffusional velocity due to boundary layer growth in zone i (cm/sec).
USTAR(I) - shear velocity, zone i (cm/sec).
RHOZ(I) - air density of zone i (g/cm^3).
VZ(I) - vertical velocity of air at center of zone i (cm/sec).
EDEPTH(I) - erosion depth, zone i (cm).
SUMTOTSUM(I) - total mass (g) of all particle sizes lofted from zone i up to time T.

3. Mass Lofting Information

APPLE 27

T= 3.0393+00 XS= 2.4919+05

I	RZ	ENERZ	TAU	VZEROZ	DOTMZ	ZMASS	SUMZ	TOTSUM
2	2.0000+04	1.5365+12	1.6633+01	1.9673+03	1.9972+05	1.8636+07	-2.6389+06	2.6856+07
3	2.5000+04	1.5102+12	1.0840+01	1.2689+03	2.4361+05	1.8159+07	-1.0512+07	2.6089+07
4	3.0000+04	1.4992+12	5.8886+00	1.1228+03	1.6414+05	3.4261+07	-1.1866+07	4.9708+07
5	3.5000+04	1.4986+12	6.9351+00	9.0290+02	2.8911+05	4.9718+07	-1.4936+07	7.4309+07
6	4.0000+04	1.4746+12	4.1150-01	2.9438+02	0.0000	3.4356+07	2.2602+06	5.1582+07
7	4.5000+04	1.4150+12	6.1410-01	1.9308+02	0.0000	4.9278+07	7.4302+06	7.6263+07
8	5.0000+04	1.2909+12	2.7296-01	2.1658+02	0.0000	7.2931+07	-2.3477+07	1.3303+08
9	5.5000+04	1.0772+12	1.3623-02	4.2636+01	0.0000	1.1876+08	-6.4130+07	1.6236+08
10	6.0000+04	8.1642+11	3.2055-03	1.0885+01	0.0000	1.2609+08	-4.2209+07	2.1937+08
11	6.5000+04	5.7173+11	4.9773-01	1.6928+02	0.0000	7.4366+07	1.0996+06	1.7103+08
12	7.0000+04	3.8995+11	8.1489-01	2.0044+02	0.0000	8.3502+07	-1.2729+08	1.1801+08
13	7.5000+04	2.6703+11	1.7459+00	1.5945+02	4.4088+05	1.3519+08	-1.4963+07	3.2125+08
14	8.0000+04	1.8126+11	5.5946-01	1.2032+02	0.0000	1.2584+08	-1.2442+08	2.5992+08
15	8.5000+04	1.1969+11	2.3156-02	1.9343+01	0.0000	1.4427+08	-2.4668+07	3.3225+08
16	9.0000+04	7.9115+10	1.0769-02	1.2813+01	0.0000	1.7093+08	-2.0104+07	4.6559+08
17	9.5000+04	5.4981+10	2.4956-01	4.5894+01	0.0000	2.2065+08	-2.7868+08	5.1492+08
18	1.0000+05	3.7869+10	1.7702-01	2.6667+01	0.0000	2.4052+08	-2.1008+08	3.1712+08
19	1.0500+05	2.6020+10	3.0150-01	3.4608+01	0.0000	1.9819+08	-9.7580+07	5.1317+08
20	1.1000+05	1.8221+10	4.1553-01	3.3800+01	0.0000	1.9233+08	-1.0608+08	4.3812+08
21	1.1500+05	1.3118+10	7.8511-01	5.4586+01	0.0000	1.0418+08	-2.1058+07	6.0214+08
22	1.2000+05	9.7670+09	2.2446+00	8.8198+01	2.6598+06	2.1429+08	-4.8256+08	5.8021+08
23	1.2500+05	7.5607+09	4.2459+00	7.4350+01	8.5721+06	1.4037+08	-7.5214+07	5.4146+08
24	1.3000+05	6.0659+09	7.5308+00	8.9551+01	1.4892+07	1.5442+08	-1.1915+09	4.8480+08
25	1.3500+05	5.0325+09	1.2249+01	1.0761+02	2.2166+07	4.1376+08	-1.6908+08	7.7003+08
26	1.4000+05	4.3037+09	1.9210+01	1.4518+02	2.7595+07	1.5178+08	-6.9465+07	4.8920+08
27	1.4500+05	3.7812+09	2.8796+01	1.1716+02	5.4035+07	1.6739+08	-1.0113+08	3.1635+08
28	1.5000+05	3.4007+09	4.1496+01	2.3197+02	4.1134+07	2.0768+08	-2.1389+08	7.7767+08
29	1.5500+05	3.1259+09	5.8213+01	2.4245+02	5.7455+07	7.1335+07	-2.0544+07	5.0321+08
30	1.6000+05	2.9208+09	8.0484+01	2.7439+02	7.2802+07	1.4990+08	-5.3335+07	6.0036+08
31	1.6500+05	2.7673+09	1.0778+02	3.2135+02	8.6121+07	2.1729+08	-9.6462+07	4.2406+08
32	1.7000+05	2.6518+09	1.4177+02	3.1203+02	1.2047+08	1.5063+08	9.1548+06	9.2624+08
33	1.7500+05	2.5676+09	1.8635+02	3.1728+02	1.6059+08	1.5009+08	0.0000	5.7389+08
34	1.8000+05	2.5074+09	2.4532+02	3.5698+02	1.9352+08	1.9228+08	0.0000	6.4469+08
35	1.8500+05	2.4667+09	3.1861+02	5.2434+02	1.7603+08	1.1462+08	-2.4831+08	2.7958+08
36	1.9000+05	2.4396+09	4.0915+02	3.5196+02	3.4610+08	2.1284+08	-7.8111+07	4.4615+08
37	1.9500+05	2.4236+09	5.2066+02	4.9928+02	3.1801+08	1.5542+08	-1.1399+08	6.4287+08
38	2.0000+05	2.4168+09	6.5784+02	4.7222+02	4.3699+08	1.2426+08	-5.7363+07	5.6671+08
39	2.0500+05	2.4178+09	8.2754+02	5.3596+02	4.9659+08	2.2781+08	0.0000	6.7179+08
40	2.1000+05	2.4256+09	1.0385+03	5.1551+02	6.6308+08	1.1674+08	-2.3738+08	7.8332+08
41	2.1500+05	2.4389+09	1.2967+03	5.7232+02	7.6457+08	1.5137+08	-2.7338+08	4.2475+08
42	2.2000+05	2.4553+09	1.5970+03	1.0215+03	5.4019+08	1.0751+08	-2.6975+07	3.2764+08
43	2.2500+05	2.4738+09	1.9484+03	6.2966+02	1.0931+09	1.4673+08	-3.9084+08	5.3756+08
44	2.3000+05	2.4982+09	2.4257+03	1.2259+03	7.1458+08	1.7392+08	-2.5551+08	4.2942+08
45	2.3500+05	2.5366+09	3.2473+03	1.2370+03	7.7498+08	9.2368+07	0.0000	9.2368+07
46	2.4000+05	2.5888+09	4.6685+03	9.7200+02	1.4482+09	1.7261+08	0.0000	1.7261+08
47	2.4500+05	2.6222+09	6.3995+03	1.3061+03	1.5083+09	1.7976+08	0.0000	1.7976+08
48	2.5000+05	0.0000	0.0000	0.0000	0.0000	0.0000	0.0000	0.0000
49	2.5500+05	0.0000	0.0000	0.0000	0.0000	0.0000	0.0000	0.0000
50	2.6000+05	0.0000	0.0000	0.0000	0.0000	0.0000	0.0000	0.0000
51	2.6500+05	0.0000	0.0000	0.0000	0.0000	0.0000	0.0000	0.0000

T = time (sec).
XS = shock front location (cm).
RZ(I) - x coordinate of center of zone i (cm).
ENERZ(I) - energy of air in zone i (ergs/g).
TAU(I) - boundary layer shear (dynes/cm^2).
VZEROZ(I,ND)* - initial velocity of lofted particle size ND in zone i (cm/sec).
DOTMZ(I,ND)* - mass lofting rate for zone i and particle size ND (g/sec).
ZMASS(I,ND)* - mass to be lofted for particle size ND in zone i (g).
TOTSUM(I,ND)* - total mass lofted for particle size ND in zone i for all time (g).

*Note that in the present calculation only one particle size was aerodynamically lofted, and only one value of this variable is printed. Other calculations using four particles would have the values for each particle size, printed in columns below the first line of particle 1 values.

4. Particle Impact Information

APPLE 27

```
OLD CYCLE= 1388. OLD TIME=   3.2181+00 NEW CYCLE= 1423. NEW TIME=   3.3968+00 DT=   1.7878-01 SHOCK POSITION=   2.5842+05
                 NO OF IMPACTS=          16          TOTAL NO OF IMPACTS=          191
                 NO OF PARTICLES=         7          TOTAL NO. OF PARTICLES=       380
                 PARTICLES KILLED=        1          TOTAL PARTICLES KILLED=         2
RESTART DUMP AT T=   3.3968+00
OLD CYCLE= 1423. OLD TIME=   3.3968+00 NEW CYCLE= 1456. NEW TIME=   3.5756+00 DT=   1.7878-01 SHOCK POSITION=   2.6230+05
                 NO OF IMPACTS=          19          TOTAL NO OF IMPACTS=          210
                 NO OF PARTICLES=         7          TOTAL NO. OF PARTICLES=       387
                 PARTICLES KILLED=        0          TOTAL PARTICLES KILLED=         2
OLD CYCLE= 1456. OLD TIME=   3.5756+00 NEW CYCLE= 1489. NEW TIME=   3.7544+00 DT=   1.7878-01 SHOCK POSITION=   2.7202+05
                 NO OF IMPACTS=          20          TOTAL NO OF IMPACTS=          230
                 NO OF PARTICLES=         5          TOTAL NO. OF PARTICLES=       391
                 PARTICLES KILLED=        1          TOTAL PARTICLES KILLED=         3
OLD CYCLE= 1489. OLD TIME=   3.7544+00 NEW CYCLE= 1536. NEW TIME=   4.0226+00 DT=   1.7878-01 SHOCK POSITION=   2.8122+05
                 NO OF IMPACTS=          26          TOTAL NO OF IMPACTS=          256
                 NO OF PARTICLES=         6          TOTAL NO. OF PARTICLES=       397
                 PARTICLES KILLED=        0          TOTAL PARTICLES KILLED=         3
OLD CYCLE= 1536. OLD TIME=   4.0226+00 NEW CYCLE= 1582. NEW TIME=   4.2907+00 DT=   2.6817-01 SHOCK POSITION=   2.9064+05
                 NO OF IMPACTS=          28          TOTAL NO OF IMPACTS=          284
                 NO OF PARTICLES=         9          TOTAL NO. OF PARTICLES=       405
                 PARTICLES KILLED=        1          TOTAL PARTICLES KILLED=         4
OLD CYCLE= 1582. OLD TIME=   4.2907+00 NEW CYCLE= 1612. NEW TIME=   4.4695+00 DT=   2.6817-01 SHOCK POSITION=   3.0027+05
                 NO OF IMPACTS=          26          TOTAL NO OF IMPACTS=          310
                 NO OF PARTICLES=         7          TOTAL NO. OF PARTICLES=       412
                 PARTICLES KILLED=        0          TOTAL PARTICLES KILLED=         4
OLD CYCLE= 1612. OLD TIME=   4.4695+00 NEW CYCLE= 1654. NEW TIME=   4.7377+00 DT=   1.7878-01 SHOCK POSITION=   3.1160+05
                 NO OF IMPACTS=          27          TOTAL NO OF IMPACTS=          337
                 NO OF PARTICLES=         7          TOTAL NO. OF PARTICLES=       419
                 PARTICLES KILLED=        0          TOTAL PARTICLES KILLED=         4
OLD CYCLE= 1654. OLD TIME=   4.7377+00 NEW CYCLE= 1696. NEW TIME=   5.0059+00 DT=   2.6817-01 SHOCK POSITION=   3.2204+05
                 NO OF IMPACTS=          33          TOTAL NO OF IMPACTS=          370
                 NO OF PARTICLES=        11          TOTAL NO. OF PARTICLES=       430
                 PARTICLES KILLED=        0          TOTAL PARTICLES KILLED=         4
OLD CYCLE= 1696. OLD TIME=   5.0059+00 NEW CYCLE= 1748. NEW TIME=   5.3634+00 DT=   2.6817-01 SHOCK POSITION=   3.3397+05
                 NO OF IMPACTS=          37          TOTAL NO OF IMPACTS=          407
                 NO OF PARTICLES=        11          TOTAL NO. OF PARTICLES=       441
                 PARTICLES KILLED=        0          TOTAL PARTICLES KILLED=         4
OLD CYCLE= 1748. OLD TIME=   5.3634+00 NEW CYCLE= 1809. NEW TIME=   5.8104+00 DT=   3.5756-01 SHOCK POSITION=   3.4527+05
                 NO OF IMPACTS=          47          TOTAL NO OF IMPACTS=          454
```

OLD CYCLE - cycle number of previous cycle of hydro input.
NEW CYCLE - cycle number of subsequent cycle of hydro input.
OLD TIME - time of old cycle (since detonation), sec.
NEW TIME - time of new cycle (since detonation), sec.
DT - time between present old and previous old cycle, sec.
SHOCK POSITION - radial location of air shock at old time, cm.
NO. OF IMPACTS - number of particle impacts in dt.
NO. OF PARTICLES - number of particles created in dt.
PARTICLES KILLED - number of particles deposited in dt.
TOTAL NO. OF IMPACTS - total number of particle impacts recorded between 0 and old time.
TOTAL NO. OF PARTICLES - total number of particles created between 0 and old time.
TOTAL PARTICLES KILLED - total number of particles deposited between 0 and old time.

5. Sweepup Dust Cloud Structure

APPLE 27

T= 3.2181+00

TOTAL MASS= 2.5617+10 SIZE-1= 1.8057+10 SIZE-2= 0.0000 SIZE-3= 0.0000 SIZE-4= 0.0000

PKILL1= 0.0000 PKILL2= 2.5765+07

I	RZ	TOTMAS	SUMS1	SUMS2	SUMS3	SUMS4	YMAX1	YMAX2	YMAX3	YMAX4
1	0.0000	0.0000	0.0000	0.0000	0.0000	0.0000	0.0000	0.0000	0.0000	0.0000
2	2.0000+04	0.0000	0.0000	0.0000	0.0000	0.0000	0.0000	0.0000	0.0000	0.0000
3	2.5000+04	0.0000	0.0000	0.0000	0.0000	0.0000	0.0000	0.0000	0.0000	0.0000
4	3.0000+04	1.4539+07	1.4539+07	0.0000	0.0000	0.0000	3.0231+03	0.0000	0.0000	0.0000
5	3.5000+04	0.0000	0.0000	0.0000	0.0000	0.0000	0.0000	0.0000	0.0000	0.0000
6	4.0000+04	6.8975+06	6.8975+06	0.0000	0.0000	0.0000	7.4746+03	0.0000	0.0000	0.0000
7	4.5000+04	0.0000	0.0000	0.0000	0.0000	0.0000	0.0000	0.0000	0.0000	0.0000
8	5.0000+04	0.0000	0.0000	0.0000	0.0000	0.0000	0.0000	0.0000	0.0000	0.0000
9	5.5000+04	2.9330+07	2.9330+07	0.0000	0.0000	0.0000	4.7069+03	0.0000	0.0000	0.0000
10	6.0000+04	2.6491+07	2.6491+07	0.0000	0.0000	0.0000	9.3518+02	0.0000	0.0000	0.0000
11	6.5000+04	1.5125+07	1.5125+07	0.0000	0.0000	0.0000	3.2481+02	0.0000	0.0000	0.0000
12	7.0000+04	1.0329+07	1.0329+07	0.0000	0.0000	0.0000	3.8283+03	0.0000	0.0000	0.0000
13	7.5000+04	5.2744+07	5.2744+07	0.0000	0.0000	0.0000	6.3650+03	0.0000	0.0000	0.0000
14	8.0000+04	0.0000	0.0000	0.0000	0.0000	0.0000	0.0000	0.0000	0.0000	0.0000
15	8.5000+04	1.2346+08	1.2346+08	0.0000	0.0000	0.0000	1.0067+04	0.0000	0.0000	0.0000
16	9.0000+04	3.4927+07	3.4927+07	0.0000	0.0000	0.0000	5.7997+03	0.0000	0.0000	0.0000
17	9.5000+04	4.4220+07	4.4220+07	0.0000	0.0000	0.0000	1.0000-06	0.0000	0.0000	0.0000
18	1.0000+05	4.5859+07	4.5859+07	0.0000	0.0000	0.0000	6.8439+02	0.0000	0.0000	0.0000
19	1.0500+05	1.0066+08	1.0066+08	0.0000	0.0000	0.0000	1.0077+04	0.0000	0.0000	0.0000
20	1.1000+05	2.6221+08	2.6221+08	0.0000	0.0000	0.0000	7.4949+03	0.0000	0.0000	0.0000
21	1.1500+05	1.2170+08	1.2170+08	0.0000	0.0000	0.0000	3.5994+03	0.0000	0.0000	0.0000
22	1.2000+05	2.5215+08	2.5215+08	0.0000	0.0000	0.0000	1.7639+04	0.0000	0.0000	0.0000
23	1.2500+05	2.2604+08	2.2604+08	0.0000	0.0000	0.0000	1.4532+04	0.0000	0.0000	0.0000
24	1.3000+05	7.0147+08	7.0147+08	0.0000	0.0000	0.0000	1.4529+04	0.0000	0.0000	0.0000
25	1.3500+05	2.3289+08	2.3289+08	0.0000	0.0000	0.0000	1.1566+04	0.0000	0.0000	0.0000
26	1.4000+05	8.1009+08	8.1009+08	0.0000	0.0000	0.0000	1.1295+04	0.0000	0.0000	0.0000
27	1.4500+05	4.6990+08	4.6990+08	0.0000	0.0000	0.0000	9.4128+03	0.0000	0.0000	0.0000
28	1.5000+05	1.0179+09	1.0179+09	0.0000	0.0000	0.0000	8.3882+03	0.0000	0.0000	0.0000
29	1.5500+05	6.7194+08	6.7194+08	0.0000	0.0000	0.0000	7.4149+03	0.0000	0.0000	0.0000
30	1.6000+05	1.1792+09	1.1792+09	0.0000	0.0000	0.0000	7.5549+03	0.0000	0.0000	0.0000
31	1.6500+05	6.7654+08	6.7654+08	0.0000	0.0000	0.0000	6.2833+03	0.0000	0.0000	0.0000
32	1.7000+05	1.0239+09	1.0239+09	0.0000	0.0000	0.0000	5.3943+03	0.0000	0.0000	0.0000
33	1.7500+05	9.8295+08	9.8295+08	0.0000	0.0000	0.0000	4.7917+03	0.0000	0.0000	0.0000
34	1.8000+05	7.1362+08	7.1362+08	0.0000	0.0000	0.0000	4.5837+03	0.0000	0.0000	0.0000
35	1.8500+05	7.5863+08	7.5863+08	0.0000	0.0000	0.0000	4.0823+03	0.0000	0.0000	0.0000
36	1.9000+05	2.3223+09	9.2229+08	0.0000	0.0000	0.0000	3.7944+03	0.0000	0.0000	0.0000
37	1.9500+05	4.3871+09	6.6712+08	0.0000	0.0000	0.0000	3.3003+03	0.0000	0.0000	0.0000
38	2.0000+05	2.3588+09	6.3881+08	0.0000	0.0000	0.0000	3.2310+03	0.0000	0.0000	0.0000
39	2.0500+05	1.7381+09	1.0981+09	0.0000	0.0000	0.0000	3.0321+03	0.0000	0.0000	0.0000
40	2.1000+05	5.7975+08	5.7975+08	0.0000	0.0000	0.0000	2.5460+03	0.0000	0.0000	0.0000
41	2.1500+05	7.0259+08	7.0259+08	0.0000	0.0000	0.0000	5.3905+02	0.0000	0.0000	0.0000
42	2.2000+05	5.4758+08	5.4758+08	0.0000	0.0000	0.0000	2.2842+03	0.0000	0.0000	0.0000
43	2.2500+05	7.5051+08	6.7051+08	0.0000	0.0000	0.0000	1.9805+03	0.0000	0.0000	0.0000
44	2.3000+05	6.0006+08	6.0006+08	0.0000	0.0000	0.0000	1.6303+03	0.0000	0.0000	0.0000
45	2.3500+05	0.0000	0.0000	0.0000	0.0000	0.0000	0.0000	0.0000	0.0000	0.0000
46	2.4000+05	2.5888+08	2.5888+08	0.0000	0.0000	0.0000	1.2121+03	0.0000	0.0000	0.0000
47	2.4500+05	3.2064+08	3.2064+08	0.0000	0.0000	0.0000	9.0899+02	0.0000	0.0000	0.0000
48	2.5000+05	4.4474+08	4.4474+08	0.0000	0.0000	0.0000	2.7917+02	0.0000	0.0000	0.0000
49	2.5500+05	0.0000	0.0000	0.0000	0.0000	0.0000	0.0000	0.0000	0.0000	0.0000
50	2.6000+05	0.0000	0.0000	0.0000	0.0000	0.0000	0.0000	0.0000	0.0000	0.0000
51	2.6500+05	0.0000	0.0000	0.0000	0.0000	0.0000	0.0000	0.0000	0.0000	0.0000

J	YZP	TOTMAS	MASS ABOVE	SUMS1	SUMS2	SUMS3	SUMS4
1	5.0000+01	3.1366+09	2.2480+10	3.1366+09	0.0000	0.0000	0.0000
2	1.0000+02	7.4912+08	2.1731+10	7.4912+08	0.0000	0.0000	0.0000
3	2.0000+02	8.4996+08	2.0882+10	8.4996+08	0.0000	0.0000	0.0000
4	3.0000+02	7.0936+08	2.0172+10	7.0936+08	0.0000	0.0000	0.0000
5	4.0000+02	5.6467+08	1.9608+10	5.6467+08	0.0000	0.0000	0.0000
6	5.0000+02	0.0000	1.9608+10	0.0000	0.0000	0.0000	0.0000
7	1.0000+03	1.6939+09	1.7914+10	1.6939+09	0.0000	0.0000	0.0000
8	2.0000+03	2.5145+09	1.5399+10	2.5145+09	0.0000	0.0000	0.0000
9	3.0000+03	1.4244+09	1.3975+10	1.4244+09	0.0000	0.0000	0.0000
10	5.0000+03	3.4960+09	1.0479+10	3.4960+09	0.0000	0.0000	0.0000
11	1.0000+04	2.5049+09	7.9739+09	2.5049+09	0.0000	0.0000	0.0000
12	2.0000+04	4.1392+08	7.5600+09	4.1392+08	0.0000	0.0000	0.0000
13	3.0000+04	5.1600+09	2.4000+09	0.0000	0.0000	0.0000	0.0000
14	5.0000+04	2.4000+09	-2.0800+04	0.0000	0.0000	0.0000	0.0000
15	1.0000+05	0.0000	-2.0800+04	0.0000	0.0000	0.0000	0.0000
16	2.0000+05	0.0000	-2.0800+04	0.0000	0.0000	0.0000	0.0000
17	3.0000+05	0.0000	-2.0800+04	0.0000	0.0000	0.0000	0.0000
18	5.0000+05	0.0000	-2.0800+04	0.0000	0.0000	0.0000	0.0000
19	1.0000+06	0.0000	-2.0800+04	0.0000	0.0000	0.0000	0.0000
20	1.5000+06	0.0000	-2.0800+04	0.0000	0.0000	0.0000	0.0000

For time T, total mass of aerodynamically lofted dust in the grid is printed, with mass of dust for each individual particle size also indicated.

PKILL1, PKILL2 - amount of mass deposited (using two particle deposition routines).
RZ(I) - x coordinate of center of zone i.
TOTMASS(I) - total dust mass in zone i for all j.
SUMS1(I) - mass of dust particles, size 1, in zone i for all j.
SUMS2(I) - mass of dust particles, size 2, in zone i for all j.
SUMS3(I) - mass of dust particles, size 3, in zone i for all j.
SUMS4(I) - mass of dust particles, size 4, in zone i for all j.
YMAX1(I) - y coordinate of maximum height reached by particle size 1.
YMAX2(I) - y coordinate of maximum height reached by particle size 2.
YMAX3(I) - y coordinate of maximum height reached by particle size 3.
YMAX4(I) - y coordinate of maximum height reached by particle size 4.
YZP(J) - y coordinate of top of vertical zone j.
TOTMASS(J) - total dust mass in zone j, for all i.
MASS ABOVE - total dust mass above zone j for all i.
SUMS1(J) - mass of dust particles, size 1, in zone j for all i.
SUMS2(J) - mass of dust particles, size 2, in zone j for all i.
SUMS3(J) - mass of dust particles, size 3, in zone j for all i.
SUMS4(J) - mass of dust particles, size 4, in zone j for all i.

6. Grid Dust Concentrations (Aerodynamically Lofted Dust)

APPLE 27

T= 3.2181+00

I	J	RZ	YZP	CONCENT	PARTS	SIZE-1	SIZE-2	SIZE-3	SIZE-4	DYN PR	HOR DYN
4	1	3.000+04	5.000+01	1.458-04	1.000+00	1.458-04	0.000	0.000	0.000	3.094+03	0.000
4	8	3.000+04	2.000+03	4.141-06	1.000+00	4.141-06	0.000	0.000	0.000	2.985+02	2.806+02
4	10	3.000+04	5.000+03	1.998-06	1.000+00	1.998-06	0.000	0.000	0.000	8.791+01	8.672+01
6	11	4.000+04	1.000+04	1.098-06	1.000+00	1.098-06	0.000	0.000	0.000	2.551+01	1.742+01
9	9	5.500+04	3.000+03	8.621-06	1.000+00	8.621-06	0.000	0.000	0.000	2.985+01	2.886-01
9	10	5.500+04	5.000+03	4.177-06	2.000+00	4.177-06	0.000	0.000	0.000	4.455+00	4.906-01
10	7	6.000+04	1.000+03	2.811-05	1.000+00	2.811-05	0.000	0.000	0.000	3.229+01	1.553+01
11	5	6.500+04	4.000+02	7.407-05	1.000+00	7.407-05	0.000	0.000	0.000	1.023+02	8.934+01
12	10	7.000+04	5.000+03	2.348-06	1.000+00	2.348-06	0.000	0.000	0.000	2.244+00	2.193+00
13	4	7.500+04	3.000+02	1.208-04	1.000+00	1.208-04	0.000	0.000	0.000	1.997+02	1.833+02
13	7	7.500+04	1.000+03	1.333-05	1.000+00	1.333-05	0.000	0.000	0.000	2.432+01	2.259+01
13	11	7.500+04	1.000+04	7.280-07	1.000+00	7.280-07	0.000	0.000	0.000	8.247-01	7.876-01
15	1	8.500+04	5.000+01	2.242-04	1.000+00	2.242-04	0.000	0.000	0.000	6.145-02	5.276-02
15	3	8.500+04	2.000+02	1.086-04	1.000+00	1.086-04	0.000	0.000	0.000	1.967-01	1.964-01
15	8	8.500+04	2.000+03	1.292-05	1.000+00	1.292-05	0.000	0.000	0.000	1.839-01	1.518-01
15	9	8.500+04	3.000+03	5.695-06	1.000+00	5.695-06	0.000	0.000	0.000	1.356-01	1.052-01
15	11	8.500+04	1.000+04	8.086-07	1.000+00	8.086-07	0.000	0.000	0.000	1.863-02	6.098-03
15	12	8.500+04	2.000+04	1.508-07	1.000+00	1.508-07	0.000	0.000	0.000	4.645-02	5.884-03
16	10	9.000+04	5.000+03	3.170-06	1.000+00	3.170-06	0.000	0.000	0.000	1.805-02	1.616-02
16	11	9.000+04	1.000+04	1.203-06	1.000+00	1.203-06	0.000	0.000	0.000	1.134-02	8.103-03
17	1	9.500+04	5.000+01	2.963-04	1.000+00	2.963-04	0.000	0.000	0.000	5.030-02	0.000
18	7	1.000+05	1.000+03	2.919-05	1.000+00	2.919-05	0.000	0.000	0.000	2.342-01	2.341-01
19	1	1.050+05	5.000+01	2.622-04	1.000+00	2.622-04	0.000	0.000	0.000	5.630-02	0.000
19	11	1.050+05	1.000+04	2.645-06	1.000+00	2.645-06	0.000	0.000	0.000	2.356-01	2.147-01
19	12	1.050+05	2.000+04	4.182-07	1.000+00	4.182-07	0.000	0.000	0.000	8.682-02	6.218-02
20	1	1.100+05	5.000+01	2.368-04	1.000+00	2.368-04	0.000	0.000	0.000	8.092-02	1.969-02
20	7	1.100+05	1.000+03	4.433-05	1.000+00	4.433-05	0.000	0.000	0.000	5.152-01	5.139-01
20	11	1.100+05	1.000+04	8.374-06	4.000+00	8.374-06	0.000	0.000	0.000	8.074-01	7.602-01
21	1	1.150+05	5.000+01	1.413-04	1.000+00	1.413-04	0.000	0.000	0.000	6.076-02	5.227-03
21	10	1.150+05	5.000+03	1.331-05	2.000+00	1.331-05	0.000	0.000	0.000	9.881-01	9.781-01
22	1	1.200+05	5.000+01	3.145-04	1.000+00	3.145-04	0.000	0.000	0.000	4.695-02	0.000
22	3	1.200+05	2.000+02	6.212-05	1.000+00	6.212-05	0.000	0.000	0.000	4.558-01	4.368-01
22	5	1.200+05	4.000+02	8.945-05	1.000+00	8.945-05	0.000	0.000	0.000	1.496+00	1.496+00
22	7	1.200+05	1.000+03	2.429-05	1.000+00	2.429-05	0.000	0.000	0.000	8.224-01	8.209-01
22	10	1.200+05	5.000+03	7.050-06	1.000+00	7.050-06	0.000	0.000	0.000	1.689+00	1.657+00
22	12	1.200+05	2.000+04	9.760-07	2.000+00	9.760-07	0.000	0.000	0.000	1.101+00	8.215-01
23	1	1.250+05	5.000+01	1.594-04	1.000+00	1.594-04	0.000	0.000	0.000	3.298-02	0.000
23	3	1.250+05	2.000+02	1.918-04	2.000+00	1.918-04	0.000	0.000	0.000	1.728+00	1.685+00
23	7	1.250+05	1.000+03	2.451-05	1.000+00	2.451-05	0.000	0.000	0.000	1.622+00	1.616+00
23	11	1.250+05	1.000+04	1.886-06	1.000+00	1.886-06	0.000	0.000	0.000	7.510-01	7.412-01
23	12	1.250+05	2.000+04	8.725-07	1.000+00	8.725-07	0.000	0.000	0.000	1.092+00	9.514-01
24	1	1.300+05	5.000+01	7.440-04	1.000+00	7.440-04	0.000	0.000	0.000	9.582-01	0.000
24	5	1.300+05	4.000+02	1.009-04	1.000+00	1.009-04	0.000	0.000	0.000	3.533+00	3.519+00
24	8	1.300+05	2.000+03	3.488-05	2.000+00	3.488-05	0.000	0.000	0.000	5.257+00	5.231+00
24	10	1.300+05	5.000+03	2.687-05	4.000+00	2.687-05	0.000	0.000	0.000	1.110+01	1.100+01
24	11	1.300+05	1.000+04	3.054-06	1.000+00	3.054-06	0.000	0.000	0.000	1.785+00	1.755+00
24	12	1.300+05	2.000+04	2.059-06	2.000+00	2.059-06	0.000	0.000	0.000	3.161+00	2.918+00
25	1	1.350+05	5.000+01	4.173-04	1.000+00	4.173-04	0.000	0.000	0.000	6.690-01	0.000
25	8	1.350+05	2.000+03	8.559-06	1.000+00	8.559-06	0.000	0.000	0.000	1.329+00	1.319+00
25	11	1.350+05	1.000+04	2.773-06	1.000+00	2.773-06	0.000	0.000	0.000	1.985+00	1.967+00

RZ(I) - x coordinate of center of zone i, cm.
YZP(J) - y coordinate of top of vertical zone j, cm.
CONCENT(I,J)- concentration of all dust particles in zone i, j, g/cc.
PARTS(I,J) - number of representative particles in zone i, j, g/cc.
SIZE-1(I,J) - concentration for dust particles, size 1, in zone i, j, g/cc.
SIZE-2(I,J) - concentration for dust particles, size 2, in zone i, j, g/cc.
SIZE-3(I,J) - concentration for dust particles, size 3, in zone i, j, g/cc.
SIZE-4(I,J) - concentration for dust particles, size 4, in zone i, j, g/cc.
DYN PR(I,J) - dynamic pressure of all dust in zone i, j, ergs/cc.
HOR DYN(I,J)- horizontal dynamic pressure of all dust in zone i, j, ergs/cc.

7. Concentration Level Printer Plots – All Dust

```
APPLE 27

CONCENTRATION LEVELS.  8=   1.00-03 T=   3.2181+00        HALF DECADE INTEGER PLOTS
   1.5000+06
   1.0000+06
   5.0000+05
   3.0000+05
   2.0000+05
   1.0000+05
   5.0000+04                                    3321   1
   3.0000+04                                    3443
   2.0000+04           1  1   11222
   1.0000+04     2      1 12  23  2223434444
   5.0000+03   2    2  2   2    43 4 444444 4444444
   3.0000+03        3     3          4 4 44   4  45  4
   2.0000+03   2          4        43  444 554 5      44 4
   1.0000+03         4  4    4 4 44  5   4     5 55 5     5
   5.0000+02
   4.0000+02          5          5 6    6  6 6
   3.0000+02            6            6      6     6        7
   2.0000+02              6      56    6   656   6  6
   1.0000+02                             7  6   8 7
   5.0000+01   6          6 6 66666766 666 7667 66777787
                         +         +         +         +         +         +         +
                                 1.1000+05           2.1000+05           3.1000+05
```

YZP(J) versus RZ(I) representation of the grid.

Shows concentration for all particle sizes for a zone i, j, where, for C_{ij} = *dust concentration* (g/cc),

8 means $10^{-3} \leq C_{ij} \leq 5 \times 10^{-3}$

7 means $5 \times 10^{-4} \leq C_{ij} \leq 10^{-3}$

6 means $10^{-4} \leq C_{ij} \leq 5 \times 10^{-4}$

5 means $5 \times 10^{-5} \leq C_{ij} \leq 10^{-4}$

4 means $10^{-5} \leq C_{ij} \leq 5 \times 10^{-5}$

3 means $5 \times 10^{-6} \leq C_{ij} \leq 10^{-5}$

2 means $10^{-6} \leq C_{ij} \leq 5 \times 10^{-6}$

1 means $5 \times 10^{-7} \leq C_{ij} \leq 10^{-6}$

0 means $C_{ij} = 0.0$

} Half Decade Integer Plots

8. Concentration Levels for Particle Size 1

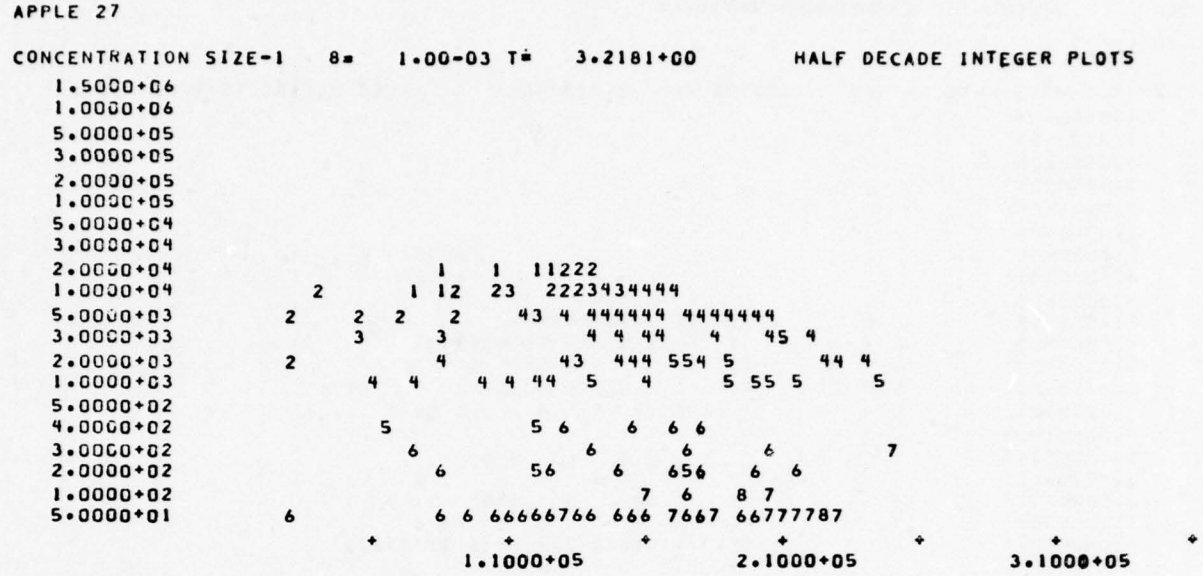

YZP(J) versus RZ(I) representation of the grid.

Shows concentrations for particle size 1 in zone i,j, where, for C_{ij} = dust concentration (g/cc),

8 means $10^{-3} \leq C_{ij} \leq 5 \times 10^{-3}$

7 means $5 \times 10^{-4} \leq C_{ij} \leq 10^{-3}$

6 means $10^{-4} \leq C_{ij} \leq 5 \times 10^{-4}$

5 means $5 \times 10^{-5} \leq C_{ij} \leq 10^{-4}$

4 means $10^{-5} \leq C_{ij} \leq 5 \times 10^{-5}$

3 means $5 \times 10^{-6} \leq C_{ij} \leq 10^{-5}$

2 means $10^{-6} \leq C_{ij} \leq 5 \times 10^{-6}$

1 means $5 \times 10^{-7} \leq C_{ij} \leq 10^{-6}$

0 means $C_{ij} = 0.0$

} Half Decade Integer Plots

Note that in calculations where more than one particle size is aerodynamically lofted, a plot for each particle size would be printed.

9. Dynamic Pressure Levels

```
APPLE 27

DYNAMIC PRES LEVELS.  8=   1.00+05 T=   3.2181+00       FULL DECADE INTEGER PLOTS
   1.5000+06
   1.0000+06
   5.0000+05
   3.0000+05
   2.0000+05
   1.0000+05
   5.0000+04                                          6655   5
   3.0000+04                                          6666
   2.0000+04                    1   1  33334
   1.0000+04          4       2 11  22  2333444555
   5.0000+03        4   3  3    1    23 4 345455 5555555
   3.0000+03          4     2           4 4 55   5   66 6
   2.0000+03        5           2          33  444 555 6      66 6
   1.0000+03             4  4     2 2 23  4    4     6 66 6     7
   5.0000+02
   4.0000+02               5           3 3    4  5 6
   3.0000+02                  5              3      5     6         7
   2.0000+02                    2       23     4   445   5  6
   1.0000+02                                  5  5   6 6
   5.0000+01        6           1 1 11111222 232 4445 33333333
                       +          +          +          +          +          +
                                1.1000+05           2.1000+05           3.1000+05
```

YZP(J) versus RZ(I) representation of the grid.

Shows dynamic pressure levels for all particle sizes in zone i, j, where dp_{ij} is the dynamic pressure (ergs/cc),

8 means $10^5 \leq dp_{ij} \leq 10^6$

7 means $10^4 \leq dp_{ij} \leq 10^5$

6 means $10^3 \leq dp_{ij} \leq 10^4$

5 means $10^2 \leq dp_{ij} \leq 10^3$

4 means $10^1 \leq dp_{ij} \leq 10^2$

3 means $1 \leq dp_{ij} \leq 10^1$

2 means $10^{-1} \leq dp_{ij} \leq 1$

1 means $10^{-2} \leq dp_{ij} \leq 10^{-1}$

0 means $dp_{ij} = 0$

} Full Decade Integer Plots

10. Horizontal Dynamic Pressures

APPLE 27

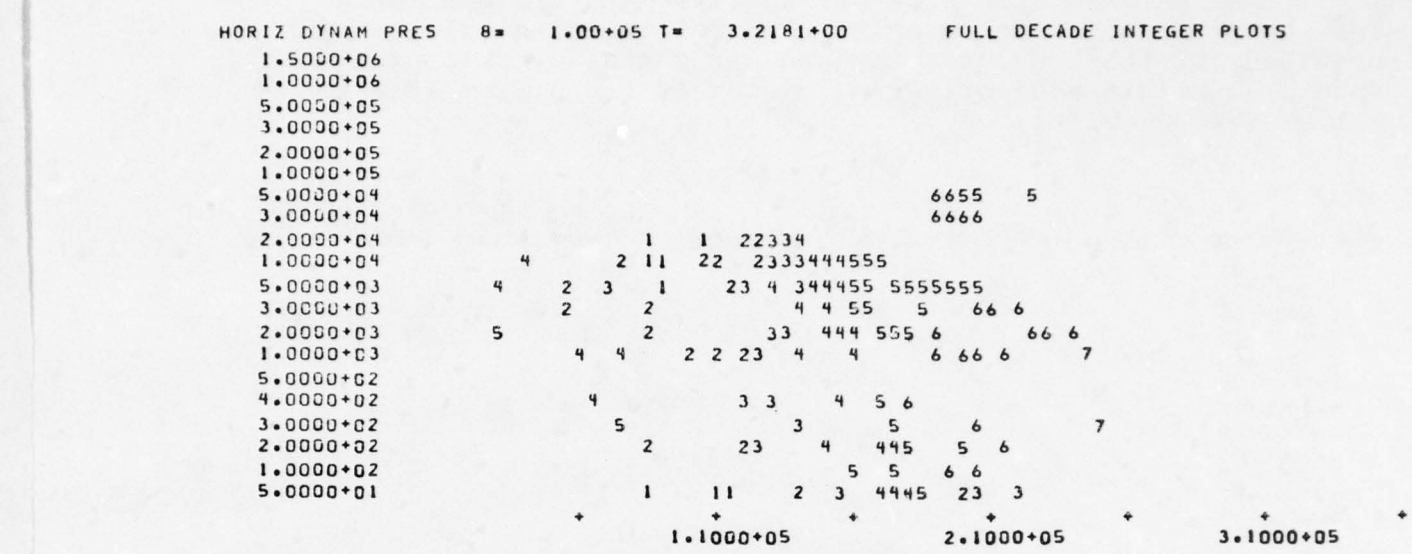

YZP(J) versus RZ(I) representation of the grid.

Shows horizontal dynamic pressure for all particle sizes in zone i,j, where dp_{ij} is the horizontal dynamic pressure (ergs/cc),

8 means $10^5 \leq dp_{ij} \leq 10^6$

7 means $10^4 \leq dp_{ij} \leq 10^5$

6 means $10^3 \leq dp_{ij} \leq 10^4$

5 means $10^2 \leq dp_{ij} \leq 10^3$

4 means $10^1 \leq dp_{ij} \leq 10^2$

3 means $1 \leq dp_{ij} \leq 10^1$

2 means $10^{-1} \leq dp_{ij} \leq 1$

1 means $10^{-2} \leq dp_{ij} \leq 10^{-1}$

0 means $dp_{ij} = 0$

} Full Decade Integer Plots

11. Preloaded Particles

The entire retinue of printout formats are available for the preload particles only. The following two plots are provided for the concentration and horizontal dynamic pressure of 1 mm diameter crater particles at t = 3.2181 secs in a 1 MT surface burst.

```
APPLE 27

CONCENTRATION LEVELS.  8=   1.00-03 T=   3.2181+00       HALF DECADE INTEGER PLOTS
   1.5000+06
   1.0000+06
   5.0000+05
   3.0000+05
   2.0000+05
   1.0000+05
   5.0000+04                                          3321   1
   3.0000+04                                          3443
   2.0000+04
   1.0000+04
   5.0000+03
   3.0000+03
   2.0000+03
   1.0000+03
   5.0000+02
   4.0000+02
   3.0000+02
   2.0000+02
   1.0000+02
   5.0000+01
                    +         +         +         +         +         +         +
                          1.1000+05           2.1000+05           3.1000+05
```

```
APPLE 27

HORIZ DYNAM PRES   8=   1.00+05 T=   3.2181+00       FULL DECADE INTEGER PLOTS
   1.5000+06
   1.0000+06
   5.0000+05
   3.0000+05
   2.0000+05
   1.0000+05
   5.0000+04                                          6655   5
   3.0000+04                                          6666
   2.0000+04
   1.0000+04
   5.0000+03
   3.0000+03
   2.0000+03
   1.0000+03
   5.0000+02
   4.0000+02
   3.0000+02
   2.0000+02
   1.0000+02
   5.0000+01
                    +         +         +         +         +         +         +
                          1.1000+05           2.1000+05           3.1000+05
```

APPENDIX B

BLAST WAVE FLOW FIELDS FOR SCOUR2 CALCULATIONS

MIDDLE GUST

To compute the dust cloud development behind the blast wave from the 100 ton MIDDLE GUST detonation, the flow conditions at the outer edge of the boundary layer were computed on the basis of an idealized flow model. An analytic fit to the air shock position as a function of time ($X_s(t)$) and values for the duration of the positive phase at a given radial location, $\Delta t_+(X_n)$, are the basic determinants of the flow field. For MIDDLE GUST, a fit to the data in Table B.1 from Reference B.1 yields

$$X_s(t) = 170 \left(\frac{t}{20}\right)^{0.525} \tag{B.1}$$

$$\dot{X}_s(t) = 4.46 \left(\frac{t}{20}\right)^{-475} \tag{B.2}$$

Values for Δt_+ are taken directly from Table B.1.

Since shock location and speed are known, we may compute the air velocity, density, and internal energy behind the shock from the shock relations for an ideal gas with specific heat ratio of 1.4. This gives us the peak values of these parameters: $(u_{peak})_N$, $(\rho_{peak})_w$, and $(E_{peak})_N$, where N designates the zone number where the shock is located; i.e.,

$$X_N - \frac{\Delta X}{2} < X_S < X_N + \frac{\Delta X}{2} , \tag{B.3}$$

where ΔX is the zone size (2.5 m for MIDDLE GUST). The flow parameters for the 100 ton MIDDLE GUST blast wave are presented in Table B.2.

Table B.1. Predicted Air Blast Parameters for MIDDLE GUST Event III

Ground Range (ft)	Arrival Time (msec)	Shock Pressure (psi)	Positive Duration (msec)	Positive Pressure Impulse (psi-msec)	Dynamic Pressure (psi)	Dynamic Pressure Impulse (psi-msec)
17	0.80	20,000	9.0	48,000	130,000	150,000
18	0.85	15,000	9.0	35,000	110,000	130,000
20	0.94	10,000	8.9	21,000	78,000	110,000
22	1.0	5,000	8.8	14,000	60,000	91,000
25	1.2	3,000	8.8	8,000	43,000	74,000
30	1.5	2,000	8.8	4,000	18,000	57,000
70	4.7	1,000	8.3	1,000	8,000	19,000
92	7.1	750	8.1	970	4,700	14,000
120	11.0	500	7.9	1,000	2,800	10,000
170	20.0	250	22.0	2,200	1,100	9,500
250	40.0	100	62.0	1,200	310	5,100
320	60.0	50	81.0	830	75	2,700
380	90.0	30	95.0	640	18	1,200
440	115.0	20	110.0	560	8	350
560	195.0	10	130.0	440	2	72

Table B.2. Idealized Flow for MIDDLE GUST II Dust Lofting Calculations Flow Parameters Just Aft of the Air Shock as the Shock Enters the Various Zones – MIDDLE GUST II

RZ ZONE LOCATION,M	N ZONE NO.	TSHOCK ARRIVAL TIME,SEC	VSHOCK SHOCK SPEED, CM/SEC	SHOCKM SHOCK MACH NUMBER	PSHOCK SHOCK OVER-PRESSURE (ERGS/CC)	RSHOCK SHOCK DENSITY (GM/CC)	ESHOCK SHOCK ENERGY, (ERGS/CC)	QSHOCK SHOCK TEMPERATURE, °K	UPEAK PEAK AIR VELOCITY, (CM/SEC)	DELTS POSITIVE PHASE DURATION,SECS.
0.00	1	0.0000	0.0000	0.0000	0.0000	0.0000	0.0000	0.0000	0.0000	0.0000
21.25	2	9.0829-03	2.8928+05	8.4437+00	7.3350+07	5.9361-03	3.0513+10	9.3047+03	2.3784+05	1.0000-02
23.75	3	9.9903-03	2.6298+05	7.8578+00	6.0594+07	5.8589-03	2.5538+10	3.6029+03	2.1560+05	9.5000-03
26.25	4	9.9837-03	2.4125+05	7.2086+00	5.0973+07	5.7774-03	2.1786+10	3.0736+03	1.9717+05	9.1000-03
28.75	5	7.0623-03	2.2299+05	6.6629+00	4.3526+07	5.6922-03	1.8882+10	2.6638+03	1.8164+05	8.7000-03
31.25	6	8.2255-03	2.0741+05	6.1974+00	3.7638+07	5.6038-03	1.6585+10	2.3398+03	1.6834+05	8.2500-03
33.75	7	9.4725-03	1.9396+05	5.7955+00	3.2897+07	5.5127-03	1.4736+10	2.0789+03	1.5682+05	7.8000-03
36.25	8	1.0603-02	1.8222+05	5.4448+00	2.9020+07	5.4193-03	1.3223+10	1.8655+03	1.4673+05	7.4000-03
38.75	9	1.2216-02	1.7188+05	5.1359+00	2.5806+07	5.3241-03	1.1969+10	1.6885+03	1.3781+05	6.9500-03
41.25	10	1.3711-02	1.6271+05	4.8618+00	2.3110+07	5.2275-03	1.0916+10	1.5401+03	1.2986+05	1.2200-02
43.75	11	1.5288-02	1.5451+05	4.6168+00	2.0825+07	5.1299-03	1.0024+10	1.4142+03	1.2272+05	1.7900-02
46.25	12	1.6947-02	1.4713+05	4.3964+00	1.8871+07	5.0317-03	9.2612+09	1.3065+03	1.1627+05	2.3600-02
48.75	13	1.8686-02	1.4046+05	4.1970+00	1.7186+07	4.9331-03	8.6027+09	1.2137+03	1.1041+05	2.9200-02
51.25	14	2.0504-02	1.3440+05	4.0158+00	1.5722+07	4.8344-03	8.0305+09	1.1329+03	1.0505+05	3.4900-02
53.75	15	2.2406-02	1.2886+05	3.8503+00	1.4441+07	4.7363-03	7.5297+09	1.0623+03	1.0014+05	4.0600-02
56.25	16	2.4386-02	1.2378+05	3.6985+00	1.3314+07	4.6388-03	7.0887+09	1.0001+03	9.5607+04	4.6300-02
58.75	17	2.6445-02	1.1910+05	3.5588+00	1.2317+07	4.5407-03	6.6903+09	9.4498+02	9.1414+04	5.2000-02
61.25	18	2.8583-02	1.1478+05	3.4297+00	1.1430+07	4.4442-03	6.3507+09	8.9595+02	8.7521+04	5.3900-02
63.75	19	3.0800-02	1.1078+05	3.3102+00	1.0637+07	4.3488-03	6.0400+09	8.5211+02	8.3892+04	5.5700-02
66.25	20	3.3096-02	1.0706+05	3.1990+00	9.9258+06	4.2546-03	5.7608+09	8.1272+02	8.0500+04	5.7600-02
68.75	21	3.5470-02	1.0360+05	3.0955+00	9.2847+06	4.1617-03	5.5090+09	7.7720+02	7.7321+04	5.9500-02
71.25	22	3.7921-02	1.0036+05	2.9987+00	8.7048+06	4.0702-03	5.2810+09	7.4504+02	7.4332+04	6.1400-02
73.75	23	4.0451-02	9.7328+04	2.9082+00	8.1785+06	3.9802-03	5.0739+09	7.1582+02	7.1516+04	6.3200-02
76.25	24	4.3058-02	9.4483+04	2.8232+00	7.6992+06	3.8918-03	4.8851+09	6.8918+02	6.8857+04	6.5100-02
78.75	25	4.5742-02	9.1807+04	2.7432+00	7.2615+06	3.8051-03	4.7124+09	6.6481+02	6.6339+04	6.7000-02
81.25	26	4.8503-02	8.9287+04	2.6679+00	6.8606+06	3.7201-03	4.5540+09	6.4247+02	6.3952+04	6.7700-02
83.75	27	5.1341-02	8.6907+04	2.5968+00	6.4925+06	3.6368-03	4.4083+09	6.2192+02	6.1683+04	6.8500-02
86.25	28	5.4256-02	8.4658+04	2.5296+00	6.1535+06	3.5553-03	4.2740+09	6.0296+02	5.9523+04	6.9200-02
88.75	29	5.7247-02	8.2527+04	2.4659+00	5.8407+06	3.4755-03	4.1498+09	5.8544+02	5.7463+04	7.0000-02
91.25	30	6.0314-02	8.0506+04	2.4055+00	5.5514+06	3.3976-03	4.0347+09	5.6920+02	5.5495+04	7.0700-02
93.75	31	6.3457-02	7.8587+04	2.3482+00	5.2832+06	3.3215-03	3.9278+09	5.5412+02	5.3612+04	7.1500-02
96.25	32	6.6675-02	7.6762+04	2.2937+00	5.0342+06	3.2472-03	3.8283+09	5.4009+02	5.1809+04	7.2200-02
98.75	33	6.9969-02	7.5023+04	2.2417+00	4.8025+06	3.1746-03	3.7355+09	5.2700+02	5.0078+04	7.3000-02
101.25	34	7.3339-02	7.3366+04	2.1922+00	4.5865+06	3.1039-03	3.6488+09	5.1477+02	4.8416+04	7.4200-02
103.75	35	7.6784-02	7.1784+04	2.1449+00	4.3848+06	3.0349-03	3.5676+09	5.0331+02	4.6817+04	7.5500-02
106.25	36	8.0303-02	7.0272+04	2.0997+00	4.1962+06	2.9677-03	3.4915+09	4.9257+02	4.5272+04	7.6700-02
108.75	37	8.3898-02	6.8825+04	2.0565+00	4.0195+06	2.9022-03	3.4199+09	4.8248+02	4.3781+04	7.8000-02
111.25	38	8.7567-02	6.7440+04	2.0151+00	3.8537+06	2.8384-03	3.3526+09	4.7298+02	4.2340+04	7.9200-02
113.75	39	9.1311-02	6.6112+04	1.9754+00	3.6979+06	2.7762-03	3.2892+09	4.6403+02	4.0945+04	8.0500-02
116.25	40	9.5129-02	6.4838+04	1.9374+00	3.5514+06	2.7157-03	3.2293+09	4.5558+02	3.9636+04	8.1700-02
118.75	41	9.9022-02	6.3615+04	1.9008+00	3.4134+06	2.6568-03	3.1726+09	4.4759+02	3.8340+04	8.3000-02
121.25	42	1.0299-01	6.2439+04	1.8657+00	3.2833+06	2.5994-03	3.1190+09	4.4002+02	3.7084+04	8.4100-02
123.75	43	1.0703-01	6.1308+04	1.8319+00	3.1604+06	2.5436-03	3.0681+09	4.3285+02	3.5866+04	8.5200-02
126.25	44	1.1114-01	6.0219+04	1.7994+00	3.0442+06	2.4892-03	3.0199+09	4.2604+02	3.4683+04	8.6400-02
128.75	45	1.1533-01	5.9170+04	1.7680+00	2.9342+06	2.4363-03	2.9740+09	4.1956+02	3.3535+04	8.7500-02
131.25	46	1.1959-01	5.8159+04	1.7378+00	2.8300+06	2.3849-03	2.9301+09	4.1340+02	3.2418+04	8.8600-02
133.75	47	1.2393-01	5.7184+04	1.7087+00	2.7312+06	2.3348-03	2.8886+09	4.0752+02	3.1331+04	8.9700-02
136.25	48	1.2833-01	5.6243+04	1.6805+00	2.6375+06	2.2861-03	2.8489+09	4.0192+02	3.0273+04	9.0900-02
138.75	49	1.3282-01	5.5333+04	1.6534+00	2.5483+06	2.2387-03	2.8109+09	3.9656+02	2.9243+04	9.2000-02
141.25	50	1.3737-01	5.4454+04	1.6271+00	2.4636+06	2.1925-03	2.7744+09	3.9144+02	2.8238+04	9.3000-02
143.75	51	1.4200-01	5.3604+04	1.6017+00	2.3829+06	2.1476-03	2.7395+09	3.8654+02	2.7258+04	9.4000-02
146.25	52	1.4670-01	5.2781+04	1.5771+00	2.3061+06	2.1039-03	2.7065+09	3.8183+02	2.6301+04	9.5000-02
148.75	53	1.5147-01	5.1985+04	1.5533+00	2.2328+06	2.0614-03	2.6746+09	3.7732+02	2.5366+04	9.6000-02
151.25	54	1.5631-01	5.1213+04	1.5303+00	2.1628+06	2.0201-03	2.6439+09	3.7299+02	2.4452+04	9.7000-02
153.75	55	1.6123-01	5.0465+04	1.5079+00	2.0960+06	1.9798-03	2.6143+09	3.6882+02	2.3559+04	9.8000-02
156.25	56	1.6622-01	4.9740+04	1.4862+00	2.0322+06	1.9406-03	2.5859+09	3.6481+02	2.2685+04	9.9000-02
158.75	57	1.7128-01	4.9036+04	1.4652+00	1.9712+06	1.9025-03	2.5585+09	3.6095+02	2.1829+04	1.0000-01
161.25	58	1.7641-01	4.8353+04	1.4448+00	1.9128+06	1.8653-03	2.5321+09	3.5722+02	2.0991+04	1.0100-01
163.75	59	1.8162-01	4.7690+04	1.4250+00	1.8568+06	1.8292-03	2.5066+09	3.5363+02	2.0170+04	1.0200-01
166.25	60	1.8690-01	4.7045+04	1.4057+00	1.8032+06	1.7940-03	2.4820+09	3.5015+02	1.9365+04	1.0300-01
168.75	61	1.9225-01	4.6419+04	1.3870+00	1.7518+06	1.7597-03	2.4582+09	3.4679+02	1.8575+04	1.0400-01
171.25	62	1.9767-01	4.5810+04	1.3688+00	1.7024+06	1.7264-03	2.4351+09	3.4354+02	1.7800+04	1.0500-01
173.75	63	2.0316-01	4.5217+04	1.3511+00	1.6551+06	1.6938-03	2.4128+09	3.4039+02	1.7039+04	1.0600-01
176.25	64	2.0872-01	4.4641+04	1.3339+00	1.6096+06	1.6622-03	2.3912+09	3.3734+02	1.6292+04	1.0700-01
178.75	65	2.1436-01	4.4079+04	1.3171+00	1.5658+06	1.6314-03	2.3702+09	3.3438+02	1.5558+04	1.0800-01
181.25	66	2.2007-01	4.3533+04	1.3008+00	1.5238+06	1.6013-03	2.3498+09	3.3150+02	1.4837+04	1.0800-01
183.75	67	2.2584-01	4.3000+04	1.2849+00	1.4833+06	1.5720-03	2.3300+09	3.2871+02	1.4127+04	1.0900-01
186.25	68	2.3169-01	4.2481+04	1.2693+00	1.4443+06	1.5435-03	2.3107+09	3.2599+02	1.3429+04	1.0900-01
188.75	69	2.3761-01	4.1975+04	1.2542+00	1.4068+06	1.5157-03	2.2919+09	3.2334+02	1.2743+04	1.0900-01
191.25	70	2.4360-01	4.1482+04	1.2395+00	1.3706+06	1.4886-03	2.2737+09	3.2076+02	1.2067+04	1.0900-01
193.75	71	2.4966-01	4.1000+04	1.2251+00	1.3358+06	1.4622-03	2.2558+09	3.1825+02	1.1402+04	1.0900-01
196.25	72	2.5580-01	4.0530+04	1.2110+00	1.3021+06	1.4364-03	2.2385+09	3.1580+02	1.0746+04	1.1000-01
198.75	73	2.6200-01	4.0072+04	1.1973+00	1.2696+06	1.4113-03	2.2215+09	3.1341+02	1.0100+04	1.1000-01

The wind field at a particular location may be approximated in the positive phase by the following prescription:[B.2]

$$\left(u_e\right)_N = \left(u_{peak}\right)_N \left(1 - \left(\frac{\Delta t}{(\Delta t_+)_N}\right)\right)^{.4} \tag{B.4}$$

$$\left(E_e\right)_N = \left(E_{peak}\right)_N - \frac{\left(u_{peak}\right)_N^2 - u_N^2}{1.4} \tag{B.5}$$

$$\left(\rho_e\right)_N = \left(\rho_{peak}\right)_N \left(\frac{u_e}{u_{peak}}\right)_N \left(\frac{E_{peak}}{E}\right)_N \tag{B.6}$$

where

$\left(u_{peak}\right)_N$ = peak air velocity in zone N

$\left(\Delta t\right)_N = \left(t - t_{A_N}\right)$, t_{A_N} = shock arrival time at zone N

$\left(\Delta t_+\right)_N$ = positive phase duration in zone N

X_N = radial location of Nth zone

E = internal energy of air

ρ = density

e *subscript refers to conditions* at outer edge of the boundary layer. Spherical divergence in the flow field is taken into account by

$$u = u_e \left(1 - \frac{Y}{X_N}\right) \qquad \text{(B.7)}$$

$$v = \frac{u_e Y}{X_N} \qquad \text{(B.8)}$$

$$\Bigg\} \; Y > \delta$$

The negative phase is prescribed to be five times as long as Δt_+. The horizontal wind velocity is constant at 0.1 u_{peak} and the air density and energy are held fixed to the values computed at the conclusion of the positive phase.

MIXED COMPANY

The hydrodynamic flow field used in the SCOUR calculations to simulate the MIXED COMPANY (500 tons TNT) blast wave flow field is a scaled version of the MIDDLE GUST flow field described above. The location of a given overpressure location, the time of air shock arrival, and positive phase duration were each scaled by a factor of 1.71, the cube root of 5, the ratio of the MIXED COMPANY yield to that of MIDDLE GUST (100 tons TNT). A tabular listing of flow field variables is provided in Table B.3.

Table B.3. Tabular Listing of Flow Field Variables — MIXED COMPANY

T= 5.9642-01

TOTAL MASS= 2.4847+08 SIZE-1= 5.6663+07 SIZE-2= 7.8942+07 SIZE-3= 5.6171+07 SIZE-4= 5.8249+07

PKILL1= 0.0000 PKILL2= 1.5293+06

I	RZ	TOTMAS	SUMS1	SUMS2	SUMS3	SUMS4	YMAX1	YMAX2	YMAX3	YMAX4
1	0.0000	6.1603+06	9.5910+05	1.4381+06	2.1374+06	1.6257+06	3.0637+01	3.0689+01	2.3771+02	6.3446+02
2	3.6337+03	2.5171+06	6.6357+05	6.4352+05	7.7142+05	4.3862+05	2.1482+01	8.3276+01	7.1675+02	4.3974+02
3	4.0612+03	2.9323+06	1.1263+06	1.2140+05	5.1073+05	1.1739+06	2.4392+02	2.3093+02	5.9589+02	6.0030+02
4	4.4887+03	9.3760+05	0.0000	0.0000	1.6616+05	7.7144+05	0.0000	0.0000	1.5516+02	1.7944+02
5	4.9162+03	1.1471+06	4.3552+05	5.1577+05	1.4578+05	0.0000	5.0425+01	2.8424+01	9.8674+01	0.0000
6	5.3437+03	1.8535+06	8.6723+05	6.1978+05	1.2723+05	2.3927+05	4.5341+01	2.5270+01	2.6153+01	4.5959+02
7	5.7712+03	1.3498+06	4.5095+05	2.4550+05	4.2911+05	2.2425+05	3.5774+01	1.6050+01	1.5842+02	1.5803+02
8	6.1987+03	1.6861+06	2.1180+05	6.0275+05	4.5461+05	4.1696+05	3.3934+01	6.5816+00	2.1437+02	4.0202+02
9	6.6262+03	2.5341+06	3.7580+05	5.4337+05	7.6542+05	8.4956+05	5.3670+01	4.6004+01	3.2054+02	6.0348+02
10	7.0537+03	2.2151+06	4.8548+05	8.2797+05	6.9505+05	2.0751+05	2.5681+01	3.4509+01	2.5816+02	5.4452+02
11	7.4811+03	5.0528+06	1.2784+06	1.7383+06	1.1055+06	1.0305+06	1.3155+02	1.3915+02	3.1805+02	4.8481+02
12	7.9086+03	4.8330+06	5.4872+05	2.1544+06	9.4736+05	9.8247+05	8.9998+01	1.4516+02	2.0995+02	2.7756+02
13	8.3361+03	5.4935+06	9.2147+05	9.9917+05	1.3843+06	1.6886+06	1.9338+02	1.8526+02	2.6527+02	4.5091+02
14	8.7635+03	6.3360+06	1.9162+06	2.6859+06	9.9727+05	7.3664+05	1.9032+02	1.9312+02	2.6852+02	5.1331+02
15	9.1911+03	7.8081+06	9.4610+05	3.3675+06	1.7236+06	1.7816+06	1.8676+02	2.0797+02	2.6811+02	5.6498+02
16	9.6186+03	6.1026+06	2.0332+06	2.0021+06	1.1448+06	9.2256+05	1.9088+02	1.5649+02	2.4541+02	3.5090+02
17	1.0046+04	4.0834+06	1.9312+06	1.0382+06	1.3031+06	7.1086+05	4.6256+01	1.9342+02	2.5727+02	5.3190+02
18	1.0474+04	5.4210+06	1.0816+06	2.0399+06	1.2405+06	1.0590+06	1.9160+02	1.8768+02	2.4484+02	6.3288+02
19	1.0901+04	5.4188+06	7.1562+05	2.0100+06	1.3313+06	1.3619+06	1.7812+02	1.6934+02	2.6114+02	4.9449+02
20	1.1329+04	8.0250+06	1.7974+06	3.2429+06	1.3777+06	1.6071+06	1.6550+02	1.9428+02	2.7428+02	5.0026+02
21	1.1756+04	6.4583+06	1.5402+06	1.7821+06	1.0738+06	2.0622+06	1.7101+02	1.7198+02	2.4941+02	5.1302+02
22	1.2184+04	5.8397+06	9.5385+05	2.2520+06	1.7196+06	9.1419+05	1.4853+02	1.8024+02	2.8483+02	1.5002+02
23	1.2611+04	6.7489+06	7.6835+05	2.4424+06	1.6187+06	1.9195+06	1.4597+02	1.7014+02	2.5313+02	5.5050+02
24	1.3039+04	4.0146+06	1.0011+06	8.4111+05	1.0364+06	1.1360+06	1.4939+02	1.5684+02	1.9742+02	5.9716+02
25	1.3466+04	6.2561+06	1.4021+06	2.1995+06	8.2106+05	1.8335+06	1.3614+02	1.4239+02	2.5964+02	3.5146+02
26	1.3894+04	6.0720+06	1.7314+06	1.5747+06	1.3820+06	1.3838+06	1.3573+02	1.5651+02	1.7548+02	5.2050+02
27	1.4321+04	4.4414+06	8.4511+05	1.3573+06	9.8231+05	1.2571+06	1.0797+01	1.4136+02	2.3115+02	4.9507+02
28	1.4749+04	5.7073+06	1.1102+06	1.6461+06	1.5309+06	1.4201+06	1.2737+02	1.5323+02	2.3579+02	4.6525+02
29	1.5176+04	6.1783+06	1.7474+06	1.8096+06	1.2425+06	1.3792+06	1.3048+02	1.3973+02	2.3283+02	5.4688+02
30	1.5604+04	5.6801+06	1.0841+06	2.4027+06	1.3345+06	8.5874+05	1.1547+02	1.3171+02	2.2634+02	4.5860+02
31	1.6031+04	2.5306+06	5.8786+05	3.9748+05	7.2426+05	8.2104+05	1.2651+01	2.8776+01	2.5784+02	2.4886+02
32	1.6459+04	5.0611+06	1.2527+06	1.9569+06	9.0871+05	8.8277+05	1.1152+02	1.2016+02	1.5108+02	5.9504+02
33	1.6886+04	6.0035+06	1.4777+06	1.9777+06	1.1112+06	1.4369+06	1.0629+02	1.2053+02	1.9626+02	5.5195+02
34	1.7314+04	3.2912+06	8.3033+05	5.6035+05	6.4386+05	1.1567+06	1.1085+02	9.2409+01	2.1040+02	5.8780+02
35	1.7741+04	4.8002+06	1.0486+06	1.3492+06	1.3818+06	1.1212+06	1.0382+02	1.0750+02	2.2287+02	3.7744+02
36	1.8168+04	5.0311+06	7.5233+05	1.8601+06	8.3587+05	1.7829+06	1.0166+02	1.1824+02	1.6463+02	5.9609+02
37	1.8596+04	4.0485+06	8.2043+05	1.2302+06	1.2891+06	7.0875+05	1.0335+02	1.1807+02	2.1866+02	5.3438+02
38	1.9023+04	4.9045+06	1.2745+06	8.3876+05	1.1554+06	1.6359+06	9.6818+01	8.5032+01	1.7251+02	5.5750+02
39	1.9451+04	3.6547+06	1.0073+06	9.6549+05	6.4265+05	1.0383+06	8.6697+01	1.0753+02	2.6212+02	6.5286+02
40	1.9878+04	3.3945+06	9.1724+05	5.1954+05	8.4248+05	1.0152+06	9.0875+01	8.6112+01	1.8026+02	4.1166+02
41	2.0306+04	4.2689+06	5.6852+05	1.6694+06	9.0322+05	1.1277+06	9.0667+01	9.6814+01	2.1768+02	1.6868+02
42	2.0733+04	4.3423+06	9.8048+05	1.2416+06	9.4827+05	1.1719+06	8.5306+01	9.7062+01	2.1048+02	3.5603+02
43	2.1161+04	3.1927+06	5.9773+05	8.8193+05	8.8137+05	8.2166+05	8.2920+01	8.5497+01	2.0066+02	7.7324+02
44	2.1588+04	3.5108+06	8.6131+05	9.1083+05	9.7107+05	7.6740+05	7.8862+01	7.8847+01	2.4294+02	6.2081+02
45	2.2016+04	3.0541+06	6.8009+05	7.6487+05	8.2492+05	7.8426+05	7.9549+01	8.6745+01	1.5704+02	7.0519+02
46	2.2443+04	2.9111+06	6.5547+05	8.5642+05	5.6751+05	8.3171+05	7.7192+01	7.6165+01	2.0036+02	7.3414+02
47	2.2871+04	2.7153+06	5.8327+05	9.3735+05	7.0961+05	4.8664+05	7.7852+01	9.5715+01	1.9215+02	1.0460+02
48	2.3298+04	3.4541+06	1.0698+06	1.0422+06	7.1522+05	6.2679+05	7.1454+01	9.3615+01	1.9898+02	7.6147+02
49	2.3725+04	2.6424+06	5.6248+05	1.3026+06	2.9487+05	4.8233+05	6.8117+01	9.2742+01	2.2394+02	9.0382+01

Table B.3. (continued)

I=	5.9643-01									
50	2.4153+04	3.0450+06	7.9833+05	6.5167+05	8.4705+05	7.4792+05	6.7848+01	7.8333+01	2.8469+02	6.0834+02
51	2.4581+04	2.1595+06	6.5773+05	6.3709+05	5.2429+05	3.4042+05	6.0082+01	7.5008+01	2.6873+02	6.7074+02
52	2.5008+04	2.8162+06	8.5085+05	7.4641+05	7.3692+05	4.8200+05	6.3867+01	7.5622+01	2.1739+02	4.7399+02
53	2.5436+04	2.1794+06	5.2704+05	8.2311+05	3.5863+05	4.6053+05	5.9641+01	7.6446+01	2.2586+02	6.5760+02
54	2.5863+04	2.0283+06	6.4080+05	6.7519+05	4.7325+05	2.3911+05	6.0565+01	7.3660+01	2.3055+02	1.1144+02
55	2.6291+04	2.1965+06	4.7437+05	7.1289+05	4.8057+05	5.2857+05	5.6572+01	8.4197+01	2.2052+02	1.9532+02
56	2.6718+04	2.2244+06	6.3975+05	8.7423+05	2.9093+05	4.1946+05	5.3150+01	6.7547+01	1.5033+02	2.5077+02
57	2.7146+04	1.5860+06	5.0860+05	1.9642+05	3.8243+05	4.8852+05	5.1615+01	7.0449+01	3.2333+02	4.6344+02
58	2.7573+04	1.7937+06	2.6532+05	9.1976+05	3.1947+05	2.8910+05	5.2561+01	6.2447+01	2.8959+02	1.2374+02
59	2.8001+04	1.7754+06	5.3797+05	5.5274+05	3.5006+05	3.3463+05	4.8108+01	6.7811+01	2.1752+02	2.0294+02
60	2.8428+04	1.6691+06	4.1323+05	5.8204+05	4.1133+05	2.6246+05	4.8092+01	6.4855+01	2.7569+02	2.4641+02
61	2.8856+04	1.3195+06	4.1437+05	3.6728+05	3.6902+05	1.6884+05	4.6495+01	6.1238+01	2.4799+02	1.1832+02
62	2.9283+04	1.6656+06	3.7266+05	6.5982+05	3.0193+05	3.3121+05	4.5482+01	6.5446+01	3.2644+02	1.4160+02
63	2.9711+04	9.2172+05	3.3463+04	3.7682+05	2.7383+05	1.7760+05	4.2487+01	6.4781+01	2.1744+02	1.3766+02
64	3.0138+04	1.3558+06	5.0853+05	3.5332+05	2.6043+05	2.3445+05	4.3799+01	5.3366+01	1.2342+02	8.7606+01
65	3.0566+04	9.9889+05	2.1411+05	4.1130+05	1.9204+05	1.8245+05	4.7385+01	6.1438+01	2.5425+02	1.3898+02
66	3.0993+04	7.9148+05	1.6358+05	3.2064+05	7.7789+04	2.2958+05	3.8150+01	5.6800+01	1.0033+02	2.4296+02
67	3.1421+04	8.7876+05	2.7635+05	3.3449+05	2.2177+05	4.6143+04	4.1054+01	5.7597+01	7.5671+01	2.0014+02
68	3.1848+04	9.3804+05	8.5944+04	3.8123+05	1.8123+05	2.8965+05	3.2986+01	5.1545+01	7.1340+01	2.0778+01
69	3.2276+04	8.9490+05	3.9056+05	2.4980+05	1.0308+05	1.5146+05	3.1630+01	4.3898+01	1.9182+02	8.6082+01
70	3.2703+04	9.7948+05	2.7752+05	3.6056+05	2.2409+05	1.1732+05	2.4174+01	3.8187+01	8.0764+01	9.9177+01
71	3.3131+04	8.0129+05	3.0261+05	2.4351+05	1.4166+05	1.1351+05	1.9150+01	2.4620+01	1.3905+02	3.4105+01
72	3.3558+04	5.1247+05	2.2462+05	1.3690+05	1.0616+05	4.4799+04	1.5233+01	4.4748+01	1.2339+02	3.4221+01
73	3.3986+04	6.4191+05	2.1862+05	2.2036+05	1.5344+05	4.9484+04	1.1842+01	2.6877+01	3.6970+01	1.4606+01
J		YZP	TOTMAS	MASS ABOVE		SUMS1	SUMS2	SUMS3	SUMS4	
1		1.1000+01	4.3938+07	2.0453+08		1.5760+07	1.3005+07	7.3346+06	7.2388+06	
2		3.5000+01	4.9089+07	1.5552+08		1.4241+07	1.8901+07	8.0025+06	7.8647+06	
3		7.0000+01	4.1956+07	1.1356+08		1.0484+07	2.2197+07	5.2398+06	4.0354+06	
4		1.4000+02	2.3220+07	9.0344+07		4.1169+06	8.9761+06	6.7876+06	3.3391+06	
5		1.2500+02	1.7014+07	7.3329+07		4.4212+06	4.6926+06	4.4484+06	3.4521+06	
6		1.5000+02	1.3351+07	5.9979+07		4.1132+06	3.6968+06	3.2333+06	2.3072+06	
7		1.7500+02	1.3265+07	4.6714+07		1.6949+06	3.3994+06	5.3499+06	2.8208+06	
8		2.0000+02	9.2670+06	3.7447+07		1.5318+06	2.4269+06	3.3017+06	2.0068+06	
9		2.5000+02	1.4015+07	2.3433+07		9.0569+04	8.0083+05	7.7572+06	5.3684+06	
10		5.0000+02	1.7348+07	6.8836+06		0.0000	0.0000	3.6518+06	1.3898+07	
11		7.5000+02	5.4985+06	5.8509+05		0.0000	0.0000	3.5496+05	5.1435+06	
12		1.0000+03	1.5173+05	4.3336+05		0.0000	0.0000	0.0000	1.5173+05	
13		1.2500+03	0.0000	4.3336+05		0.0000	0.0000	0.0000	0.0000	
14		1.5000+03	0.0000	4.3336+05		0.0000	0.0000	0.0000	0.0000	

Table B.3. (continued)

I	TSHOCK	VSHOCK	SHOCKM	PSHOCK	RSHOCK	ESHOCK	QSHOCK	UPEAK	DELTS
1	5.5786-03	3.2131+05	9.6157+00	9.0808+07	6.0084-03	3.7320+10	5.2658+03	2.6527+05	0.0000
2	6.9817-03	2.8928+05	8.6437+00	7.3350+07	5.9361-03	3.0513+10	4.3047+03	2.3784+05	1.7100-02
3	8.5333-03	2.6298+05	7.8578+00	6.0594+07	5.8589-03	2.5538+10	3.6029+03	2.1560+05	1.6245-02
4	1.0232-02	2.4125+05	7.2086+00	5.0973+07	5.7774-03	2.1786+10	3.0736+03	1.9717+05	1.5581-02
5	1.2076-02	2.2293+05	6.6629+00	4.3526+07	5.6922-03	1.8882+10	2.6638+03	1.8164+05	1.4877-02
6	1.4065-02	2.0741+05	6.1974+00	3.7638+07	5.6038-03	1.6585+10	2.3398+03	1.6834+05	1.4107-02
7	1.6198-02	1.9396+05	5.7955+00	3.2897+07	5.5127-03	1.4736+10	2.0789+03	1.5682+05	1.3338-02
8	1.8473-02	1.8222+05	5.4448+00	2.9020+07	5.4193-03	1.3223+10	1.8655+03	1.4673+05	1.2825-02
9	2.0889-02	1.7188+05	5.1359+00	2.5806+07	5.3241-03	1.1969+10	1.6885+03	1.3781+05	1.1115-02
10	2.3446-02	1.6271+05	4.8618+00	2.3110+07	5.2275-03	1.0916+10	1.5401+03	1.2986+05	2.0862-02
11	2.6143-02	1.5451+05	4.6168+00	2.0825+07	5.1299-03	1.0024+10	1.4142+03	1.2272+05	3.0609-02
12	2.8979-02	1.4713+05	4.3984+00	1.8871+07	5.0317-03	9.2612+09	1.3085+03	1.1627+05	4.0355-02
13	3.1953-02	1.4046+05	4.1970+00	1.7186+07	4.9331-03	8.6027+09	1.2137+03	1.1041+05	4.9931-02
14	3.5065-02	1.3440+05	4.0158+00	1.5722+07	4.8344-03	8.0305+09	1.1329+03	1.0505+05	5.9678-02
15	3.8313-02	1.2886+05	3.8513+00	1.4441+07	4.7360-03	7.5297+09	1.0623+03	1.0014+05	6.9425-02
16	4.1699-02	1.2378+05	3.6985+00	1.3314+07	4.6380-03	7.0867+09	1.0001+03	9.5607+04	7.9172-02
17	4.5220-02	1.1910+05	3.5538+00	1.2317+07	4.5407-03	6.6983+09	9.4498+02	9.1414+04	8.8919-02
18	4.8876-02	1.1478+05	3.4297+00	1.1430+07	4.4442-03	6.3567+09	8.9595+02	8.7521+04	9.2168-02
19	5.2668-02	1.1078+05	3.3172+00	1.0637+07	4.3488-03	6.0480+09	8.5211+02	8.3892+04	9.5246-02
20	5.6593-02	1.0706+05	3.1940+00	9.9258+06	4.2546-03	5.7608+09	8.1272+02	8.0500+04	9.8495-02
21	6.0652-02	1.0360+05	3.0955+00	9.2847+06	4.1617-03	5.5090+09	7.7720+02	7.7321+04	1.0174-01
22	6.4845-02	1.0036+05	2.9986+00	8.7048+06	4.0702-03	5.2810+09	7.4504+02	7.4332+04	1.0499-01
23	6.9170-02	9.7328+04	2.9082+00	8.1785+06	3.9802-03	5.0739+09	7.1582+02	7.1516+04	1.0807-01
24	7.3628-02	9.4483+04	2.8232+00	7.6992+06	3.8918-03	4.8851+09	6.8918+02	6.8857+04	1.1132-01
25	7.8218-02	9.1837+04	2.7432+00	7.2615+06	3.8051-03	4.7124+09	6.6481+02	6.6339+04	1.1457-01
26	8.2940-02	8.9287+04	2.6679+00	6.8606+06	3.7201-03	4.5540+09	6.4247+02	6.3952+04	1.1577-01
27	8.7793-02	8.6907+04	2.5968+00	6.4925+06	3.6368-03	4.4083+09	6.2192+02	6.1683+04	1.1713-01
28	9.2776-02	8.4658+04	2.5296+00	6.1535+06	3.5553-03	4.2740+09	6.0298+02	5.9523+04	1.1833-01
29	9.7891-02	8.2527+04	2.4658+00	5.8407+06	3.4755-03	4.1498+09	5.8544+02	5.7463+04	1.1970-01
30	1.0314-01	8.0506+04	2.4055+00	5.5514+06	3.3976-03	4.0347+09	5.6920+02	5.5495+04	1.2090-01
31	1.0851-01	7.8587+04	2.3482+00	5.2832+06	3.3215-03	3.9278+09	5.5412+02	5.3612+04	1.2226-01
32	1.1401-01	7.6762+04	2.2937+00	5.0342+06	3.2472-03	3.8283+09	5.4009+02	5.1809+04	1.2346-01
33	1.1965-01	7.5023+04	2.2417+00	4.8025+06	3.1746-03	3.7355+09	5.2700+02	5.0078+04	1.2483-01
34	1.2541-01	7.3366+04	2.1922+00	4.5865+06	3.1039-03	3.6488+09	5.1477+02	4.8416+04	1.2688-01
35	1.3130-01	7.1784+04	2.1449+00	4.3848+06	3.0349-03	3.5676+09	5.0331+02	4.6817+04	1.2910-01
36	1.3732-01	7.0272+04	2.0997+00	4.1962+06	2.9677-03	3.4915+09	4.9257+02	4.5277+04	1.3116-01
37	1.4346-01	6.8825+04	2.0565+00	4.0195+06	2.9022-03	3.4199+09	4.8248+02	4.3793+04	1.3338-01
38	1.4974-01	6.7440+04	2.0151+00	3.8537+06	2.8384-03	3.3526+09	4.7298+02	4.2360+04	1.3543-01
39	1.5614-01	6.6112+04	1.9754+00	3.6979+06	2.7762-03	3.2892+09	4.6403+02	4.0975+04	1.3765-01
40	1.6267-01	6.4836+04	1.9374+00	3.5514+06	2.7157-03	3.2293+09	4.5558+02	3.9636+04	1.3971-01
41	1.6932-01	6.3615+04	1.9013+00	3.4134+06	2.6568-03	3.1726+09	4.4759+02	3.8340+04	1.4193-01
42	1.7611-01	6.2439+04	1.8667+00	3.2833+06	2.5994-03	3.1190+09	4.4002+02	3.7084+04	1.4381-01
43	1.8302-01	6.1308+04	1.8319+00	3.1604+06	2.5436-03	3.0681+09	4.3285+02	3.5866+04	1.4569-01
44	1.9005-01	6.0219+04	1.7994+00	3.0442+06	2.4892-03	3.0199+09	4.2604+02	3.4683+04	1.4774-01
45	1.9721-01	5.9170+04	1.7680+00	2.9342+06	2.4363-03	2.9740+09	4.1956+02	3.3535+04	1.4962-01
46	2.0450-01	5.8159+04	1.7378+00	2.8300+06	2.3849-03	2.9303+09	4.1340+02	3.2418+04	1.5150-01
47	2.1191-01	5.7184+04	1.7087+00	2.7312+06	2.3348-03	2.8886+09	4.0752+02	3.1331+04	1.5338-01
48	2.1945-01	5.6243+04	1.6805+00	2.6375+06	2.2861-03	2.8489+09	4.0192+02	3.0273+04	1.5544-01
49	2.2711-01	5.5333+04	1.6534+00	2.5483+06	2.2387-03	2.8109+09	3.9656+02	2.9243+04	1.5732-01
50	2.3490-01	5.4454+04	1.6271+00	2.4636+06	2.1925-03	2.7746+09	3.9144+02	2.8238+04	1.5903-01

Table B.3. (concluded)

51	2.4241-01	[illegible]	1.6017+00	[illegible]	2.1476-03	2.7395+09	3.6654+02	2.7256+04	1.6074-01
52	2.5085-01	5.2781+04	1.5771+00	2.3861+06	2.1039-03	2.7065+09	3.8183+02	2.6301+04	1.6245-01
53	2.5901-01	5.1985+04	1.5533+00	2.2328+06	2.0614-03	2.6746+09	3.7732+02	2.5366+04	1.6416-01
54	2.6729-01	5.1213+04	1.5303+00	2.1628+06	2.0201-03	2.6439+09	3.7239+02	2.4452+04	1.6587-01
55	2.7570-01	5.0465+04	1.5079+00	2.0960+06	1.9798-03	2.6143+09	3.6882+02	2.3559+04	1.6758-01
56	2.8423-01	4.9742+04	1.4862+00	2.0322+06	1.9406-03	2.5859+09	3.6481+02	2.2685+04	1.6929-01
57	2.9289-01	4.9026+04	1.4652+01	1.9712+06	1.9025-03	2.5585+09	3.6095+02	2.1829+04	1.7100-01
58	3.0165-01	4.8353+04	1.4448+00	1.9128+06	1.8653-03	2.5321+09	3.5722+02	2.0991+04	1.7271-01
59	3.1057-01	4.7690+04	1.4251+01	1.8568+06	1.8292-03	2.5066+09	3.5363+02	2.0170+04	1.7442-01
60	3.1959-01	4.7045+04	1.4057+00	1.8032+06	1.7940-03	2.4820+09	3.5015+02	1.9365+04	1.7613-01
61	3.2874-01	4.6419+04	1.3871+00	1.7518+06	1.7597-03	2.4582+09	3.4679+02	1.8575+04	1.7784-01
62	3.3801-01	4.5811+04	1.3688+00	1.7024+06	1.7264-03	2.4351+09	3.4354+02	1.7800+04	1.7955-01
63	3.4740-01	4.5217+04	1.3511+00	1.6551+06	1.6938-03	2.4128+09	3.4039+02	1.7039+04	1.8126-01
64	3.5691-01	4.4641+04	1.3339+00	1.6096+06	1.6622-03	2.3912+09	3.3734+02	1.6292+04	1.8297-01
65	3.6655-01	4.4079+04	1.3171+00	1.5658+06	1.6314-03	2.3702+09	3.3438+02	1.5558+04	1.8468-01
66	3.7631-01	4.3533+04	1.3008+00	1.5238+06	1.6013-03	2.3498+09	3.3150+02	1.4837+04	1.8468-01
67	3.8619-01	4.3001+04	1.2849+00	1.4833+06	1.5720-03	2.3300+09	3.2871+02	1.4127+04	1.8639-01
68	3.9619-01	4.2481+04	1.2693+00	1.4443+06	1.5435-03	2.3107+09	3.2599+02	1.3429+04	1.8639-01
69	4.0631-01	4.1975+04	1.2542+00	1.4068+06	1.5157-03	2.2919+09	3.2334+02	1.2743+04	1.8639-01
70	4.1655-01	4.1482+04	1.2395+00	1.3706+06	1.4886-03	2.2737+09	3.2076+02	1.2067+04	1.8639-01
71	4.2692-01	4.1001+04	1.2251+00	1.3358+06	1.4622-03	2.2558+09	3.1825+02	1.1402+04	1.8639-01
72	4.3740-01	4.0531+04	1.2110+00	1.3021+06	1.4364-03	2.2385+09	3.1581+02	1.0746+04	1.8810-01
73	4.4801-01	4.0072+04	1.1973+00	1.2696+06	1.4113-03	2.2215+09	3.1341+02	1.0100+04	1.8810-01

REFERENCES, APPENDIX B

B.1 Hodgson, G. W., Capt. and S. Melzer, 1st Lt., "Preliminary Test Plan for Project MIDDLE GUST," Civil Engineering Research Division, Air Force Weapons Laboratory, 30 April 1971.

B.2 Bannister, J. R. and R. J. Emrich, "Preliminary Investigation of Dust Raised by Blast Waves," Report SC-3610-TR, Sandia Corporation, 3 January 1955.

DISTRIBUTION LIST

DEPARTMENT OF DEFENSE

Assistant to the Secretary of Defense
ATTN: Honorable Donald R. Cotter

Director
Defense Advanced Rsch. Proj. Agency
ATTN: NRMO
ATTN: PMO
ATTN: STO
ATTN: Technical Library

Director
Defense Civil Preparedness Agency
Assistant Director for Research
ATTN: Admin. Officer

Defense Communications Agency
WWMCCS System Engineering Org.
ATTN: Thomas Neighbors

Defense Documentation Center
Cameron Station
12 cy ATTN: TC

Director
Defense Intelligence Agency
ATTN: DT-1C
ATTN: DI-7E
ATTN: DB-4C, Edward O'Farrell

Director
Defense Nuclear Agency
ATTN: DDST
ATTN: TISI, Archives
2 cy ATTN: SPSS
3 cy ATTN: TITL, Tech. Library

Under Secretary of Defense for Rsch. & Engineering
ATTN: S&SS (OS)

Commander
Field Command
Defense Nuclear Agency
ATTN: FCPR

Director
Interservice Nuclear Weapons School
ATTN: Document Control

Director
Joint Strat. Tgt. Planning Staff, JCS
ATTN: STINFO, Library

Chief
Livermore Division, Fld. Command, DNA
Lawrence Livermore Laboratory
ATTN: FCPRL

DEPARTMENT OF THE ARMY

Director
BMD Advanced Tech. Ctr.
Huntsville Office
ATTN: 1CRDABH-X
ATTN: CRDABH-S

DEPARTMENT OF THE ARMY (Continued)

Dep. Chief of Staff for Rsch. Dev. & ACQ
ATTN: Technical Library

Chief of Engineers
ATTN: DAEN-RDM
ATTN: DAEN-MCE-D

Deputy Chief of Staff for Ops. & Plans
ATTN: Technical Library

Commander
Harry Diamond Laboratories
ATTN: DRXDO-NP
ATTN: DRXDO-TI, Tech. Lib.

Commander
Redstone Scientific Information Ctr.
U.S. Army Missile Command
ATTN: Chief, Documents

Director
U.S. Army Ballistic Research Labs.
ATTN: DRXBR-X, Julius J. Meszaros
ATTN: Tech. Lib., Edward Baicy
ATTN: W. Taylor
ATTN: J. H. Keefer, DRDAR-BLE

Commander
U.S. Army Engineer Center
ATTN: ATSEN-SY-L

Division Engineer
U.S. Army Engineer Div., Huntsville
ATTN: HNDED-SR

Division Engineer
U.S. Army Engineer Div., Ohio River
ATTN: Technical Library

Director
U.S. Army Engr. Waterways Exper. Sta.
ATTN: John N. Strange
ATTN: Guy Jackson
ATTN: Technical Library
ATTN: Leo Ingram
ATTN: William Flathau

Commander
U.S. Army Mat. & Mechancis Rsch. Ctr.
ATTN: Technical Library

Commander
U.S. Army Materiel Dev. & Readiness Cmd.
ATTN: Technical Library

Commander
U.S. Army Nuclear Agency
ATTN: Technical Library

DEPARTMENT OF THE NAVY

Chief of Naval Material
ATTN: MAT, 0323

DEPARTMENT OF THE NAVY (Continued)

Chief of Naval Operations
ATTN: OP 981
ATTN: OP 03EG

Chief of Naval Research
ATTN: Code 464, Thomas P. Quinn
ATTN: Technical Library
ATTN: Code 464, Jacob L. Warner
ATTN: Nicholas Perrone

Officer-in-Charge
Civil Engineering Laboratory
Naval Construction Battalion Center
ATTN: Technical Library
ATTN: Stan Takahashi

Commander
David W. Taylor Naval Ship R&D Ctr.
ATTN: Code L42-3, Library

Commander
Naval Electronics System Command
Naval Electronic Systems Cmd. Hqs.
ATTN: PME 117-21A

Commander
Naval Facilities Engineering Command
Headquarters
ATTN: Technical Library
ATTN: Code 03A
ATTN: Code 04B

Superintendent (Code 1424)
Naval Postgraduate School
ATTN: Code 2124, Tech. Rpts. Librarian

Director
Naval Research Laboratory
ATTN: Code 2600, Tech. Lib.

Commander
Naval Sea Systems Command
ATTN: ORD-91313, Lib.

Commander
Naval Ship Engineering Center
ATTN: Technical Library

Commander
Naval Ship Rsch. and Development Ctr.
Underwater Explosive Research Division
ATTN: Technical Library

Officer-In-Charge
Naval Surface Weapons Center
ATTN: Code WA501, Navy Nuc. Prgms. Off.

Commander
Naval Surface Weapons Center
Dahlgren Laboratory
ATTN: Technical Library

President
Naval War College
ATTN: Technical Library

Commanding Officer
Naval Weapons Evaluation Facility
ATTN: Technical Library

DEPARTMENT OF THE NAVY (Continued)

Director
Strategic Systems Project Office
ATTN: NSP-43, Tech. Lib.

DEPARTMENT OF THE AIR FORCE

AF Geophysics Laboratory, AFSC
ATTN: SUOL, Rsch. Lib.

AF Institute of Technology, AU
ATTN: Library AFIT, Bldg. 640, Area B

AF Weapons Laboratory, AFSC
ATTN: DES-C, Robert Henny
ATTN: SUL
ATTN: DES-S, M. A. Plamondon
ATTN: DYT

Headquarters
Air Force Systems Command
ATTN: Technical Library
ATTN: DLCAW

Commander
Foreign Technology Division, AFSC
ATTN: NICD, Library

Hq. USAF/IN
ATTN: INATA

Hq. USAF/PR
ATTN: PRE

Hq. USAF/RD
ATTN: RDQSM

Commander
Rome Air Development Center, AFSC
ATTN: EMTLD, Doc. Library

SAMSO/MN
ATTN: MMH

Commander in Chief
Strategic Air Command
ATTN: NRI-STINFO, Library

DEPARTMENT OF ENERGY

Department of Energy
Albuquerque Operations Office
ATTN: Doc. Con. for Tech. Library

Department of Energy
Division of Headquarters Services
ATTN: Doc. Con. for Class. Tech. Lib.

Department of Energy
Nevada Operations Office
ATTN: Doc. Con. for Tech. Lib.

University of California
Lawrence Livermore Laboratory
ATTN: Tech. Info. Dept., L-3

Los Alamos Scientific Laboratory
ATTN: Doc. Con. for R. J. Bridwell
ATTN: Doc. Con. for Reports Lib.
ATTN: Doc. Con. for G. R. Spillman

DEPARTMENT OF ENERGY (Continued)

Sandia Laboratories
Livermore Laboratory
ATTN: Doc. Con. for Tech. Library

Sandia Laboratories
ATTN: Doc. Con. for 3141, Sandia Rpt. Coll.

Union Carbide Corporation
Holifield National Laboratory
ATTN: Doc. Con. for Tech. Lib.
ATTN: Civil Def. Res. Proj.

OTHER GOVERNMENT AGENCIES

Department of the Interior
Bureau of Mines
ATTN: Tech. Lib.

Department of the Interior
U.S. Geological Survey
ATTN: Cecil B. Raleigh
ATTN: J. H. Healy

DEPARTMENT OF DEFENSE CONTRACTORS

Aerospace Corporation
ATTN: Tech. Info. Services

Agbabian Associates
ATTN: M. Agbabian

Applied Theory, Inc.
2 cy ATTN: John G. Trulio

Avco Research & Systems Group
ATTN: Research Lib. A830, Rm. 7201

Battelle Memorial Institute
ATTN: Technical Library

The BDM Corporation
ATTN: Technical Library

The Boeing Company
ATTN: R. M. Schmidt
ATTN: Aerospace Library

California Research & Technology, Inc.
ATTN: Sheldon Shuster
ATTN: Technical Library
ATTN: Ken Kreyenhagen

Calspan Corporation
ATTN: Technical Library

Civil/Nuclear Systems Corp.
ATTN: Robert Crawford

University of Dayton
Industrial Security Super, KL-505
ATTN: Hallock F. Swift

University of Denver
Colorado Seminary
Denver Research Institute
ATTN: Sec. Officer for J. Wisotski

EG&G, Inc.
Albuquerque Division
ATTN: Technical Library

DEPARTMENT OF DEFENSE CONTRACTORS (Continued)

Gard, Incorporated
ATTN: G. L. Neidhardt

General Electric Company
TEMPO-Center for Advanced Studies
ATTN: DASIAC

IIT Research Institute
ATTN: Technical Library

Institute for Defense Analyses
ATTN: IDA Librarian, Ruth S. Smith

Kaman AviDyne
Division of Kaman Sciences Corp.
ATTN: Technical Library
ATTN: E. S. Criscione

Kaman Sciences Corporation
ATTN: Library

Lockheed Missiles & Space Co., Inc.
ATTN: Technical Library

Lockheed Missiles & Space Co., Inc.
ATTN: Tech. Info. Ctr., D/Coll.
ATTN: Tom Geers, D/52-33, Bldg 205

McDonnell Douglas Corporation
ATTN: Robert W. Halprin

Merritt CASES, Inc.
ATTN: J. L. Merritt
ATTN: Technical Library

The Mitre Corporation
ATTN: Library

Nathan M. Newmark
Consulting Engineering Services
ATTN: Nathan M. Newmark

Physics International Company
ATTN: Doc. Con. for Fred M. Sauer
ATTN: Doc. Con. for Larry A. Behrmann
ATTN: Doc. Con. for Robert Swift
ATTN: Doc. Con. for Dennis Orphal
ATTN: Doc. Con. for Tech. Lib.
ATTN: Doc. Con. for Charles Godfrey
ATTN: Doc. Con. for E. T. Moore

R&D Associates
ATTN: Henry Cooper
ATTN: Robert Port
ATTN: Harold L. Brode
ATTN: Jerry Carpenter
ATTN: J. G. Lewis
ATTN: Technical Library
ATTN: Cyrus P. Knowles
ATTN: William B. Wright, Jr.
ATTN: Jerry Stockton

Science Applications, Inc.
ATTN: D. E. Maxwell
ATTN: David Bernstein

Science Applications, Inc.
ATTN: Technical Library

DEPARTMENT OF DEFENSE CONTRACTORS (Continued)

Southwest Research Institute
ATTN: Wilfred E. Baker
ATTN: A. B. Wenzel

SRI International
ATTN: Burt R. Gasten
ATTN: George R. Abrahamson

Systems, Science and Software, Inc.
ATTN: Technical Library
ATTN: Donald R. Grine
ATTN: Ted Cherry
ATTN: Thomas D. Riney
ATTN: J. W. Kirsch

Terra Tek, Inc.
ATTN: Sidney Green
ATTN: Technical Library

Tetra Tech., Inc.
ATTN: Li-San Hwang
ATTN: Technical Library

TRW Defense & Space Sys. Group
ATTN: D. H. Baer, R1-2136
ATTN: Tech. Info. Center/S-1930
ATTN: R. K. Plebuch, R1-2078
ATTN: I. E. Alber, R1-1008
2 cy ATTN: Peter K. Dai, R1/2170

TRW Defense & Space Sys. Group
San Bernardino Operations
ATTN: E. Y. Wong, 527/712

Universal Analytics, Inc.
ATTN: E. I. Field

DEPARTMENT OF DEFENSE CONTRACTORS (Continued)

URS Research Company
ATTN: Technical Library

The Eric H. Wang
Civil Engineering Rsch. Fac.
ATTN: Larry Bickle
ATTN: Neal Baum

Washington State University
Administrative Organization
ATTN: Arthur Miles Hohorf for George Duval

Weidlinger Assoc. Consulting Engineers
ATTN: J. W. Wright
ATTN: Melvin L. Baron

Weidlinger Assoc. Consulting Engineers
ATTN: J. Isenberg

Westinghouse Electric Corp.
Marine Division
ATTN: W. A. Volz